Dissertation

Presenilin-1-mediated ER Ca^{2+} leak is an essential trigger for β-cell responsiveness to glucose

submitted by

Christiane KLEC, MSc

for the Academic Degree of

Doctor of Philosophy

(PhD)

at the

Medical University of Graz

Institute of Molecular Biology and Biochemistry

under the supervision of

Univ.-Prof. Dr. Wolfgang F. GRAIER

2019

DECLARATION

I hereby declare that this dissertation is my own original work and that I have fully acknowledged by name all of those individuals and organizations that have contributed to the research for the dissertation. Due acknowledgement has been made in the text to all other material used. Throughout this dissertation and in all related publications I followed the guidelines of “Standards of Good Scientific Practice and Ombuds Committee at the Medical University of Graz”.

Graz, Date

DISCLOSURES

Part of this thesis has been published in:

Klec C, Madreiter-Sokolowski CT, Stryeck S, Sachdev V, Duta-Mare M, Gottschalk B, Depaoli MR, Rost R, Hay J, Waldeck-Weiermair M, Kratky D, Madl T, Malli R and Graier WF. Glycogen synthase kinase 3 beta controls presenilin-1-mediated endoplasmic reticulum Ca^{2+} leak directed to mitochondria in pancreatic islets and β-cells. Cellular Physiology and Biochemistry 2018.

During my PhD thesis I also contributed to the following publications:

- Depaoli MR, Karsten F, Bischof H, Eroglu E, Madreiter-Sokolowski CT, **Klec C**, Gottschalk B, Waldeck-Weiermair M, Simmen T, Graier WF, Malli R Real-time imaging of mitochondrial ATP dynamics discloses the metabolic setting of single cells.
  Cell Reports. 2018; 25(2): 501-512
- Gottschalk, B; **Klec, C**; Waldeck-Weiermair, M; Malli, R; Graier, WF Intracellular Ca^{2+} release decelerates mitochondrial cristae dynamics within the junctions to the endoplasmic reticulum.
  Pflugers Arch. 2018; 470(8):1193-1203
- Eroglu, E; Rost, R; Bischof, H; Blass, S; Schreilechner, A; Gottschalk, B; Depaoli, MR; **Klec, C**; Charoensin, S; Madreiter-Sokolowski, CT; Ramadani, J; Waldeck-Weiermair, M; Graier, WF; Malli, R Application of Genetically Encoded Fluorescent Nitric Oxide (NO center dot) Probes, the geNOps, for Real-time Imaging of NO center dot Signals in Single Cells
  JOVE-J VIS EXP. 2017; (121): e55486
- Madreiter-Sokolowski, CT; Győrffy, B; **Klec, C**; Sokolowski, AA; Rost, R; Waldeck-Weiermair, M; Malli, R; Graier, WF UCP2 and PRMT1 are key prognostic markers for lung carcinoma patients.
  Oncotarget. 2017; 8(46): 80278-80285.
- Madreiter-Sokolowski, CT; Gottschalk, B; Parichatikanond, W; Eroglu, E; **Klec, C**; Waldeck-Weiermair, M; Malli, R; Graier, WF Resveratrol Specifically Kills Cancer Cells by a Devastating Increase in the Ca2+ Coupling Between the

Greatly Tethered Endoplasmic Reticulum and Mitochondria. Cell Physiol Biochem. 2016; 39(4):1404-1420

- Madreiter-Sokolowski, CT; **Klec, C**; Parichatikanond, W; Stryeck, S; Gottschalk, B; Pulido, S; Rost, R; Eroglu, E; Hofmann, NA; Bondarenko, AI; Madl, T; Waldeck-Weiermair, M; Malli, R; Graier, WF PRMT1-mediated methylation of MICU1 determines the UCP2/3 dependency of mitochondrial Ca(2+) uptake in immortalized cells. Nat Commun. 2016; 7: 12897-12897
- Waldeck-Weiermair, M; Bischof, H; Blass, S; Deak, AT; **Klec, C**; Graier, T; Roller, C; Rost, R; Eroglu, E; Gottschalk, B; Hofmann, NA; Graier, WF; Malli, R Generation of Red-Shifted Cameleons for Imaging Ca^{2+} Dynamics of the Endoplasmic Reticulum. Sensors (Basel). 2015; 15(6):13052-13068
- Waldeck-Weiermair, M; Malli, R; Parichatikanond, W; Gottschalk, B; Madreiter-Sokolowski, CT; **Klec, C**; Rost, R; Graier, WF Rearrangement of MICU1 multimers for activation of MCU is solely controlled by cytosolic Ca(2+). Sci Rep. 2015; 5(10):15602-15602
- Hofmann, NA; Barth, S; Waldeck-Weiermair, M; **Klec, C**; Strunk, D; Malli, R; Graier, WF TRPV1 mediates cellular uptake of anandamide and thus promotes endothelial cell proliferation and network-formation. Biol Open. 2014; 3(12):1164-1172

Co-authors of my publication

Corina T. Madreiter-Sokolowski[1], Sarah Stryeck[1], Vinay Sachdev[1], Madalina Duta-Mare[1], Benjamin Gottschalk[1], Maria R. Depaoli[1], Rene Rost[1], Jesse Hay[1,2], Markus Waldeck-Weiermair[1], Dagmar Kratky[1], Tobias Madl[1], Roland Malli[1,3] and Wolfgang F. Graier [1,3.]

[1]Medical University of Graz, Neue Stiftingtalstraße 6/6, 8010 Graz, Austria

[2]University of Montana, Campus Drive 32, Missoula, Montana, USA

[3]BioTechMed Graz, Graz, Austria

I confirm that all co-authors have agreed to use their data in my thesis. I have obtained permission from Cellular Physiology and Biochemistry to reproduce figures published in Klec et al. (1). The journal is part of the Karger Publishing Company which allows the reuse of published data in a PhD thesis at any time after publication (please visit the journal website for rights and permission statements https://www.karger.com/Services/RightsPermissions).

DANKSAGUNG

As a PhD student I have received funding by the Medical University of Graz through the PhD program DK-MCD (DK for Metabolic and Cardiovascular Disease).

An dieser Stelle möchte ich mich bei allen bedanken, die mir während der Arbeit an meiner Dissertation zur Seite gestanden sind. Zuallererst will ich mich bei meiner Familie und meinen Freunden bedanken, die mir stets Rückhalt gegeben und mich auf dem herausfordernden Weg ermutigend begleitet haben.

Ich danke meinen lieben Kollegen für ihre Unterstützung bei der Durchführung von Experimenten, die lebhaften wissenschaftlichen und nicht-wissenschaftlichen Diskussionen und den stetigen Zusammenhalt, alles entscheidende Faktoren für die Entstehung dieser Arbeit. Das freundschaftliche Miteinander im Laboralltag war sehr hilfreich, Rückschläge besser zu verkraften und neue Energie zu schöpfen. Mein besonderer Dank gilt hier Corina, Maria und Benjamin, die mich auf dem größten Teil dieser Reise begleitet haben und stets ein offenes Ohr für mich hatten. Ein weiteres großes Danke geht an Markus, der mir von Beginn an alle meine – vor allem am Anfang häufigen – Fragen stets mit Geduld beantwortet und mir so ziemlich alles im Labor gezeigt und beigebracht hat. Ein herzliches Dankeschön gebührt Sonja, für ihr stets offenes Ohr und die oft langen und intensiven Gespräche. Danke auch an die Kollegen der „AG Malli“ Jeta, Helmut, Sandra und Emrah, sowie an Anna, René und Sandra für die gute Zusammenarbeit über die gesamte Zeit hinweg.

Für die wissenschaftliche Begleitung während meines PhD-Studiums danke ich den Mitgliedern meines Dissertations-Komitees Roland Malli und Klaus Groschner.

Zuletzt gilt mein besonderer Dank meinem Supervisor Wolfgang F. Graier, der mir einerseits die Möglichkeit gab, an vielen spannenden Projekten sowie an meiner Dissertation zu arbeiten und andererseits auch in schwierigen Zeiten nie den Glauben an mich verloren und mich stets tatkräftig mit wertvollen Ratschlägen und Ideen unterstützt hat.

TABLE OF CONTENTS

LIST OF FIGURES

LIST OF ABBREVIATIONS

ADP/ATP	adenosine diphosphate/adenosine triphosphate
APH-1	anterior pharynx-defective 1
APP	amyloid precursor protein
$[ATP]_{mito}$	mitochondrial free ATP concentration
BCA	bicinchoninic acid assay
Bcl-2	B-cell lymphoma 2
BHQ	2,5-di-tert-butylhydroquinone
$[Ca^{2+}]_{cyto}$	cytosolic free Ca^{2+} concentration
$[Ca^{2+}]_{ER}$	endoplasmic reticulum free Ca^{2+} concentration
$[Ca^{2+}]_{mito}$	mitochondrial free Ca^{2+} concentration
Cch	carbachol
cDNA	complementary DNA
cds	coding sequence
CFP/YFP	cyan/yellow fluorescent protein
CHIR99021	6-[[2-[[4-(2,4-Dichlorophenyl)-5-(5-methyl-1*H*-imidazol-2-yl)-2- pyrimidinyl]amino]ethyl] amino]-3-pyridinecarbonitrile
D1ER	ER targeted Ca^{2+} sensor
DAG	diacylglycerol
DMEM	Dulbecco's modified eagle medium
dNTPs	desoxynucleotide triphosphate
DRP1	dynamin related protein 1
EB	experimental buffer
EGTA	ethylene glycol tetraacetic acid
ELISA	enzyme-linked immunosorbent assay
EMRE	essential MCU regulator
ER/SR	endo/sarcoplasmic reticulum
ETC	electron transport chain
$FAD/FADH_2$	flavin adenine dinucleotide: oxidized/reduced
FCCP	carbonyl cyanide-4-(trifluoromethoxy)phenylhydrazone
FCS	fetal calf serum

FP	fluorescent protein
FRET	Förster resonance energy transfer
Fura-2/AM	Fura-2 acetoxymethyl ester
GAPDH	glyceraldehyde-3-phosphate dehydrogenase
GPCR	G-protein coupled receptor
GSK3β	glycogen synthase kinase 3 beta
HBSS	Hank's balanced salt solution
HEPES	4-(2-Hydroxyethyl)piperazine-1-ethanesulfonic acid, N-(2-Hydroxyethyl)piperazine-N'-(2-ethanesulfonic acid)
His	histamine
IMM/OMM	inner/outer mitochondrial membrane
IMS	inter membrane space
INM/ONM	inner/outer nuclear membrane
INS-1	insulinoma cell line
IP_3	inositol 1,4,5-trisphosphate
IP_3R	inositol 1,4,5-trisphosphate receptor
kDa	kilodalton
LETM1	leucine zipper EF-hand containing transmembrane protein 1
MAMs	mitochondria-associated ER membranes
MCU	mitochondrial calcium uniporter
MCUb	mitochondrial calcium uniporter b
MCUR1	mitochondrial calcium uniporter regulator 1
MEF	mouse embryonic fibroblasts
MFN-2	mitofusin 2
MICU1/2	mitochondrial calcium uptake 1/2
mPTP	mitochondrial permeability transition pore
mRYR	mitochondrial ryanodine receptor
mtDsRed	mitochondrial *Discosoma sp*. red fluorescent protein
NAD/NADH	nicotinamide adenine dinucleotide: oxidized/reduced
NCLX	mitochondrial sodium/calcium exchanger
NCX	plasmamembrane located sodium/calcium exchanger
NO	nitric oxide
OCR	oxygen consumption rate

Opa1	optic atrophy 1
Orai1	calcium release-activated calcium channel protein 1
PBS	phosphate buffered saline
qPCR/RT-PCR	quantitative/real time polymerase chain reaction
PEN-2	presenilin enhancer 2
Pink1	PTEN-induced putative kinase 1
PIP_2	phosphatidylinositol 4,5-bisphosphate
PLC	phospholipase C
PMCA	plasma membrane Ca^{2+} ATPase
PS1/PSEN1	presenilin-1
Pyr6	N-[4-[3,5-Bis(trifluoromethyl)-1H-pyrazol-1-yl]phenyl]-3-fluoro-4-pyridinecarboxamide
RNA	ribonucleic acid
rpm	revolutions per minute
RT	reverse transcription
Sec61	ER protein translocator
SERCA	sarcoendoplasmic reticular calcium ATPase
siRNA	short interfering RNA
SOCE	store operated calcium entry
STIM1	stromal interacting molecule 1
TCA cycle	tricarboxcylic acid cycle
TMD	transmembrane domain
TRPC	transient receptor potential channel
UCP2/3	uncoupling protein 2/3
VDAC	voltage dependent anion channel

ABSTRACT

Mitochondrial activity serves as a key factor for the initiation of insulin release in β-cells. However, it is still unclear how β-cells precisely sense exclusively (blood) glucose. In fact, in non β-cells ATP production is under the control of mitochondrial Ca^{2+} that stimulates matrix dehydrogenases, while in β-cells mitochondrial ATP production is solely controlled by (blood) glucose. Our aim was to elucidate the molecular mechanism that makes mitochondrial ATP production in β-cells uniquely controlled by (blood) glucose. We hypothesize that in resting β-cells the Ca^{2+}-dependent mitochondrial dehydrogenases are already fully stimulated by Ca^{2+}, thus, making the redox-equivalents (i.e. NADH + H^+, $FADH_2$) derived from glucose metabolism the exclusive trigger for respiratory chain and mitochondrial ATP production. This would ensure a fast and precise insulin response upon glucose stimulation in β-cells that is independent from any mitochondrial Ca^{2+} signal and all-triggered by (blood) glucose. In the two insulin-producing cell lines, INS-1 and MIN-6 we found an increased ER Ca^{2+} leak which was not detectable in the non-insulin producing cell lines HeLa and the human umbilical vein endothelial cell line, EA.hy926. ER Ca^{2+} leak in β-cells was not a result from differences in SERCA activity and was compensated by continuous ER Ca^{2+} refilling by TRPC3. ER Ca^{2+} leak in β-cells was established by presenilin-1 that is phosphorylated at serine 353/357 by glycogen synthase kinase 3 (GSK3β). Subsequently to the ER Ca^{2+} leak, resting mitochondrial Ca^{2+} and basal mitochondrial dehydrogenase activity, measured as enhanced basal respiration and organelle ATP content was enhanced in β-cells. By preventing ER Ca^{2+} leak, responsiveness of β-cells to increased extracellular glucose, measured as lag time to cytosolic Ca^{2+} spiking, and, ultimately, insulin release were strongly delayed. The increased ER Ca^{2+} leak in β-beta cells appears to be of great physiological importance for the proper responsiveness of β-cells to elevated glucose, thus, possibly representing the molecular link between diabetes and Alzheimer's disease (AD). As presenilin-1, which was found herein to be essential for β-cells sensitivity, is also of utmost importance in the development of Alzheimer's disease further work will focus on verifying this potential link between diabetes and Alzheimer's disease.

ZUSAMMENFASSUNG

Die Insulinfreisetztung durch β-Zellen hängt grundlegend von deren mitochondrieller Aktivität ab. Jener Mechanismus, der es β-Zellen ermöglicht, ausschließlich Änderungen des (Blut-) Glukosespiegels zu detektieren, ist jedoch weiterhin ein Mysterium. In Zellen, die kein Insulin produzieren, steht die zelluläre ATP-Produktion unter der Kontrolle von mitochondriellem Ca^{2+}, das Dehydrogenasen (DH) in der mitochondriellen Matrix aktiviert. Im Gegensatz dazu wird die ATP-Produktion in β-Zellen ausschließlich durch einen Anstieg des (Blut-) Glukosespiegels stimuliert. Ziel dieser Arbeit war es den molekularen Mechanismus aufzudecken, der die Abhängigkeit mitochondrieller ATP-Produktion von der (Blut-) Glukosekonzentration in β-Zellen reguliert. Die Hypothese dieser Arbeit lautet, dass Ca^{2+}-abhängige mitochondrielle DH in β-Zellen im Ruhezustand bereits zur Gänze durch Ca^{2+} stimuliert sind und in Folge dessen Reduktionsäquivalente aus dem Glukosemetabolismus, als alleinige Auslöser für die Aktivierung der Atmungskette und der mitochondriellen ATP-Produktion verantwortlich sind. Dieser Vorgang würde eine schnelle und präzise Insulinausschüttung in Folge eines Glukosesignals durch β-Zellen sicherstellen. In den zwei untersuchten Insulin-produzierenden Zelllinien, INS-1 und MIN-6 konnte ein erhöhter passiver Ca^{2+}-Ausstrom aus dem endoplasmatischen Retikulum (ER) nachgewiesen werden, jedoch nicht in den Kontrollzelllinien, HeLa und EA.hy926. Dieser erhöhte passive Ca^{2+}-Ausstrom in β-Zellen resultiert nicht aus unterschiedlichen SERCA-Aktivitäten und wird durch eine kontinuierliche Ca^{2+}-Zufuhr durch den TRPC3 Kanal kompensiert. Weiters konnte gezeigt werden, dass Presenilin-1 für diesen Ca^{2+}-Ausstrom verantwortlich ist und dass dessen Aktivität durch die Glykogen-Synthase-Kinase 3 (GSK3β) reguliert wird. Als Konsequenzen des erhöhten Ca^{2+}-Ausstroms aus dem ER, konnten basal erhöhte mitochondrielle Ca^{2+}- Levels, verstärkte DH-Aktivitäten, sowie gesteigerte zelluläre Atmung und ATP-Levels in β-Zellen gemessen werden. Diese Daten scheinen von großer physiologischer Bedeutung zu sein und könnten die lange gesuchte Verbindung zwischen Diabetes und Alzheimer sein, weshalb zukünftige Forschung in diese Richtung von großer Wichtigkeit ist.

1. Introduction

Two cellular organelles namely mitochondria and the endoplasmic reticulum, as well as insulin producing β-cells are the main actors of my project. For that reason, I will address both organelles regarding their history, structure, function, Ca^{2+} handling properties and their implications in health and disease on the one hand and the mechanism how β-cells are able to produce insulin upon a rise of blood glucose and their role in physiological and pathophysiological processes on the other hand.

1.1. Mitochondria – structure, function and physiological relevance

1.1.1. Facts & history

The first observations of intracellular structures which are today known as mitochondria go back in the 1840s but the first definite description of “bioblasts” dates back until 1890. In the beginnings of their discovery mitochondria were supposed to be “elementary organisms living inside cells” and indeed the theory of the symbiotic origin of mitochondria was revived decades later (2). According to this endosymbiont theory more than two billion years ago a nucleus-bearing ancient eukaryotic cell incorporated today’s mitochondria by actively phagocyting an α-proteobacterium (3). Mitochondria owe their double-membrane character to their ancestors and also kept the ability for ATP-production, but during evolution their shape and composition drastically altered and a multitude of new functions were gained. “Modern” mitochondria possess a 16 kb, circular genome which is encoding for only 13 proteins mainly involved in the respiratory complex. The remaining approximately 1500 mitochondrial proteins are nuclear encoded and need to be transported to and imported into the mitochondria (4, 5). Since their discovery mitochondria have been well studied and the milestones of mitochondrial research are shown in **Figure 1**.

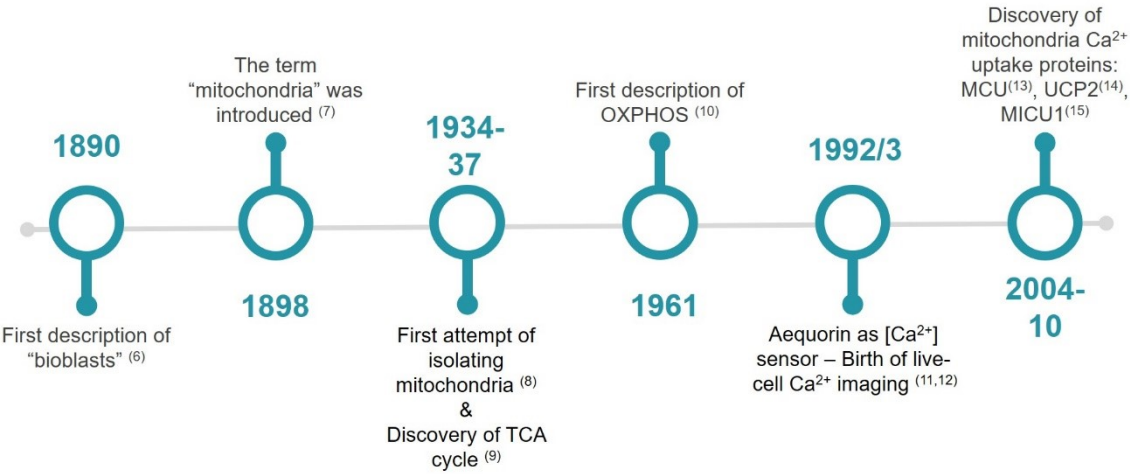

Figure 1 I History of mitochondrial research

1.1.2. Structure

As already mentioned, mitochondria are organelles composed of two functionally diverse membranes creating several compartments within this unique organelle (**Figure 2**).

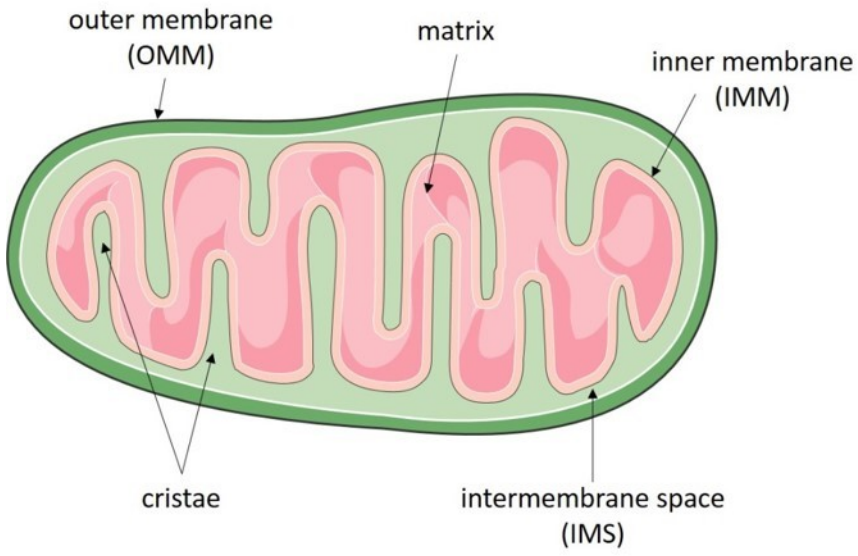

Figure 2 | Schematic representation of the basic mitochondrial structure

The mitochondrial outer membrane (OMM) is separating the intermembrane space (IMS) from the cytosolic environment. Ions and small uncharged molecules are able to passively diffuse through the OMM via pore forming proteins, also called porins,

such as the voltage-dependent anion channel (VDAC). Larger molecules and proteins depend on active transport via specialized translocases (16, 17). The inner mitochondrial membrane (IMM) functions as boarder separating IMS and matrix and is only freely permeable to oxygen, carbon dioxide and water. The IMM has a highly complex structure and exhibits an extraordinary high protein to phospholipid ratio since this membrane harbours the components of the electron transport chain, the ATP synthase complexes and all the specialized translocation machineries, needed for the active transport of molecules across this predominantly impermeable membrane (18, 19). Infoldings of the IMM, the so called cristae, highly increase the surface of the IMM, consequently creating enough space for the multitude of IMM proteins (20). The innermost compartment of mitochondria is the matrix. Its high pH is the main driving force for the electrochemical gradient, which is essential for ATP production. The matrix also harbours the mitochondrial DNA, numerous enzymes and is the site of the citric acid cycle (16).

1.1.3. Mitochondrial dynamics

Mitochondria are highly dynamic organelles, which is essential for maintaining their health since dysregulation of their dynamics is associated with pathological conditions including cancer, neurodegenerative and metabolic diseases as well as age-related processes (21, 22). The following four processes compose the most important dynamic actions. *i*; fusion – the fusion of two organelles into one, regulated by a subset of special GTPases including optic atrophy 1 (OPA1), mitofusin 1 (Mfn1) and mitofusin 2 (Mfn2). *ii*; fission – separation of one organelle into two, executed for example by dynamin-related protein 1 (Drp1). *iii*; transport – active movement within the cell, e.g. allowing mitochondria to locate at hotspots with a high ATP demand to supply sufficient energy (Woolley 1970) and *iv*; mitophagy – targeted destruction via autophagy, where Pink1 and Parkin are so far the best studied proteins involved in mitophagic processes (23). For a good review please see *Mishra et.al 2016*.

1.1.4. Mitochondrial function

The production of the cellular energy currency ATP via oxidative phosphorylation is considered to be the most important task of mitochondria (10, 24). Besides energy supply mitochondria execute processes such as the Krebs cycle (24), β-oxidation of fatty acids (25), heme biosynthesis (26), Ca^{2+} handling (27, 28), and regulate various physiological functions such as cell cycle control (29, 30), intracellular signaling (31) and cell death mechanisms (32). The enormous involvement of mitochondria in the cell's function prove the importance of this organelle but also lead to a high grade of vulnerability i.e. dysregulation or malfunction of mitochondrial performance are causative factors for various pathological diseases, such as cancer (33, 34), neurodegenerative diseases (35-37) as well as cardiovascular dysfunction (38, 39) and diabetes mellitus type 2 (40). Since mitochondrial metabolism and Ca^{2+} handling are crucial parts of my work, these two topics will be highlighted within the next chapters.

1.1.5. Energy supply and mitochondrial respiration

Mitochondria are the sites within a cell where most of the essentially needed ATP is produced. Processes such as oxidative decarboxylation and beta-oxidation provide acetyl-CoA fuelling the TCA cycle to produce NADH or $FADH_2$, that are used as electron donors for the electron transport chain (ETC). The electron transport chain is required for oxidative phosphorylation (OXPHOS), the process in which ATP is formed as a result of electron transfer, and consists of four complexes namely *i.* NADH dehydrogenase, *ii.* succinate dehydrogenase, *iii.* ubiquinone, bc1 complex and *iv.* cytochrome oxidase. The transport of electrons via these complexes is coupled to proton pumping from the mitochondrial matrix into the intermembrane space (IMS) leading to a negatively charged matrix and a positive charged IMS and thus to an electrochemical gradient. As a consequence, protons return into the matrix through the ATP synthase, also known as complex V, thereby releasing energy for ATP production by the ATP synthase (41).

1.1.6. Mitochondrial Ca^{2+} homeostasis

Upon elevations of intracellular Ca^{2+} levels, mitochondria are able to take up huge amounts of Ca^{2+} to ensure balanced conditions. This mitochondrial Ca^{2+} buffering capability is either linked to the capacitive Ca^{2+} influx through the plasma membrane (42) or to Ca^{2+} release from the main internal Ca^{2+} store, the endoplasmic reticulum (43). In excitable cells voltage-gated Ca^{2+} channels in the plasma membrane are the main routes for cellular Ca^{2+} (44), influx while in non-excitable cells Ca^{2+} enters the cytosol via ligand-gated, receptor-mediated, second messenger-operated, store-operated or stretch-operated channels (45, 46). In order to control Ca^{2+} homeostasis, the Na^{+}/Ca^{2+} exchanger (NCX) as well as the plasma membrane Ca^{2+}-ATPase (PMCA) ensure the extrusion of Ca^{2+} (47) and an intensive interplay between the plasma membrane and ER as well as plasma membrane and mitochondria takes place (**Figure 3**).

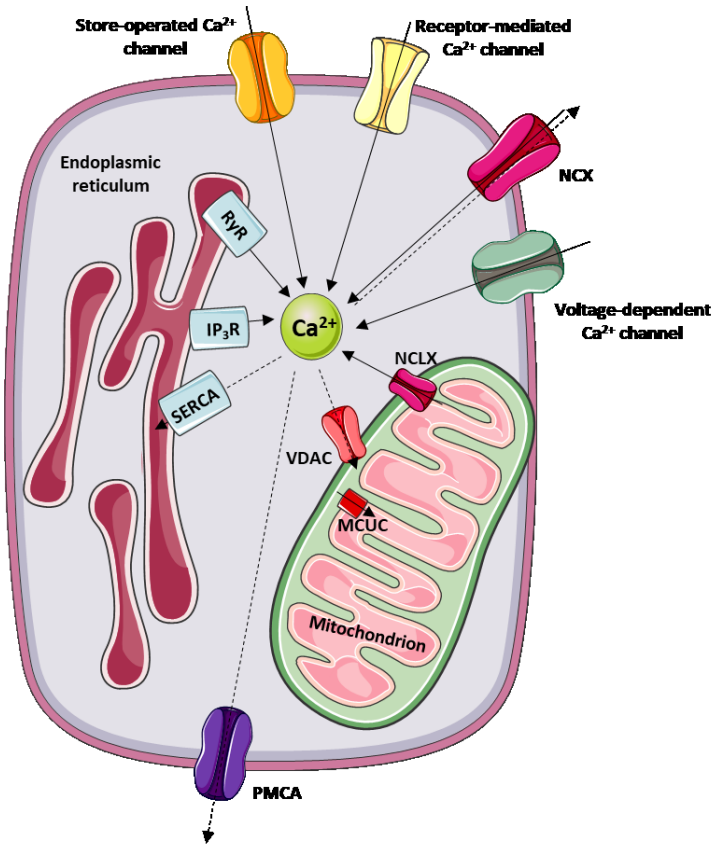

Figure 3 | Schematic representation of cellular Ca^{2+} homeostasis including Ca^{2+} channels. Full arrows indicate Ca^{2+} flux into the cytosol or the mitochondrial matrix and dotted arrows indicate Ca^{2+} flux out of the cytosol. NCX… Na^{+} Ca^{2+} exchanger (bidirectional), NCLX… mitochondrial Na^{+} Ca^{2+} exchanger, MCUC… mitochondrial Ca^{2+} uniporter complex, VDAC…voltage dependent anion channel, RyR… ryanodin receptor, IP_3R… inositol triphosphate receptor, SERCA… sarco/endoplasmic reticulum Ca^{2+}-ATPase, PMCA… plasma membrane Ca^{2+}-ATPase

1.1.7. Mitochondrial contribution to Glucose Stimulated Insulin Secretion (GSIS)

Nutrient-derived glucose is transported into the cytosol of β-cells via GLUT-2 (48) and subsequently subjected to glycolysis. During glycolysis reduction equivalents are generated, which are then transported into mitochondria where they accelerate mitochondrial metabolism (49). The resulting increased mitochondrial ATP levels cause a depolarization of the plasma membrane and opening of L-type Ca^{2+} channels, ultimately leading to exocytosis of insulin granules (50, 51). Mitochondrial Ca^{2+} uptake was shown to be essentially involved in glucose stimulated insulin secretion (GSIS) in β-cells (52) where the mitochondrial Ca^{2+} uniporter (MCU) as well as the mitochondrial Ca^{2+} uptake 1 (MICU1) were shown to have essential functions in GSIS (53).

1.2. Endoplasmic reticulum – its structure, function and physiological relevance

1.2.1. Facts & history

The endoplasmic reticulum was discovered in 1902 by Emilio Veratti, a student of Camillo Golgi – the identifier of the Golgi apparatus, but the existence of this organelle was ignored until the 1950s when it was rediscovered by electron microscopy (54, 55). Since then the ER shifted into the focus of numerous researchers and its importance acknowledged. This organelle is involved in many cellular processes of which the most important ones concerning my work are discussed below.

1.2.2. Structure & function

The endoplasmic reticulum is an interconnected network consisting of the nuclear envelope and the peripheral ER. Two lipid bilayers form the nuclear envelope i.e. the inner nuclear membrane (INM) and the outer nuclear membrane (ONM) which function as a selective barrier controlling nuclear transport. These two membranes are spanned by nuclear pores allowing the diffusion of proteins and RNAs between the nuclear and cytoplasmic compartment. The peripheral ER can be divided into

rough sheets and smooth tubules. The term rough ER derives from the ribosomes attached to the cytoplasmic side of the sheets and it is the site of protein synthesis, folding and posttranslational modifications. The smooth ER lacks attached ribosomes and mainly consists of highly curved, dynamic tubules and is the site of lipid and carbohydrate synthesis and metabolism as well as steroid hormone production (56, 57). The ER is also involved in protein biosynthesis, lipid and carbohydrate metabolism and secretion – more information concerning these issues can be found in this review (56).

1.2.3. Endoplasmic reticulum Ca^{2+} homeostasis

The ER is the biggest internal Ca^{2+} store with a [Ca^{2+}] of 100-800 µM in the lumen, a concentration which is much higher than the 100 nM in the cytosol. The ER has two main Ca^{2+} channels that are responsible for Ca^{2+} release from the organelle into the cytoplasma i.e. ryanodine receptors (RyR) and inositol 1,4,5-trisphosphate receptors (IP_3R) (58). RyRs work via Ca^{2+}-induced Ca^{2+} release when Ca^{2+} binds to the receptor in response to elevated cytoplasmic Ca^{2+} concentrations (59). Concerning IP_3R, Ca^{2+} release is triggered when phospholipase C (PLC) is stimulated through G protein-coupled receptor (GPCR) activation which leads to cleavage of phosphatidylinositol 4,5 bisphosphate (PIP_2) into diacyl-glycerol (DAG) and IP_3, which then binds to IP_3R leading to Ca^{2+} release. The sarcoendoplasmic reticular Ca^{2+} ATPase (SERCA) works into the other direction and actively pumps Ca^{2+} from the cytosol into the ER (58). Ca^{2+} is a global second messenger molecule involved in many cellular processes including protein localization, function and interactions with other proteins, organelles or nucleic acids (56).

1.2.4. ER Ca^{2+} leak channels

As already mentioned above, ER Ca^{2+} leak channels play a crucial role in keeping ER Ca^{2+} levels in balance, counteracting SERCA activity and, thus, avoiding store overfilling by clearing the organelle of excess Ca^{2+} ions through a permanent passive leak. Several membrane proteins – originally assigned for other duties - seem to occupy a function as ER Ca^{2+} leak channels and are shortly discussed in the following section (**Figure 4**).

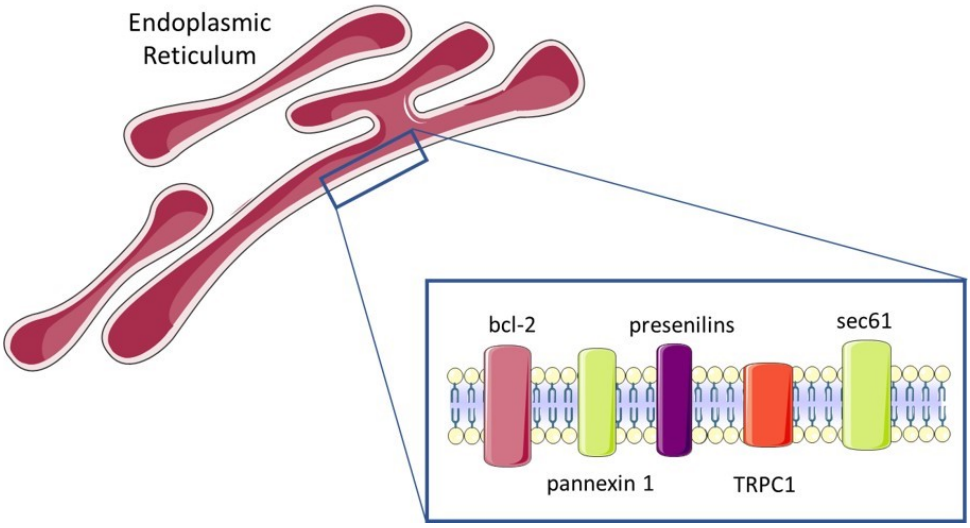

Figure 4 | Schematic representation of the known ER Ca^{2+} leak channels. These channels counteract SERCA activity to avoid ER Ca^{2+} overfilling and keeping the organelle's Ca^{2+} homeostasis in balance.

1.2.4.1. Bcl-2

The anti-apoptotic function of B-cell lymphoma 2 (Bcl-2) was first described in human lymphoma (60) and it is now known to have implications in several human cancers (61). Gene amplification (62), increased expression (63) and t(14;18) chromosomal translocation (64) of Bcl-2 are amongst other mechanisms responsible for its implications in human malignancies. Bcl-2 was found to localize at several cellular compartments i.e. *i.* the nuclear envelope (65), *ii.* the mitochondrial inner/outer membrane (66) – adequately matching it's regulatory function in apoptosis and *iii.* the endoplasmic reticulum (67). Beside its function as anti-apoptotic oncogene, Bcl-2 was recently found to contribute to decreased ER Ca^{2+} levels and increased permeability of the ER membranes (68, 69). The Bcl-2-driven passive ER Ca^{2+} leak is considered to facilitate avoiding apoptotic mechanisms (70) and was shown to form ion-conducting, cation-selective channels in lipid-bilayer experiments (71).

1.2.4.2. Pannexin

Pannexins are homologues of the connexin family whose more than 20 known members are responsible for cellular gap junction formation (72, 73). In addition to their function in conducting cellular connections via gap junctions, connexins and later also pannexins were shown to have channel properties involved in ATP signalling (74, 75). Pannexins are located in the plasma as well as the ER membrane and were recently shown to form Ca^{2+}-permeable channels. Overexpression of pannexin-1 leads to a decrease of total ER Ca^{2+} content and to a reduction of the amount of intracellular released Ca^{2+} upon stimulation (76). Regarding the crucial role of the ER as internal Ca^{2+} store, alterations in cellular pannexin expression could disturb ER Ca^{2+} homeostasis and, thus, lead to pathophysiologic conditions.

1.2.4.3. Transient receptor potential canonical type 1 (TRPC1)

The majority of the more than 30 members of the TRP channel family are non-selective Ca^{2+} permeable cation channels. The TRPC subfamily members are not only non-selective cation channels but are responsible for the so-called slow sustained mode of Ca^{2+} currents (77). TRPC channels are widely expressed in a variety of cell types and function as store-operated as well as second messenger operated channels (78). Normally, all members of the TRPC subfamily are located in plasma membrane (79) but a recent study showed that TRPC1 is also located at the sarcoplasmic reticulum of skeletal muscles and has an ER Ca^{2+} leak function, potentially contributing to the pathophysiology of muscle dystrophy caused by permanently elevated resting $[Ca^{2+}]_{cyto}$ (80).

1.2.4.4. Sec61

The Sec61 protein is one of the components of the so-called translocon complex located in the endoplasmic reticulum (81) forming a channel in the ER which is responsible for the translocation of freshly synthesized secretory proteins into the ER lumen and the integration of membrane proteins into the membrane (82) (Rapoport 1996). The Sec61 complex also is capable of transporting misfolded

proteins from the ER to the cytosol where they ultimately get degraded (83). Recently the contribution of Sec61 to ER Ca^{2+} leak function was confirmed by experiments showing *i.* Ca^{2+} permeable channel activity of Sec61 in planar lipid bilayer experiments and *ii.* a reduction of Ca^{2+} efflux from the ER upon knock-down of the Sec61 gene (84).

1.2.4.5. Presenilins

Due to their proteolytic function, presenilin-1 and 2 are well-known as contributors to Alzheimer's disease (85). Together with nicastrin, PEN-2 and APH-1 they form the γ-secretase complex (86, 87), where they constitute the catalytic part responsible for cleaving the amyloid-β precursor protein (APP) to the mature amyloid-β (88, 89), which is prone to plaque formation in the brain. Within the last decade a different function of presenilin-1 came into spotlight, i.e. its function as ER Ca^{2+} leak channel. Planar lipid bilayer experiments revealed that presenilins form cation-permeable ion channels and presenilin-1 accounts for approximately 80% of ER Ca^{2+} leak in mouse embryonic fibroblasts (MEF's), whereas mutated versions of the protein lose both abilities (90, 91).

2. Hypothesis and aims

Based on the knowledge above and considering the mechanism of insulin production and the necessity of a fast and precise response to glucose stimuli, a pre-stimulation of β-cells, ensuring an immediate response to a rise in cellular glucose levels, is of major importance. For that reason, we hypothesize that β-cells have a permanent passive ER Ca^{2+} leak which is directly sequestered to the mitochondrial matrix where it is pre-stimulating Ca^{2+}-dependent dehydrogenases of the citric acid cycle. This pre-stimulation allows a quantitative conversion of blood glucose to ATP, which is then triggering and regulating insulin secretion. In preceding experiments an increased ER Ca^{2+} leak could be demonstrated to be exclusively present in β-cells. To investigate this issue the current work was performed to achieve the following objectives:

- Characterization and comparison of ER Ca^{2+} leakage properties of β-cells and non-β-cell controls. To conduct this, ER Ca^{2+} leak was compared between two insulin-producing β-cell lines (INS-1 and MIN-6) and two non-insulin producing cell lines as controls (HeLa and EA.hy926) by using either direct ER Ca^{2+} measurements or an optimized indirect protocol for ER Ca^{2+} leakage.
- Identification of the engaged protein(s), determination of their regulation, i.e. what property makes this uniquely happen in β-cells.
- Mapping of the cellular consequences of an increased ER Ca^{2+} leak in β-cells, i.e. step-by-step investigation of the impact on the involved mechanisms for glucose stimulated insulin secretion from mitochondrial respiration over mitochondrial ATP production and cytosolic Ca^{2+} oscillations upon glucose stimulus to insulin secretion.

3. Materials and Methods

3.1. Chemicals and buffer solutions

All cell culture materials were obtained from Greiner Bio-One (Kremsmünster, Austria). The compounds histamine, antimycin A, oligomycin A, carbonyl cyanide p-trifluoromethoxyphenylhydrazone (FCCP), 2,5-di-t-butyl-1,4-benzohydroquinone (BHQ), ethylene glycol tetraacetic acid (EGTA), 2-Hydroxyethyl-trimethylammonium (carbachol), efonidipine hydrochloride monoethanolate and N-[4-[3,5-Bis(trifluoromethyl)-1H-pyrazol-1-yl]phenyl]-3-fluoro-4-pyridinecarboxamide (Pyr6) were purchased from Sigma Aldrich (Vienna, Austria). The selective GSK3β inhibitor 6-[[2-[[4-(2,4-Dichlorophenyl)-5-(5-methyl-1*H*-imidazol-2-yl)-2-pyrimidinyl]amino]ethyl] amino]-3-pyridinecarbonitrile (CHIR99021) was purchased from Tocris (Bristol, UK). All other chemicals were purchased from Carl Roth (Karlsruhe, Germany) unless otherwise specified. (1)

3.2. Cell culture and transfection

INS-1 832/13 cells were cultured in RPMI 1640 containing 11 mM D-glucose supplemented with 10 mM HEPES, 10% fetal calf serum (FCS), 1 mM sodium pyruvate, 50 µM β-mercaptoethanol, 50 µg penicillin and 100 µg streptomycin. MIN-6 cells were cultured in Dubelcco's Modified Eagle Medium (DMEM) supplemented with 25 mM D-glucose, 10 mM HEPES, 10% FCS, 1 mM sodium pyruvate, 50 µM β-mercaptoethanol, 50 µg penicillin and 100 µg streptomycin. HeLa and EA.hy926 cells were grown in DMEM supplemented with 10% fetal calf serum (FCS), 100 U/ml penicillin and 100 µg/ml streptomycin as well as 2 mM glutamine (Gibco, Life Technologies, Vienna, Austria), further on mentioned as full DMEM. (1)

3.3. Transfection with siRNAs and plasmids

For Ca^{2+} and ATP imaging, cells were plated on 30 mm glass coverslips in 6-well plates and transiently transfected at 60 – 80% confluency with 1.5 µg plasmid DNA alone or with 100 nM siRNA using 2.5 µl TransFast® transfection reagent (Promega, Madison, USA) in 1 ml of serum-and antibiotic-free medium. Cells were maintained in a humidified incubator (37°C, 5% CO_2, 95% air) for 16 – 20 hours. Afterwards, transfection mix was replaced by the appropriate full medium for each cell line. For treatment with the GSK3β inhibitor CHIR99021 cells were incubated in their

respective media containing 2.5 µM CHIR99021. All experiments were performed 48 hours after transfection or treatment. siRNAs were obtained from Microsynth (Balgach, Switzerland) or Thermofisher Scientific (Vienna, Austria). Sequences are listed in **Table 1**. Presenilin-1 wildtype as well as the mutated versions presenilin-$1^{S353/357A}$ and presenilin-$1^{S353/357D}$ overexpression plasmids were designed by us and synthesized by General Biosystems (Morrisville, USA). All presenilin-1 versions were cloned into a pcDNA3.1 backbone and are flanked by XbaI and EcoRI restriction sites. (1)

3.4. mRNA isolation, real-time and detection PCRs

Total RNA isolation was done using the PEQLAB total RNA isolation kit (Peqlab, Erlangen, Germany) and reverse transcription was performed in a thermal cycler (Peqlab) using a high-capacity cDNA reverse transcription kit (Applied Biosystems, Foster City, USA). For detection of presenilin-1 and GSK3β in INS-1, MIN-6, HeLa and EA.hy926 cells, specific primers were designed and purchased from Invitrogen (Vienna, Austria) and used for standard PCR. mRNA was isolated from the cell lines and transcribed to cDNA, which together with the GoTaq Green Master Mix (Promega, Mannheim, Germany) was used to set up the PCR reaction. Expression levels of presenilin-1, GSK3β as well as the respective knock-down and overexpression efficiency was determined by RT-PCR. A GoTaq® qPCR master mix (Promega) was used to perform real-time PCR on a LightCycler 480 (Roche Diagnostics, Vienna, Austria). Relative expression of specific genes was normalized to human, rat or mouse GAPDH, as a reference gene. Primers for real-time PCR and detection PCR were obtained from Invitrogen (Vienna, Austria). The respective sequences are listed in **Table 1**. (1)

Table 1 | List of primer and siRNA sequences. Gene and species specific detection and real time primer as well as siRNA sequences. h: *homo sapiens*, m: *mus musculus*, r: *rattus norvegicus*

APPLICATION	GENE	SEQUENCES
DETECTION PCR	h,m,rPSEN1	5'- GGTCCACTTCGTATGCTGGT -3'
		5'- TTGCTGAGGCTTTACCAACC -3'
	hGSK3β	5‘- TGTGATTCAGGAGAACTGGTCG-3‘
		5‘-ATCCAACAAGAGGTTCTGCGGT-3‘
	rGSK3β	5‘-GAGAACTGGTGGCCATCAAGAA-3‘
		5‘-CTGTATCAGGATCCAGCAAGAG-3‘
	mGSK3β	5‘-GTGATTCTGGAGAACTGGTTGC-3‘
		5‘-ATCCAACAAGAGGTTCTGTGGT-3‘
RT-PCR	hPSEN1	QuantiTect Hs_PSEN1 Primer Qiagen
	rPSEN1	QuantiTect Rn_PSEN1 Primer Qiagen
	mPSEN1	QuantiTect Mm_PSEN1 Primer Qiagen
	hGSK3β	5'- ACCTCCTTTGCGGAGAGCTG -3'
		5'- TGCCACCACTGTTGTCACCT -3'
	r,mGSK3β	5'- ACCTCCTTTGCGGAGAGCTG -3'
		5'- TGCCACCACTGTTGTTACCT-3'
siRNA	hPSEN1_1	5'-UUG UGU GGU UGG UGA AUA UTT -3'
	hPSEN1_2	5'- CCA CCU GAG CAA UAC UGU ATT -3'
	m,rPSEN1_1	5'-UUG UGU GGU UGG UGA AUA UTT -3'
	m,rPSEN1_2	5'- GGA GAG UAU CCA AAA AUU CTT - 3'

3.5. Total and pS9 GSK3β enzyme-linked immunosorbent assay (ELISA)

To determine the levels of total and pS9 (inactive) GSK3β the ELISA kit ab205711 (Abcam, Cambridge, UK) was used. In short, MIN-6, INS-1, HeLa and EA.hy926 cells were cultured until they reached approx. 80% confluency and lysed with the lysis buffer supplied with the kit. Protein concentration was measured using the Pierce™ BCA Protein Assay Kit (Thermofisher Scientific) and 5 µg protein were used for the ELISA. The remaining procedure was performed according to the manufacturer's protocol. (1)

3.6. Mitochondrial respiration measurements

INS-1, MIN-6, HeLa and EA.hy926 cells, untreated or treated with siRNA against presenilin-1 or GSK3β inhibitor CHIR99021, were plated in XF96 polystyrene cell culture microplates (Seahorse Bioscience) at a density of 60.000 cells/well for HeLa and EA.hy926, 120.000 cells/well for MIN-6 and 140.000 cells/well for INS-1 cells. After overnight incubation, cells were washed and incubated for 40 min in unbuffered XF assay medium supplemented with 1 mM sodium pyruvate at 37°C in a non-CO_2 environment. Basal oxygen consumption rate (OCR) was measured using an XF96 extracellular flux analyzer (Seahorse Bioscience). A standard protocol with 15 min basal measurement followed by 10 µM oligomycin, addition of 0.3 µM for HeLa as well as 0.7 µM for EA.hy926, INS-1 and MIN-6 carbonyl cyanide p-trifluoromethoxyphenylhydrazone (FCCP), and 2.5 µM antimycin A was performed. Oxygen consumption was normalized to protein content (pmol O_2/min × µg protein). (1)

3.7. Insulin measurements

For determination of insulin secretion rate INS-1 cells were routinely plated on 6-well plates and transfected at a confluency of 70 – 80% with either scrambled control siRNA or siRNA against presenilin-1. 48 h after transfection cells were washed twice with HBSS buffer containing 3 mM D-glucose, followed by a 30 min incubation in this buffer to record basal insulin secretion. For stimulation of insulin secretion buffer was changed to HBSS buffer containing 16 mM D-glucose and media was sampled

for the next 2 – 45 minutes. Samples were stored on ice and centrifuged at 3000 rpm for 5 min to remove residual cells. The supernatant was transferred into fresh tubes, stored at -20°C and assayed with Mercodia Rat Insulin ELISA (Mercodia, Uppsala, Sweden). Samples were diluted and total protein lysate was diluted 1:1000 in Calibration buffer #0. Insulin secretion rate was calculated by dividing the difference in insulin concentration of 2 consecutive time points by the time elapsed between sampling and normalized to total protein content (REF – Lorenz 2012).

3.8. Cytosolic Ca^{2+} imaging

Cells were incubated with 2 µM Fura-2/AM (TEFLabs, Austin, TX, USA) for 40 min in loading buffer (EHL) containing 135 mM NaCl, 5 mM KCl, 2 mM $CaCl_2$, 1 mM $MgCl_2$, 10 mM Hepes, 2.6 mM $NaHCO_3$, 440 µM KH_2PO_4, 340 µM Na_2HPO_4, 10 mM D-glucose, 0.1% vitamins, 0.2% essential amino acids, and 1% penicillin-streptomycin, pH adjusted to 7.4 and were alternately illuminated at 340 and 380 nm, whereas fluorescence emission was recorded at 510 nm. Results of Fura-2/AM measurements are shown as the ratio of F_{380}/F_{340}. For titration of cytosolic Ca^{2+} to visualize ER Ca^{2+} leak, after Fura-2/AM loading, cells were incubated for the indicated times in an experimental buffer without Ca^{2+} consisting of 138 mM NaCl, 1 mM $MgCl_2$, 5 mM KCl, 10 mM Hepes, 10 mM D-glucose and 1 mM EGTA and subsequently stimulated with 100 µM of IP_3-generating agonists (INS-1 and MIN-6: carbachol, HeLa and EA.hy926: histamine) in the presence of 15 µM of the SERCA inhibitor BHQ as described by Klec et al. (1). For D-glucose-induced cytosolic Ca^{2+} measurements, cells were loaded with 2 µM Fura-2/AM as described above, followed by a 20 min incubation in D-glucose free buffer (0G; 10 mM mannitol substitute the glucose) before imaging, to minimize the cytosolic oscillations on the one hand and to improve the signal upon exposure to high D-glucose on the other hand. On the microscope, cells were perfused with 0G buffer for 2 min before switching to 16 mM D-glucose (16G) during acquisition. To evaluate the maximal Ca^{2+} uptake via L-type Ca^{2+} channels, cells were depolarized with a high K^+ buffer, where 25 mM NaCl were substituted with KCl.

3.9. FRET measurements using genetically encoded sensors

$[Ca^{2+}]_{mito}$, $[Ca^{2+}]_{ER}$ and $[ATP]_{mito}$ were measured in cells expressing 4mtD3cpv, D1ER and mtAT1.03 (NGFI, *ngfi.eu*, Graz, Austria), respectively. Culture medium was removed and cells were kept in a HEPES-buffered solution described above. Single cell measurements were performed on an advanced wide-field fluorescent microscope (Till Photonics, Graefling, Germany) equipped with a motorized sample stage, a polychrome V (Till Photonics), a 40x objective (alpha Plan Fluar 40x, Zeiss, Göttingen, Germany) and a charge-coupled device camera (ATV Stingray F145B, Allied Vision Technologies, Stadtroda, Germany). The FRET-based Ca^{2+} sensors 4mtD3cpv and D1ER as well as the ATP sensor mtAT1.03 were excited at 430 nm and emission was collected using the dichrotome dual emission filter set (dichroic 535dcxr, CFP emitter 482/18nm and YFP emitter 535/3 nm). Data acquisition and control was carried out by the Live Acquisition 2.0.0.12 software (Till Photonics). (1)

3.10. NMR Metabolic profiling

Cells were washed twice with phosphate buffered saline and metabolic flux was quenched by mixing one volume of cell lysate (or medium) with two volumes of ice-cold methanol. Cells were lysed using Precellys® homogenisator with 1.4 mm ceramic beads (2 x 20 sec). The lysate was incubated at −20°C for at least 1 hour, and centrifuged at 13000 rpm for 30 min to pellet proteins and cell debris. Supernatants were transferred to fresh vials and lyophilized for 5 hours at room temperature. 500 µL of NMR buffer in D_2O were added to the samples, re-dissolved and transferred to 5 mm NMR tubes. Metabolites were measured as described previously (92, 93) and detailed below.

Methanol, sodium phosphate, dibasic (Na_2HPO_4), sodium hydroxide, hydrochloric acid (32% m/v), and sodium azide (NaN_3) were obtained from VWR International (Darmstadt, Germany). 3(trimethylsilyl)propionic acid-2,2,3,3-d4 sodium salt (TSP) was obtained from Alfa Aesar (Karlsruhe, Germany). Deuterium oxide (D_2O) was obtained from Cambridge Isotope laboratories, Inc. (Tewksbury, MA). Deionized water was purified using an inhouse Milli-Q® Advantage Water Purification System from Millipore (Schwalbach, Germany). The phosphate buffer solution was prepared by dissolving 5.56 g of anhydrous NaH_2PO_4, 0.4 g of TSP, and 0.2 g NaN_3, in 400

ml of deionized water and adjusted to pH 7.4 with 1M NaOH and HCl. Upon addition of D_2O to a final volume of 500 ml the pH was readjusted to pH 7.4 with 1 M NaOH and HCl.

All NMR experiments were performed at 310 K on a Bruker Avance III 500 MHz spectrometer equipped with a TXI probe head. The 1D CPMG (Carr−Purcell−Meiboom−Gill) pulse sequence (cpmgpr1d, 512 scans, 73728 points in F1, 12019.230 Hz spectral width, 1024 transients, recycle delay 4 s), with water suppression using pre-saturation, was used for 1H 1D NMR experiments.

Bruker Topspin version 3.1 was used for NMR data acquisition. The spectra for all samples were automatically processed (exponential line broadening of 0.3 Hz), phased, and referenced to TSP at 0.0 ppm using Bruker Topspin 3.1 software (Bruker GmbH, Rheinstetten, Germany).

Spectra pre-processing and statistical data analysis has been carried out using the state-of-the-art data analysis pipeline proposed by the group of Prof. Jeremy Nicholson at Imperials College London and using Matlab scripts. Statistical analysis includes Principle Component Analysis (PCA), Orthogonal Partial Least Squares Discriminant Analysis (O-PLS-DA) and all associated data consistency checks and cross-validation.

Normalized intensity matrix was exported and fold changes of metabolites of interest at distinct time points was determined. Standard deviation was calculated using error propagation.

3.11. Statistics

Data shown represent the mean ± SEM. ‘n’ values refer to the number of individual experiments performed. For life cell imaging numbers indicate the numbers of cells/independent repeats. If applicable analysis of variance (ANOVA) was used for data evaluation and statistical significance of differences between means was estimated by Bonferroni post hoc test or two-tailed Student’s t-test assuming unequal variances was used, where applicable using GraphPad Prism 5.0f (GraphPad Software, La Jolla, CA, USA). (1)

4. Results

4.1. The ER of β-cells is untypically leaky

4.1.1. Increased ER Ca^{2+} leak in β-cells

In most cell types the passive Ca^{2+} leak from the ER is compensated by SERCA activity which actively fuels the organelle with Ca^{2+} ions yielding a rather stable ER Ca^{2+} content even in the absence of extracellular Ca^{2+}. To test our hypothesis of the existence of an increased ER Ca^{2+} leak specifically in β-cells, we examined two β-cell lines – INS-1 and MIN-6 (insulinoma β-cell lines derived from pancreatic tissue of *rattus norvegicus* and *mus musculus*, respectively) as well as two widely used non-insulin producing cell lines – HeLa and EA.hy926 – as controls. We were able to develop an optimized protocol for visualizing the ER Ca^{2+} leak i.e. after removal of extracellular Ca^{2+}, the ER Ca^{2+} content was indirectly measured after given times as the cytosolic Ca^{2+} elevation upon cell stimulation with inositol 4,5-trisphosphate-(IP_3-) generating agonists and subsequent emptying of the ER Ca^{2+} store (**Figure 5**) (1).

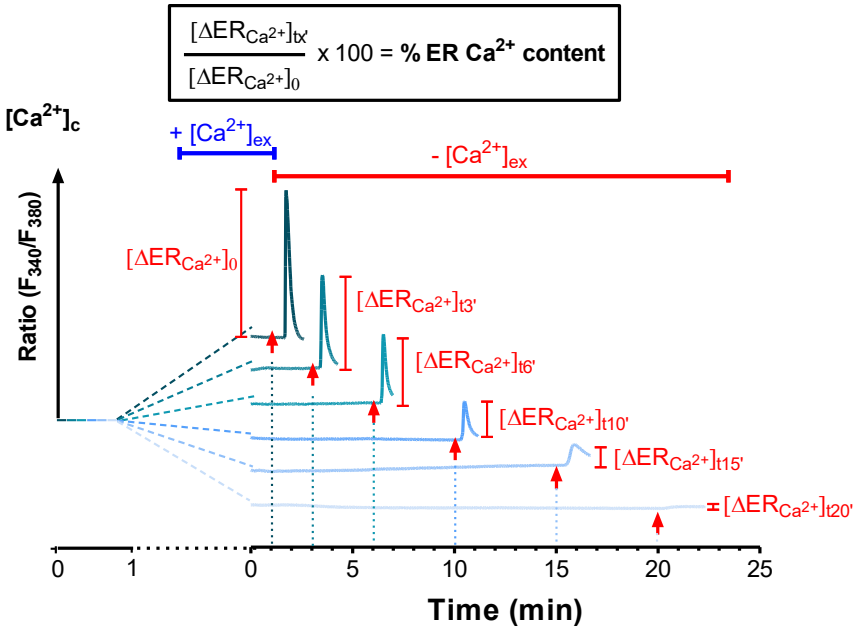

Figure 5 | Protocol for visualization of ER Ca^{2+} leakage. After loading cells with the cytosolic Ca^{2+} indicator Fura-2/AM, they were perfused with Ca^{2+} containing buffer for one minute before switching to Ca^{2+}-free buffer for predefined periods of time. For evaluation of ER Ca^{2+} content, ER Ca^{2+} stores were fully depleted by applying IP_3-generating agonists (100 µM carbachol for β-cells or histamine for non-β-cells) together with 15 µM of the SERCA inhibitor BHQ at the time points indicated with an arrow. The maximal ER store depletion was measured as maximal releasable ER Ca^{2+} in the cytosol whereas the ER is considered as fully filled at the one-minute time point and used as reference for calculating ER Ca^{2+} content as depicted in the formula. (1)

This simple protocol revealed no changes in ER Ca^{2+} content of control cells (HeLa and EA.hy926) over 20 minutes but a significant drop of IP_3-releasable Ca^{2+} was observed in the two β-cell lines (INS-1 and MIN-6) (**Figure 6A,B**). These data were generated by measuring cytosolic Ca^{2+} dynamics with the intracellular Ca^{2+} indicator Fura-2/AM and demonstrate the existence of an uncompensated ER Ca^{2+} loss present in β-cells. Also, direct measurements of ER Ca^{2+} content after removal of extracellular Ca^{2+} with the ER-targeted genetically encoded Ca^{2+} sensor D1ER reflect the observed ER leakage in β-cells but not in the control cells (**Figure 6C**) under basal conditions. We were able to reproduce these results in isolated murine pancreatic islets. Therefore, islets were incubated in Ca^{2+}-free buffer for one or 20 minutes and the IP_3-releasable ER Ca^{2+} - representing the ER Ca^{2+} content at the given time - was measured with Fura2/AM. As shown in **Figure 7** the signal was significantly lower after a long incubation under Ca^{2+}-free conditions, indicating that the ER of the islets passively lost the Ca^{2+} over time or in other words the ER of the islets is leaky as the one of the tested β-cell lines (1).

Since for the indirect protocol the fluorescent dye Fura-2/AM is used which is staining all cells on the coverslip and is not dependent on transfection efficiency or intensity of the sensor, this method was preferred when applicable.

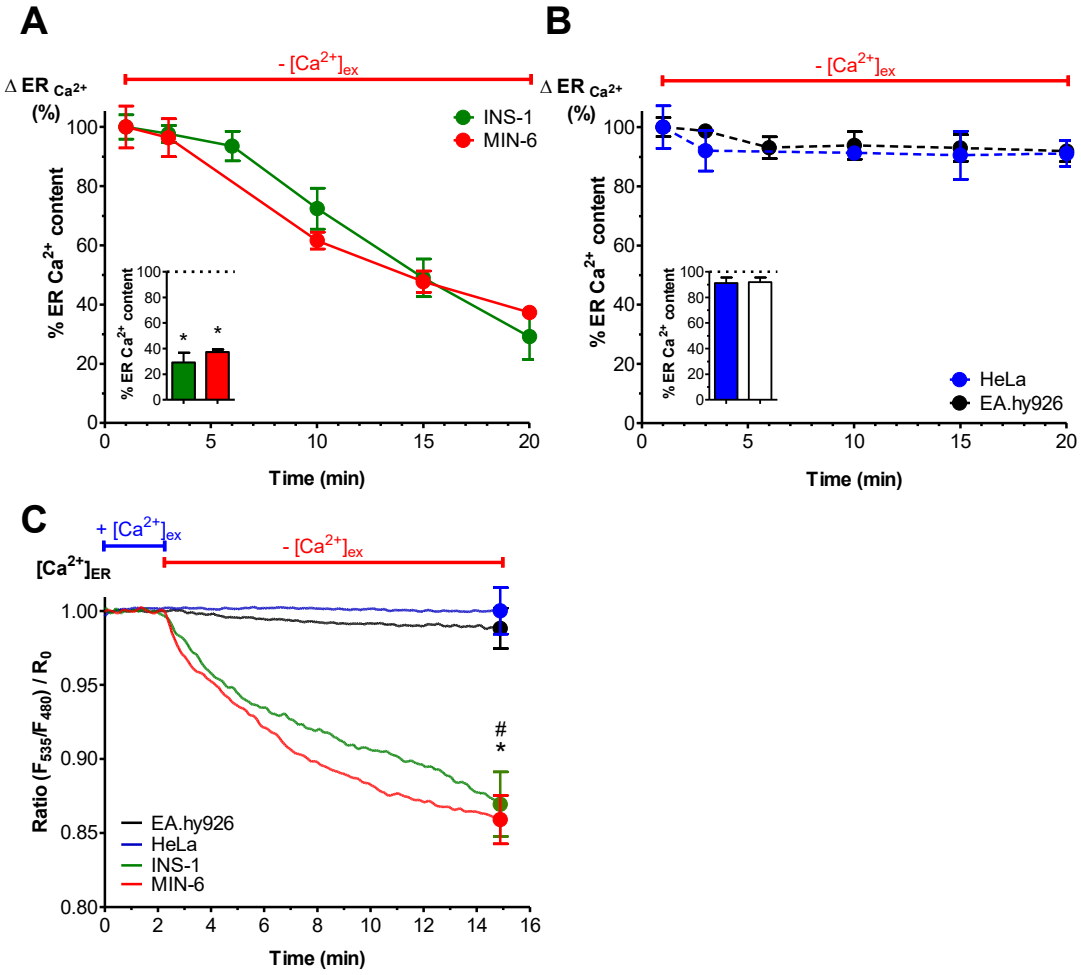

Figure 6 | β-cells have an untypical leaky ER **(A,B)** Percentage of ER Ca^{2+} leak, representing the maximal amount of Ca^{2+} released from the ER, under Ca^{2+}-free conditions in β-cells (A) or non-β-cells (B) stimulated with the IP_3-generating agonists carbachol (100 µM) in MIN-6 (red values) and INS-1 cells (green values) or histamine (100 µM) in HeLa (blue values) and EA.hy926 cells (black values) together with the SERCA-inhibitor BHQ (15 µM) at the indicated time points. Bar graphs represent percentage of ER Ca^{2+} content still present after 20 minutes incubation under Ca^{2+}-free conditions. (n≥6). **(C)** Curves reflect normalized $[Ca^{2+}]_{ER}$ ratio signals over time measured with the genetically encoded Ca^{2+} probe D1ER in HeLa (blue curve), EA.hy926 (black curve), INS-1 (green curve) and MIN-6 (red curve) cells perfused with experimental buffer containing 2 mM Ca^{2+} for two minutes before switching to 0 mM Ca^{2+} and EGTA-containing buffer, (n≥6). (1)

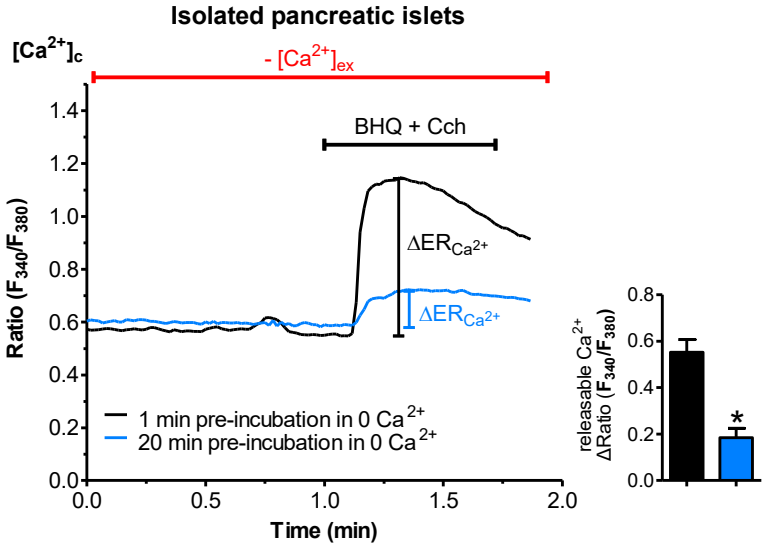

Figure 7 | ER Ca^{2+} leak is also present in isolated pancreatic islets. Curves reflect cytosolic Ca^{2+} measurements with Fura2/AM in isolated pancreatic islets after one (black curve) or 20 minutes (blue curve) of incubation in Ca^{2+}-free EGTA-buffered solution. Cells were placed on the microscope after the indicated incubation period and ER Ca^{2+} stores were depleted by applying 100 µM of the IP_3-generating agonist carbachol together with 15 µM of the SERCA inhibitor (BHQ). Bars on the right represent the released Ca^{2+}. *p<0.05 compared to 1-minute control using the Student's t-test, (n≥4). (1)

4.1.2. Enhanced ER Ca^{2+} loss is compensated by store operated Ca^{2+} channels

In β-cells the ER Ca^{2+} content remained constant in the presence of extracellular Ca^{2+} and the mobilization of intracellular Ca^{2+} with an IP_3-generating agonist resulted in a total depletion of ER Ca^{2+} stores (**Figure 8A** – black curve). Upon removal of extracellular Ca^{2+}, β-cells show the above described ER leak, leading to a complete emptying of ER Ca^{2+} stores after approximately 20 minutes, thus preventing any further reduction of the ER Ca^{2+} content in response (**Figure 8A** – red curve). When β-cells are perfused with Ca^{2+}-containing buffer, ER Ca^{2+} content stays stable over the whole period, since the ER Ca^{2+} leak is compensated by extracellular Ca^{2+} (black curve). Under both conditions, a total refilling of the store with Ca^{2+} is possible. With the next experiment we wanted to clarify the source of Ca^{2+} or more precisely where the Ca^{2+} leaking out of the ER is originating. For this purpose, we examined plasma-membrane located Ca^{2+} channels i.e. store operated channels (SOCE) via Orai1, the transient receptor potential channel 3 (TRPC3) and L-type Ca^{2+} channels. To realize this, we used pharmacological inhibitors to determine the ER Ca^{2+} content of pancreatic β-cells in Ca^{2+}-containing buffer in the

presence of 20 µM efonidipine (94), 1 or 40 µM Pyr6, and 3 µM Pyr10 (95) to inhibit Ca^{2+} entry via L-TCC, Orai1 and TRPC3, respectively. The inhibition of TRPC3 with 40 µM Pyr6 or 3 µM Pyr10 resulted in a consistent ER Ca^{2+} depletion **(Figure 8B)**, but the inhibition of L-TCC or Orai1 did not affect the ER Ca^{2+} content of the β-cells (**Figure 9**). These results demonstrate that extracellular Ca^{2+} is transported into the cell via TRPC3 and is directly transported into the ER fuelling it with the necessary Ca^{2+} needed for the leak or in other words β-cells require the activity of store-operated Ca^{2+} channels to compensate enhanced ER Ca^{2+} leakage (**Figure 8B, Figure 9**) (1).

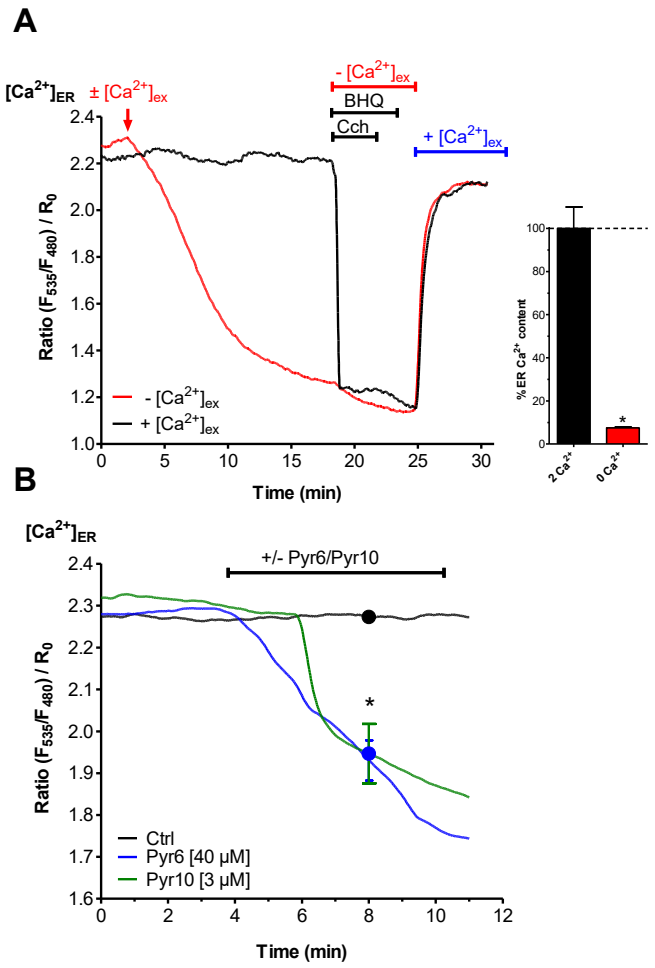

Figure 8 | Enhanced ER Ca^{2+} loss in β-cells is compensated by store-operated Ca^{2+} entry. **(A)** Representative curves for β-cells (depicted INS-1) reflect $[Ca^{2+}]_{ER}$ ratio signals over time in the presence (2 mM Ca^{2+}; black curve) or absence (0 mM Ca^{2+}; red curve) of Ca^{2+} measured with D1ER. The ER Ca^{2+} store was depleted using carbachol (100 µM) and BHQ (15 µM) in Ca^{2+}-free EGTA-buffered solution. Afterwards external Ca^{2+} (2 mM) was added. Bar graphs represent the percentage of the releasable ER Ca^{2+} content after 18 minutes of incubation in Ca^{2+}-free (red bar) or Ca^{2+}-containing (black bar) buffer. (n≥6). **(B)** Curves for β-cells (depicted INS-1) reflect $[Ca^{2+}]_{ER}$ ratio signals over time measured with D1ER in experimental buffer containing 2 mM Ca^{2+} under control conditions (black curve) or with the SOCE inhibitor Pyr6 (40 µM) (blue curve) or Pyr10 (3 µM) (green curve), (n≥6). (1)

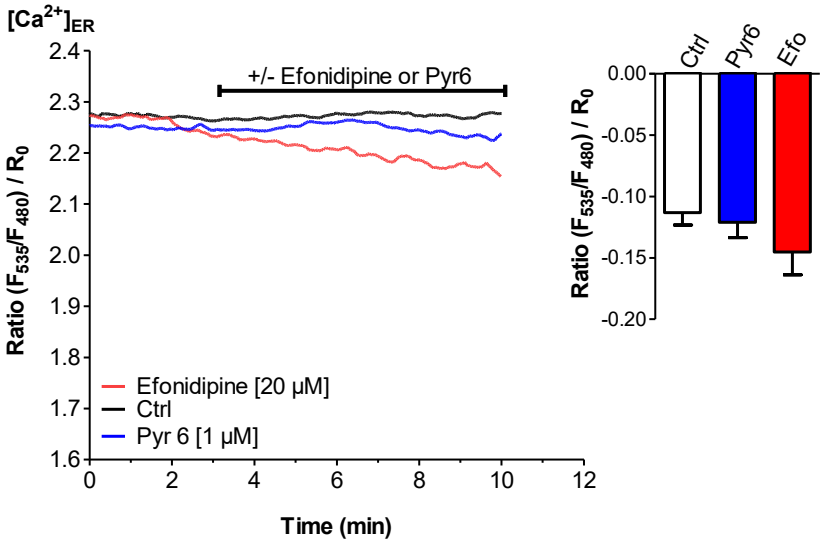

Figure 9 | L- and T-type Ca^{2+} channels do not compensate ER Ca^{2+} leak. Curves for β-cells (depicted INS-1) reflect $[Ca^{2+}]_{ER}$ ratio signals over time measured with D1ER in experimental buffer containing 2mM Ca^{2+} under control conditions (black curve) and with the L- and T-type Ca^{2+} channel blocker efonidipine [20 µM] (red curve) or Pyr6 [1 µM] (blue curve), (n=6). (1)

4.1.3. β-cell ER Ca^{2+} loss is independent of SERCA

Basically, there are two phenomena that may yield an enhanced Ca^{2+} loss of the ER: *i*, reduced SERCA activity that does not compensate a rather "normal" ER Ca^{2+} leakage, or, *ii*, enhanced ER Ca^{2+} leakage that is not compensated by normal-active SERCA since leaked Ca^{2+} is rapidly trapped by a SERCA-unserviceable "pool". To test these possibilities, SERCA activity was tested by measuring the kinetics of Ca^{2+} refilling of an ER that was pre-emptied by the SERCA inhibitor BHQ and the IP_3-generating agonists histamine for HeLa and EA.hy926 or carbachol for INS-1 and MIN-6 cells. After completely emptying the ER Ca^{2+} store and washing out BHQ, stores were again filled with Ca^{2+}. Notably, the Ca^{2+} refilling kinetics of pre-emptied ER was comparable in all the used cell lines, thus, excluding a reduced SERCA activity as cause for the observed ER Ca^{2+} loss in β-cells (**Figure 10**) (1).

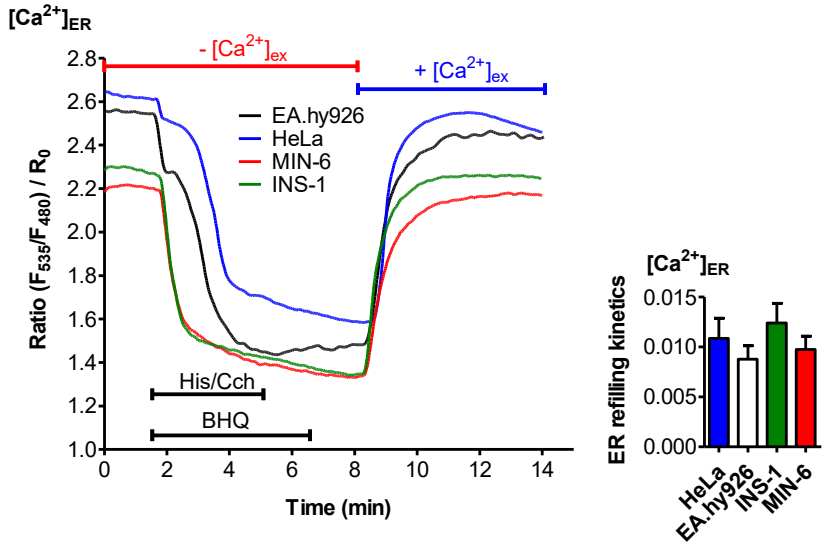

Figure 10 | β-cells ER Ca^{2+} loss is independent of SERCA activity. Representative curves reflect $[Ca^{2+}]_{ER}$ ratio signals over time in HeLa (blue curve), EA.hy926 (black curve), INS-1 (green curve) and MIN-6 (red curve) cells, measured by D1ER. ER Ca^{2+} store was depleted using 100 µM histamine (His) for HeLa and EA.hy926 or 100 µM carbachol (Cch) for INS-1 and MIN-6 together with 15 µM BHQ in Ca^{2+}-free EGTA-buffered solution. To compare SERCA activity between the cell lines, external Ca^{2+} (2 mM) was added after agonists were washed out. Corresponding statistical analysis is depicted in the bar graph on the right side showing the calculated ER refilling kinetics of the tested cell lines, (n≥6). (1)

4.2. Presenilin-1 is responsible for enhanced ER Ca^{2+} loss in β-cells

According to literature research there are several proteins supposed to execute ER leak channel function i.e. Bcl2 (68, 69), pannexin (76), presenilins (90), TRPC1 (80) and Sec61 (84) in several cell types, but none of these were investigated in β-cells so far. We decided to have a closer look on presenilin-1, since it was shown to execute an ER leak function in several cell types and to account for up to 80% of ER Ca^{2+} leak in MEF cells (mouse embryonic fibroblasts) (90, 91, 96). The expression of preseniln-1 in the used cell lines was verified by standard PCR, using gene and species-specific primers (**Table 1**). An equal gene expression was verified by quantitative real-time PCR (**Figure 11A**) and is shown in the representative gel (**Figure 11B**). To check our hypothesis that presenilin-1 indeed contributes to ER leak function in β-cells, we designed specific siRNAs to knock-down presenilin-1 (**Table 1**). Knock-down efficiency was validated by qRT-PCR (**Figure 11C**) (1).

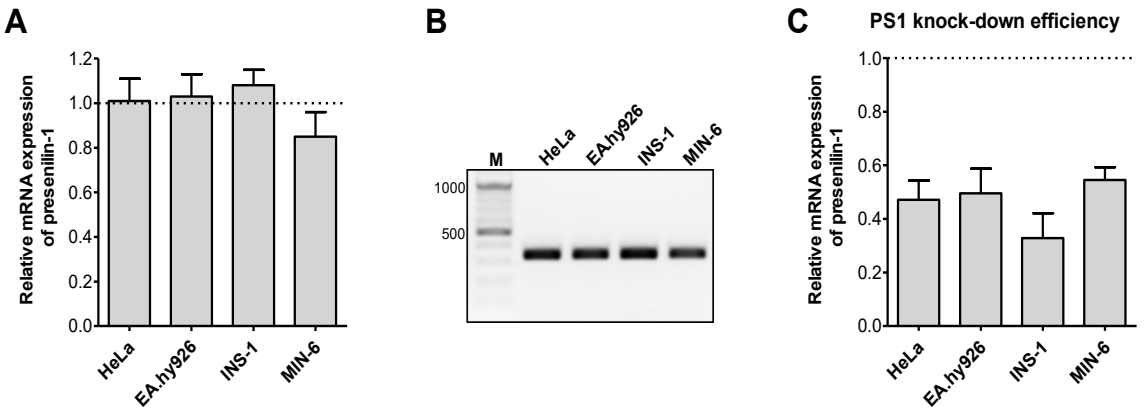

Figure 11 | Increased ER Ca^{2+} loss in β-cells is presenilin-1 mediated. **(A)** Quantitative evaluation of presenilin-1 expression levels by real-time PCR in HeLa, EA.hy926, INS-1 and MIN-6 cells using GAPDH as reference gene. For comparison between the cell lines expression values were normalized to HeLa expression which was set 100%. (n=3). **(B)** Representative gel showing detection of mRNA levels of presenilin-1 in HeLa, EA.hy926, INS-1 and MIN-6 cells conducted via standard PCR using gene and species specific primers. **(C)** Validation of siRNA-mediated knock-down efficiency of presenilin-1 in the tested cell lines via qRT-PCR. Bars represent relative mRNA expression compared to control cells transfected with negative control siRNA. All values were normalized to the houskeeping gene GAPDH. (n=3). (1)

To observe a possible effect of a reduced presenilin-1 expression on ER Ca^{2+} leak capacity we applied the improved ER leakage protocol in the four used cell lines and measured the cytosolic Ca^{2+} signal after emptying the stores representing the ER Ca^{2+} content at the given time point. Knock-down of presenilin-1 abolished the enhanced ER Ca^{2+} leak in both β-cell lines after 20 minutes (**Figure 12A**) while no effect was observed in the non-β-cells, HeLa and EA.hy926 (**Figure 12B**) (1).

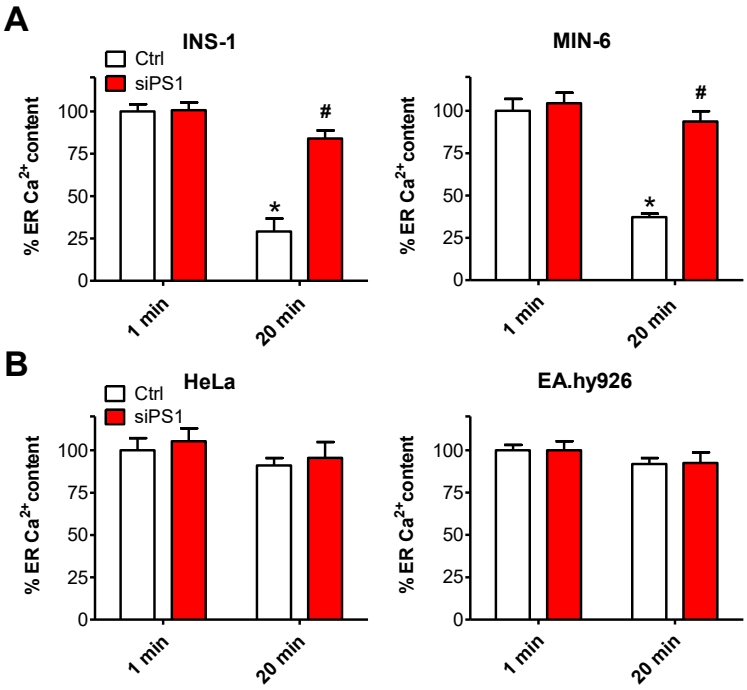

Figure 12 | ER Ca^{2+} leak is dependent on presenilin-1. **(A,B)** Evaluation of the influence of presenilin-1 knock-down on ER Ca^{2+} leakage – depicted is the percentage of the ER Ca^{2+} content in **(A)** INS-1 (*left panel*) and MIN-6 (*right panel*) as well as in **(B)** HeLa (left panel) and EA.hy926 (*right panel*) under control conditions (white bars) or after knock-down of presenilin-1 (red bars) after one or 20 minutes of incubation under Ca^{2+}-free conditions. ER Ca^{2+} stores were depleted at the indicated time points by treating the cells with 15 µM of the SERCA inhibitor BHQ and either 100 µM of the IP_3-generating agonists carbachol for INS-1 and MIN-6 or histamine for HeLa and EA.hy926 cells. Bars represent mean ± SEM, (n≥5). (1)

These results strongly suggest the implication of presenilin-1 in the leak function of β-cells, but further experiments were needed to support this hypothesis. Thus, we overexpressed presenilin-1 in our cell lines and documented the resulting consequences on ER leak function. If presenilin-1 was responsible for the ER Ca^{2+} leak an overexpression of this protein should augment the leakiness of the organelle. Indeed, overexpression of presenilin-1 resulted in an even more increased ER Ca^{2+} leak in the two β-cell lines – INS-1 and MIN-6 (**Figure 13A&B**) while no leak was detected in the control cells – HeLa and EA.hy926 (**Figure 13C**), underlining the exclusive and expression-level dependent involvement of presenilin-1 mediated ER Ca^{2+} leak in β-cells (1).

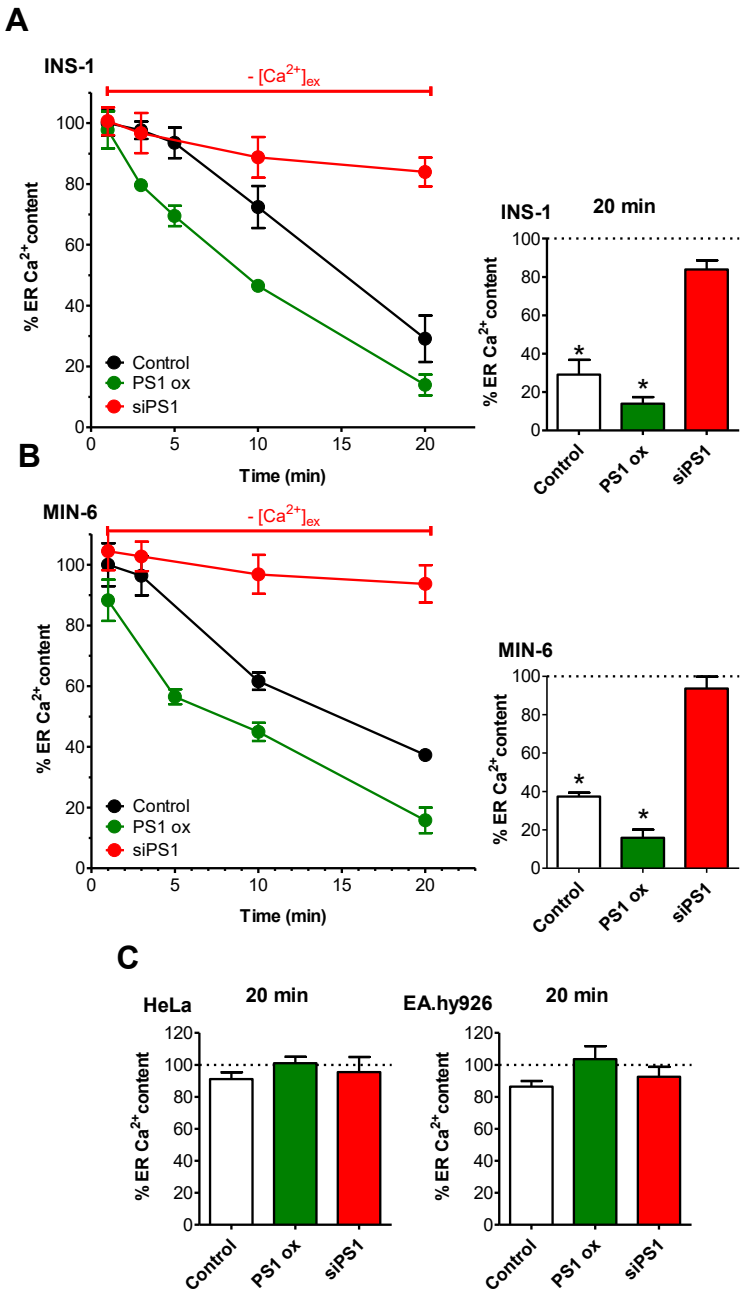

Figure 13 | Overexpression of presenilin-1 is increasing ER leak in β-cells. **(A,B)** Time course experiments in INS-1 **(A)** and MIN-6 **(B)**. Percentage of ER Ca^{2+} content under Ca^{2+}-free conditions is depicted either under control conditions (black values), knock-down of presenilin-1 (red values) or overexpression of presenilin-1 wild type (green values). Cells were stimulated with the IP_3-generating agonist carbachol (100 µM) and the SERCA inhibitor BHQ (15 µM) at the given time points. Bars represent mean ± SEM. Bars on the right represent percentage of ER Ca^{2+} content at time point 20 minutes. (n≥6). **(C)** Percentage of ER Ca^{2+} content in HeLa and EA.hy926 cells after incubation under Ca^{2+}-free conditions for one and 20 minutes under the same conditions as in A,B. ER Ca^{2+} stores were depleted at the indicated time points with 100 µM histamine and 15 µM of the SERCA inhibitor BHQ. Values for one minute under control conditions were set 100%. *p<0.05 versus control at one minute using one-way ANOVA. (n≥6). (1)

There are findings showing that presenilin-1 is involved in ER Ca^{2+} leakage via modulation of IP_3R – especially of type 1 IP_3R (97). Therefore, we performed Ca^{2+} leak experiments in β-cells and non-β-cells. First, expression levels of the IP_3R subtypes in INS-1 and HeLa cells were evaluated on mRNA level, showing a high expression of IP_3R3 in INS-1 cells and a comparable expression of the three subtypes in HeLa cells (**Figure 14A**). Second, INS-1 and HeLa cells were transfected with specific siRNAs against the IP_3R subtypes and knock-down

efficiency was verified with qRT-PCR (**Figure 14B**). Third, knock-down efficiency was also functionally verified by measuring Cch- or histamine induced intracellular Ca^{2+} release using the Fura-2/AM technique (**Figure 15A**). Fourth, ER Ca^{2+} leak measurements under IP_3R knock-down conditions show that the ER Ca^{2+} leak was persisting in β-cells. Since IP_3-generating agonists are not applicable under IP_3R knock-down conditions, global ER Ca^{2+} release was evoked by applying 0.2 µM ionomycin, a concentration of the ionophore known to specifically deplete ER Ca^{2+} (98) (**Figure 15B**). These data indicate on the one hand that IP_3R subtypes 1 and 2 are not essential for IP_3-mediated ER Ca^{2+} release in β-cells and on the other hand that IP_3R do not contribute to ER Ca^{2+} leakage – at least not in β-cells, so we speculate that these data might be the explanation for a persisting ER Ca^{2+} leak in β-cells.

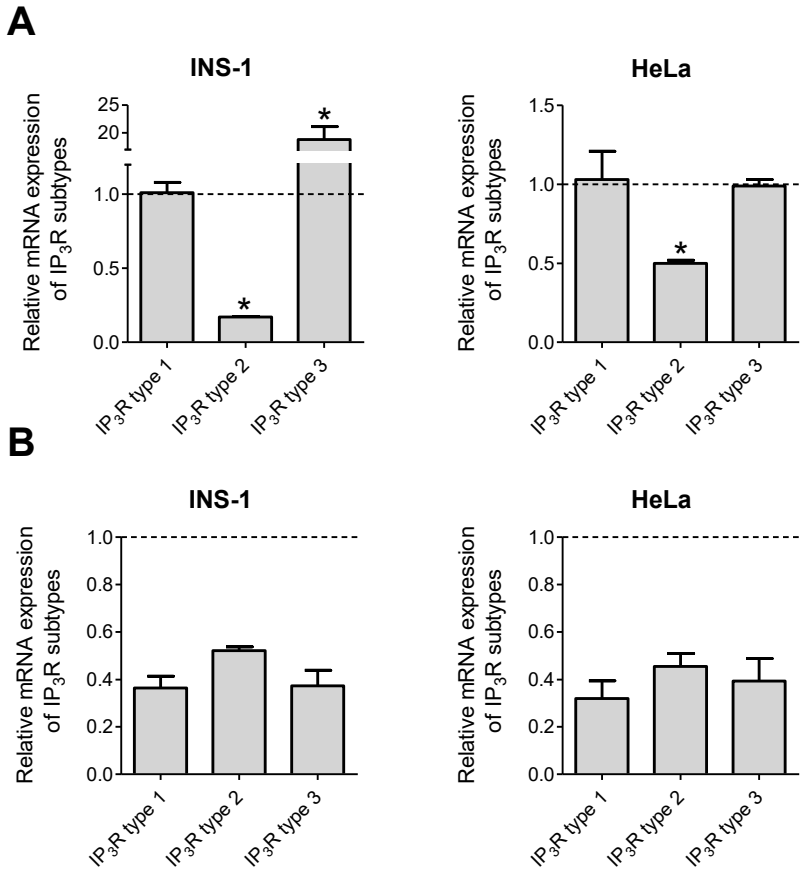

Figure 14 | IP_3R does not influence ER Ca^{2+} leakage in β-cells (I). **(A)** mRNA expression levels of the three IP_3R subtypes in INS-1 (*left panel*) and HeLa cells (*right panel*) using the housekeeping gene GAPDH as reference and normalized to the expression levels of IP_3R type 1 for comparison. *p<0.05 tested with one-way ANOVA, (n=3). **(B)** siRNA mediated knock-down efficiency of IP_3R subtypes in INS-1 (left panel) or HeLa cells (right panel) was measured with qRT-PCR, (n=5).

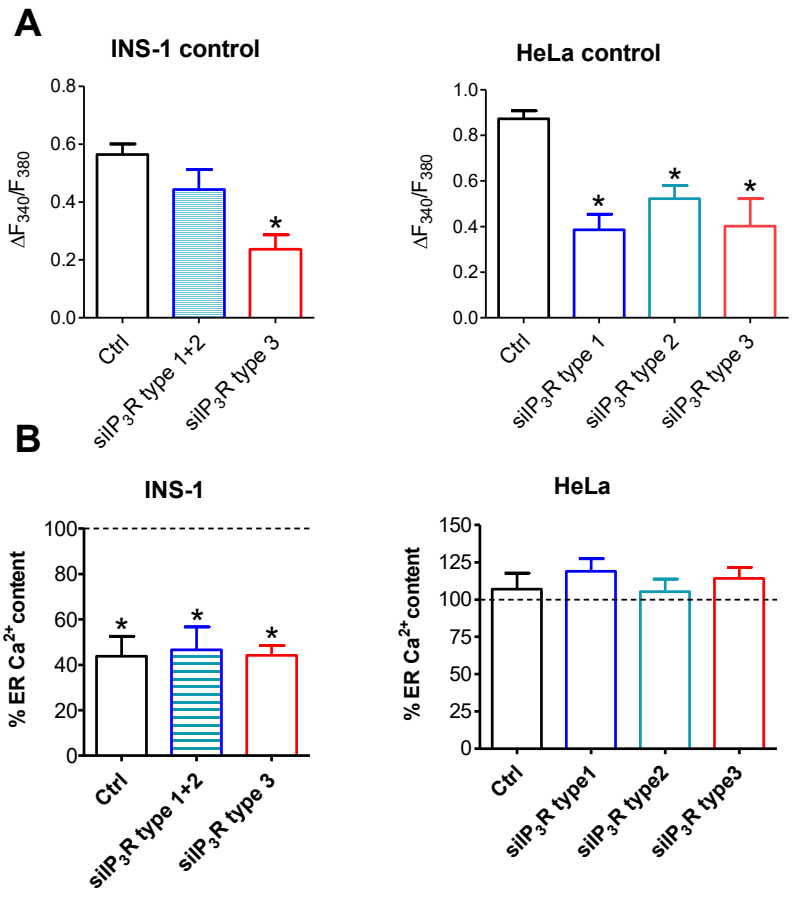

Figure 15 | IP_3R does not influence ER Ca^{2+} leakage in β-cells (II). **(A)** Functional verification of knock-down efficiency by stimulating the cells with IP_3-generating agonists i.e. 100 µM carbachol for INS-1 *(left panel)* and 100 µM histamine for HeLa cells (*right panel*) together with 15 µM BHQ, (n≥5). **(B)** Percentage of ER Ca^{2+} content in INS-1 (*left panel*) or HeLa (*right panel*) cells after 20 minutes of incubation under Ca^{2+}-free conditions either under control conditions (white bars) or after knock-down of certain IP_3R subtypes (coloured bars). ER stores were depleted after 20 minutes by applying 0.2 µM of ionomycin (a concentration known to specifically empty ER Ca^{2+} stores) together with the SERCA inhibitor BHQ (15 µM), (n≥5). (1)

In the next step we wanted to investigate the underlying basis for the ER Ca^{2+} leak exclusively appearing in β-cells. After verifying comparable expression levels of presenilin-1 between β-cells i.e. INS-1 and MIN-6 and non-β-cells i.e. HeLa and EA.hy926 (**Figure 11**), the results that presenilin-1 modulation exclusively affected ER Ca^{2+} leak in β-cells (**Figure 6, 12, 13**) and the exclusion of a contribution of IP_3Rs to ER Ca^{2+} leak in β-cells (**Figure 14, 15**), we speculate if a post-translational modification of presenilin-1 is a causative factor for the increased leak in β-cells and respective experiments and results are discussed in the following section.

4.3. Presenilin-1-dependent ER Ca^{2+} leakage in β-cells is regulated by GSK3β

The group of Maesako was able to show that presenilin-1 is phosphorylated by GSK3β at two serine residues, namely serine 353 and 357 (99). This post-translational modification leads to an increased presenilin-1 activity (96). Therefore, the involvement of this kinase in the increased ER Ca^{2+} leak of β-cells was explored by verifying the expression and the activity of GSK3β in the tested β-cells and non-β-cells. The expression levels of GSK3β are comparable in all cell lines on the mRNA level (**Figure 16A**). Interestingly, an enzyme-linked immunosorbent assay, designed to detect the total amount of GSK3β as well as its inactive version (pS9) (100), shows elevated GSK3β activity in both β-cell lines compared with the two non-β-cell lines, highlighting the correlation between ER Ca^{2+} leak and GSK3β activity, i.e. increased ER Ca^{2+} leak involves increased GSK3β activity (**Figure 16B**) (1).

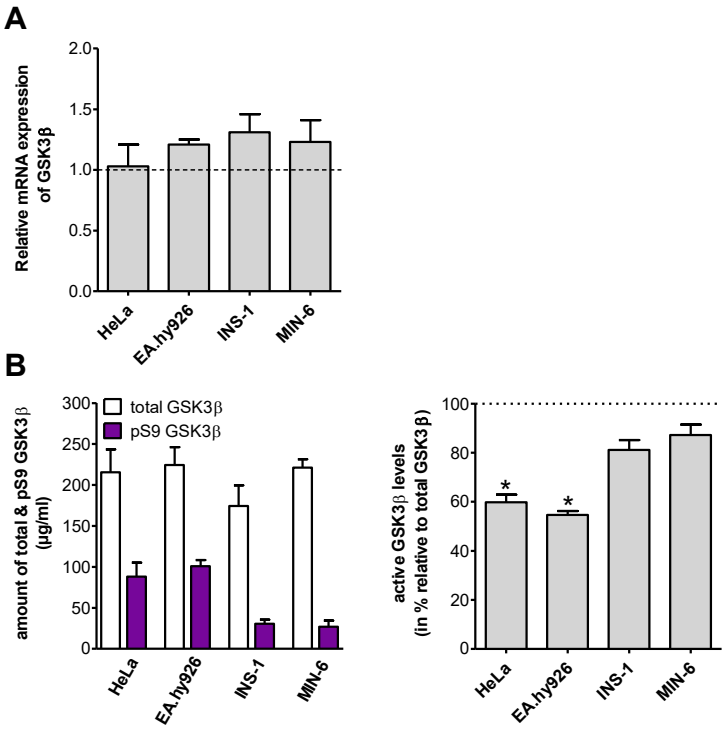

Figure 16 | GSK3β regulates presenilin-1-dependent ER Ca^{2+} leakage in β-cells (I). **(A)** Quantification of mRNA levels of GSK3β by qRT-PCR using the housekeeping gene GAPDH as reference gene. For comparison between the cell lines expression levels were normalized to expression in HeLa cells. (n=3). **(B)** (*left panel*) Evaluation of the levels of total GSK3β (white bars) and its inactive version pS9 GSK3β (violet bars) as well as

(*right panel*) the ratio of pS9 (inactive) GSK3β versus total GSK3β in HeLa, EA.hy926, INS-1 and MIN-6 cells using a specific ELISA. *p<0.05 refers to pS9 levels of EA.hy926 and HeLa compared to β-cells, (n≥4). (1)

Accordingly, we hypothesized that GSK3β-mediated phosphorylation of presenilin-1 caused its enhanced activity in β-cells and, thus, the observed enhanced ER Ca^{2+} leak in this very cell type. To challenge this hypothesis, cells were pre-incubated for 24 to 48 h with the GSK3β inhibitor CHIR99021 (101, 102) and applied the same leakage protocol as mentioned above. Pre-incubation of β-cells with the GSK3β inhibitor completely prevented enhanced ER Ca^{2+} leak in β-cells (**Figure 17A**) while in non-β-cells with their tight ER an inhibition of GSK3β had no effect on ER Ca^{2+} leak (**Figure 17B**). Strikingly, we could also abolish ER Ca^{2+} leak by inhibiting GSK3β in murine pancreatic islets, providing evidence for the physiologic importance of this leak even in primary cells (1).

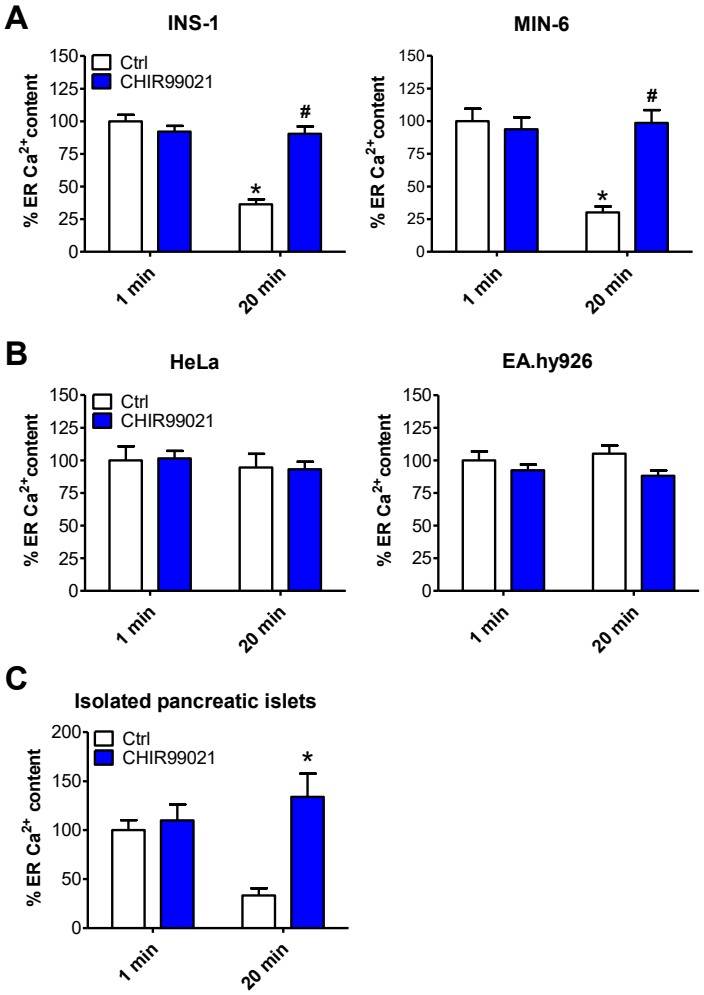

Figure 17 | GSK3β regulates presenilin-1-dependent ER Ca^{2+} leakage in β-cells (II). **(A-C)** Percentage of ER Ca^{2+} content under Ca^{2+}-free conditions. At the indicated time points ER Ca^{2+} stores were depleted using the SERCA inhibitor BHQ (15 µM), together with carbachol (100 µM) for INS-1, MIN-6 cells and isolated murine pancreatic islets or histamine (100 µM) for HeLa and EA.hy926 cells. **(A)** $[Ca^{2+}]_{cyto}$ in INS-1 (*left panel*) and MIN-6 cells (*right panel*) as well as **(B)** in HeLa (*left panel*) and EA.hy926 cells (*right panel*) and **(C)** in isolated murine pancreatic islets under control conditions (white bars) and after treatment with the GSK3β inhibitor CHIR99021 (2.5 µM) for 48 h (blue bars). (n≥6). (1)

The crucial role of the GSK3β-mediated phosphorylation of presenilin-1 in the enhanced ER Ca^{2+} leak in β-cells was further investigated using a presenilin-1

mutant where the two serine residues at position 353 and 357 are replaced by alanines (presenilin-1$^{S353/357A}$), thus, designing a presenilin-1 mutant that does not serve as target for GSK3β. During our standard ER-leakage protocol, expression of presenilin-1$^{S353/357A}$ in β-cells abolished the leak (**Figure 18A**), thus, supporting our concept that GSK3β-mediated phosphorylation of presenilin-1 yields the enhanced ER Ca^{2+} leak in β-cells (1).

To further investigate the regulatory role of GSK3β on presenilin-1, another presenilin-1 mutant was used in which the two serine residues at positions 353 and 357 were replaced by aspartic acids that mimic GSK3β-phosphorylated serines (presenilin-1$^{S353/357D}$). Expression of presenilin-1$^{S353/357D}$ in β-cells enhanced the intrinsic ER Ca^{2+} leak (**Figure 18B**) that was comparable to that observed by overexpression of wild type presenilin-1 (**Figure 13A,B**). This enhancement of the ER Ca^{2+} leak in β-cells expressing presenilin-1$^{S353/357D}$ was not affected by the GSK3β inhibitor CHIR99021 (**Figure 18C**) thus, indicating that the presenilin-1$^{S353/357D}$ mutant establishes an ER Ca^{2+} leak that is independent from GSK3β activity. Strikingly, expression of presenilin-1$^{S353/357D}$, the mutant that mimics GSK3β-phosphorylation on presenilin-1, introduced an enhanced ER Ca^{2+} leak for the first time in non-β-cells (**Figure 19**) (1).

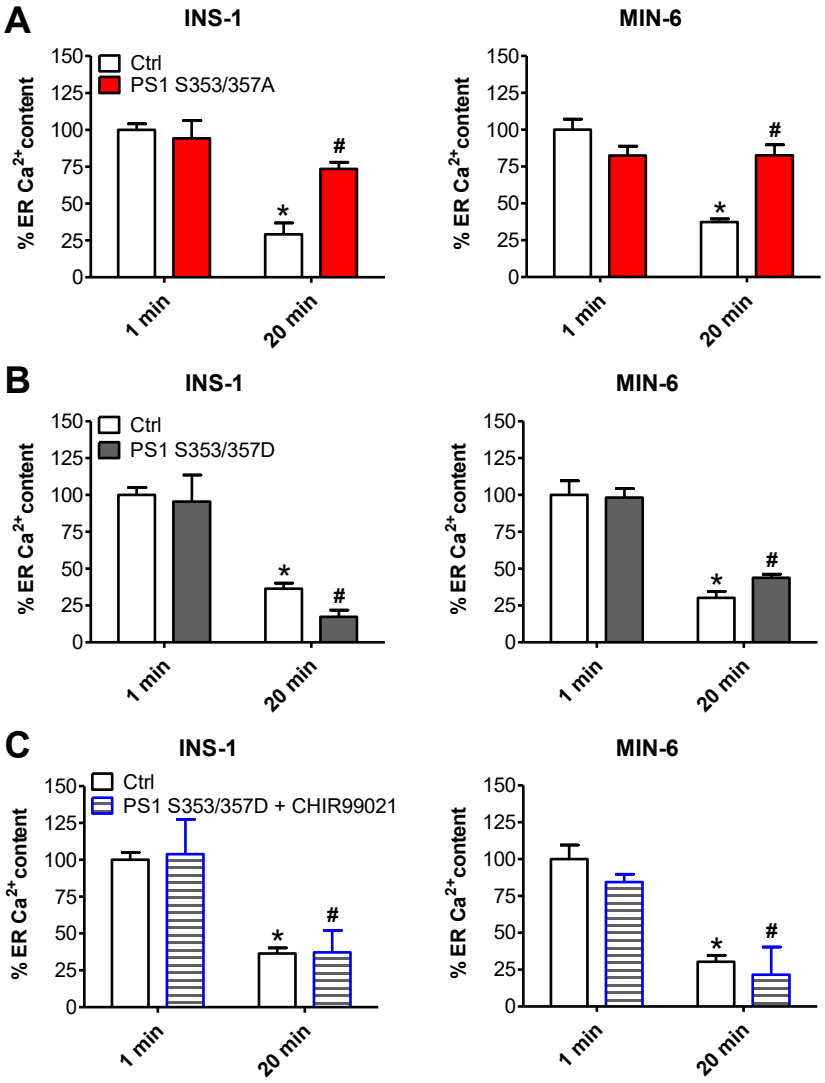

Figure 18 | GSK3β regulates presenilin-1-dependent ER Ca^{2+} leakage in β-cells (III). **(A-C)** Percentage of ER Ca^{2+} content under Ca^{2+}-free conditions. At the indicated time points ER Ca^{2+} stores were depleted using the SERCA inhibitor BHQ (15 μM), together with histamine (100 μM) for HeLa and EA.hy926 cells or carbachol (100 μM) for INS-1 and MIN-6 cells. **(A)** Percentage of ER Ca^{2+} content in INS-1 (*left panel*) and MIN-6 cells (*right panel*) under control conditions (white bars) or after overexpression of presenilin-1 mutated version which cannot be phosphorylated (PS1 S353/357A) (red bars). **(B)** Percentage of ER Ca^{2+} content in INS-1 (*left panel*) and MIN-6 cells (*right panel*) under control conditions (white bars) or after overexpression of a consecutively active presenilin-1 mutated version (PS1 S353/357D) (grey bars). **(C)** Percentage of ER Ca^{2+} content in INS-1 (*left panel*) and MIN-6 cells (right *panel*) under control conditions (white bars) or after a combination of overexpression of PS1 S353/357D and treatment with 2.5 μM of the GSK3β inhibitor CHIR99021 (striped bars). Bars represent mean ± SEM. In each graph the one-minute control value was set 100%. *p<0.05 versus respective one-minute control using one-way ANOVA. (n≥6). (1)

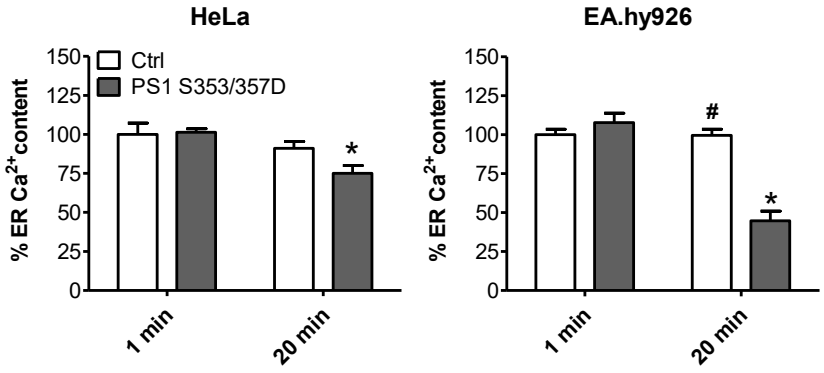

Figure 19 | GSK3β regulates presenilin-1-dependent ER Ca^{2+} leakage in β-cells (IV). Percentage of ER Ca^{2+} content in HeLa (*left panel*) and EA.hy926 cells (*right panel*) under control conditions (white bars) or after overexpression of PS1 S353/357D (grey bars). Bars represent mean ± SEM. In each graph the one-minute control value was set 100%. *p<0.05 versus respective one-minute control using one-way ANOVA. (n≥6). (1)

4.4. Mitochondria serve as Ca^{2+} sink for ER leakage in β-cells

Our data above indicate that basal cytosolic Ca^{2+} in the two β-cell lines does not differ to that found in the two non-β-cell lines, despite a largely enhanced ER Ca^{2+} leak in the β-cells. Because SERCA activity is similar in all cell types, one has to assume that the leaked Ca^{2+} is rapidly moved to a non-cytosolic, SERCA-unserviceable "Ca^{2+} sink". Considering the tight package between the ER and mitochondria in nearly all cells including β-cells (103), it is tempting to speculate that the "Ca^{2+} sink" for the enhanced ER Ca^{2+} leak are mitochondria. To test this hypothesis, mitochondrial Ca^{2+} was prevented by specific siRNA-mediated knock-down of the pore forming unit of the mitochondrial uniporter complex, the mitochondrial Ca^{2+} uniporter (MCU) (104). These experiments showed, that in β-cells that were depleted from MCU and, thus, have a strongly reduced mitochondrial Ca^{2+} uptake activity (53), the cytosolic Ca^{2+} is elevated compared with the two non-β-cell controls (**Figure 20A,B**). Hence, when the ER Ca^{2+} leakage is inhibited by knock-down of presenilin-1 or by reducing the channel activity by treatment with GSK3b inhibitor, there is no increase of basal cytosolic Ca^{2+} in β-cells with MCU knock-down (**Figure 20A,B**). These data support our hypothesis that in β-cells the Ca^{2+} leaking from the ER is instantly sequestered by mitochondria. This assumption is further supported by our findings that removal of extracellular Ca^{2+} results in a small yet significant decrease in mitochondrial Ca^{2+} levels in β-cells (**Figure 21A**) but not the non-β-cell controls (**Figure 21B**). These data suggest that once ER

refilling is not anymore compensated by Ca^{2+} influx, ER Ca^{2+} leak is reduced to a level that is not further sensed by the rather moderate sensitive Ca^{2+} uptake machinery of the mitochondria (105). In line with these findings are the increased mitochondrial and decreased endoplasmic reticulum Ca^{2+} levels in β-cells compared to the non-β-cells under basal conditions (**Figure 22A,B**). These results strongly support our hypothesis (1).

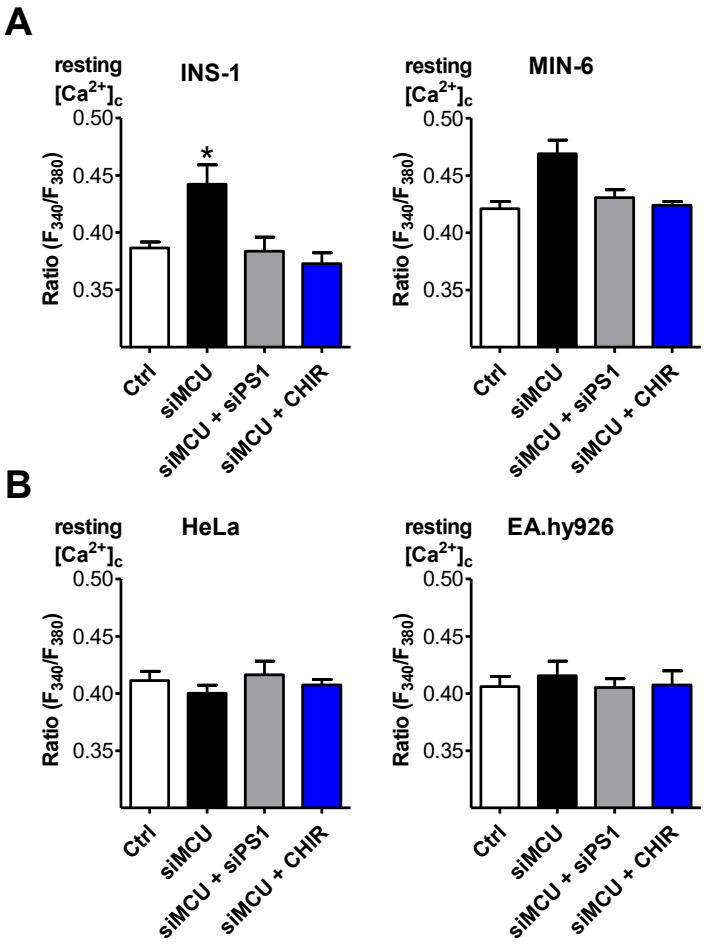

Figure 20 | Mitochondria serve as Ca^{2+} sink for ER leakage in β-cells (I). **(A,B)** Bars represent the basal ratio of $[Ca^{2+}]_{cyto}$ measured with Fura-2/AM under Ca^{2+}-free conditions in INS-1 (*left panel in A*), MIN-6 (*right panel in A*), HeLa (*left panel in B*) and EA.hy926 (*right panel in B*) cells under control conditions (white bars), siRNA against MCU (black bars), a combination of siRNA against MCU and PS1 (grey bars) or a combination of siRNA against MCU and treatment with CHIR99021 (2.5 μM; blue bars). * $p<0.05$ versus control using one-way ANOVA. ($n\geq6$). (1)

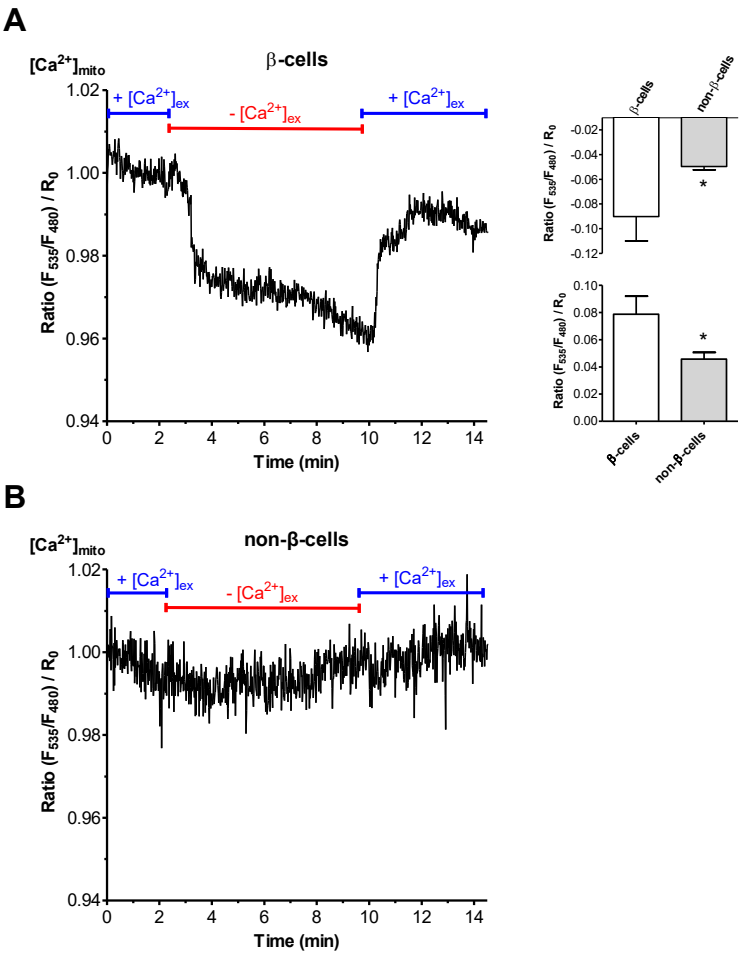

Figure 21 | Mitochondria serve as Ca^{2+} sink for ER leakage in β-cells (II). Normalized $[Ca^{2+}]_{mito}$ ratio signals measured over time in **(A)** INS-1 (representative for β-cells) and **(B)** in HeLa (representative for non-β-cells) in 2 mM Ca^{2+} ($2Ca^{2+}$) containing or Ca^{2+}-free-EGTA buffered experimental solution as indicated in the graph. Absolute drop in mitochondrial Ca^{2+} upon removal of extracellular Ca^{2+} (upper right panel) as well as rise in mitochondrial Ca^{2+} after re-addition of extracellular Ca^{2+} (lower right panel). * $p<0.05$ versus β-cells using the unpaired Student's t-test. ($n\geq6$). (1)

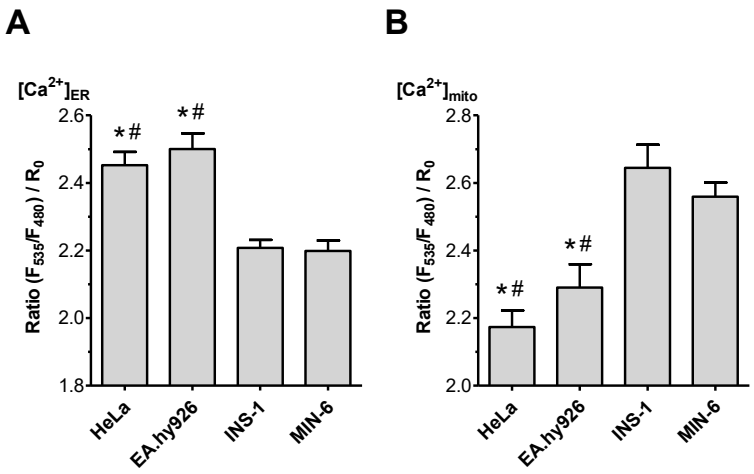

Figure 22 | Mitochondria serve as Ca^{2+} sink for ER leakage in β-cells (III). (A,B) Bar charts show **(A)** basal ER $[Ca^{2+}]$ and **(B)** basal mitochondrial $[Ca^{2+}]$ in HeLa, EA.hy926, INS-1 and MIN-6 cells measured with the genetically encoded probes D1ER and 4mtD3cpv, respectively. *p<0.05 compared to INS-1; # compared to MIN-6, measured with one-way ANOVA. (n≥6). (1)

4.5. ER Ca^{2+} leak fuels increased basal mitochondrial activity

Mitochondrial activity, in particular the dehydrogenases as source of the redox equivalents that serve as substrate for the respiratory chain, are known to be activated by entering Ca^{2+} (106, 107). Considering the continuous Ca^{2+} transit from the leaking ER towards mitochondria in β-cells shown above, we next tested its consequence on mitochondrial basal respiratory activity. Our measurements of basal mitochondrial respiration indeed showed a strongly increased basal and maximal mitochondrial respiration in β-cells compared to the non-β-cells (**Figure 23**) by app. 450±48 and 365±68%, respectively. Manipulating the ER Ca^{2+} leakage by siRNA-mediated knock-down of presenilin-1 resulted in normalized basal and maximal respiration in β-cells (**Figure 24A**) while the depletion of presenilin-1 had no effect on basal and maximal respiration in the non-β-cells (**Figure 24B**), thus indicating the increase ER Ca^{2+} leak being responsible for the enhanced respiratory activity in β-cells (1).

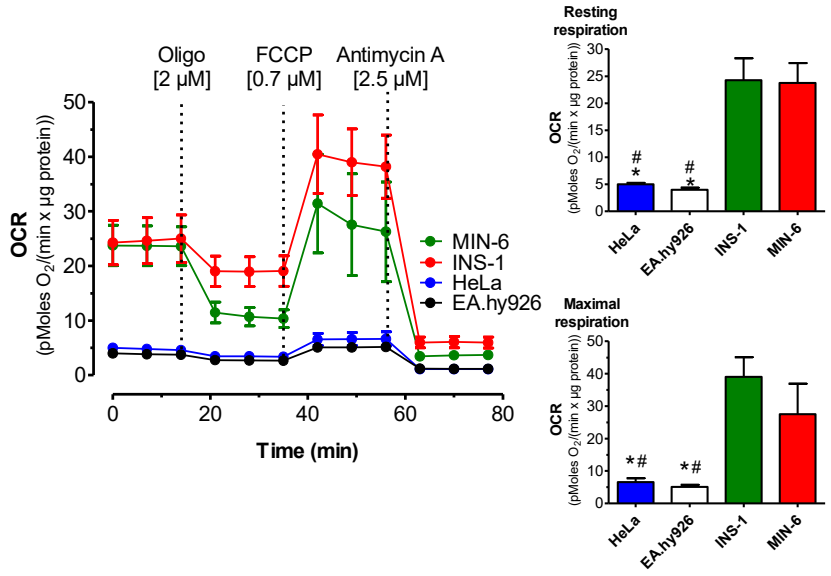

Figure 23 | ER Ca^{2+} leak fuels increased basal mitochondrial activity (I). Comparison of the OCR of β-cells as well as of non-β-cells under control conditions. OCR was normalized to protein content. As indicated, cells were treated with 2 µM oligomycin, 0.7 µM FCCP for INS-1, EA.hy926 and MIN-6 and 0.3 µM for HeLa, and 2.5 µM antimycin A. Data are presented as mean values ± SEM of triplicate repeats (n=6). *p<0.05 versus INS-1, #p<0.05 versus MIN-6, using one-way ANOVA. (1)

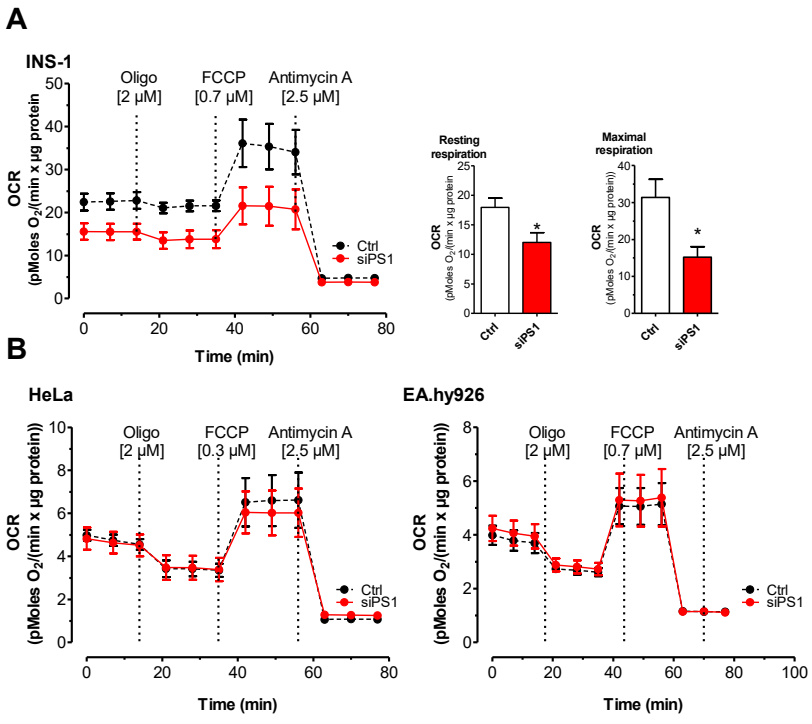

Figure 24 | ER Ca^{2+} leak fuels increased basal mitochondrial activity (II). **(A)** OCR of INS-1 cells under control conditions (black dotted curve) or knock-down of presenilin-1 (red curve), bars represent corresponding basal and maximal respiration (*right panel*), *p<0.05 versus untreated control using the unpaired Student's t-test. **(B)** OCR of HeLa (*left panel*) and EA.hy926 cells (*right panel*) under control conditions (black dotted curve) or knock-

down of presenilin-1 (red curve). OCR was normalized to protein content. As indicated, cells were treated with 2 µM oligomycin, 0.7 µM FCCP for INS-1, EA.hy926 and 0.3 µM for HeLa, and 2.5 µM antimycin A. Data are presented as mean values ± SEM of triplicate repeats (n=6). *p<0.05 versus control using the unpaired Student's t-test. (1)

In line with these experiments, the inhibition of GSK3β-induced phosphorylation of presenilin-1, the process that yields enhanced ER Ca^{2+} leakage, by a pre-treatment with the GSK3β inhibitor CHIR99021 showed a significant decrease in basal and maximal respiration in INS-1 and a significant decreased basal respiration in MIN-6 as well as a strong tendency for a decrease in maximal respiration (**Figure 25A&B**), but no difference could be observed in the non- β-cells (**Figure 25C**). To test whether or not the enhanced mitochondrial respiration that is due to the increased ER Ca^{2+} leak in β-cells is coupled to an enhanced basal ATP production in the organelle, basal mitochondrial ATP levels were measured using the genetically encoded and mitochondrial-targeted ATP sensor, mtAT1.03. In comparison with the non-β-cells, β-cells have been found to have significant elevated mitochondrial ATP levels (**Figure 26A**), while in presenilin-1 depleted or with GSK3β inhibitor CHIR99021 pre-treated β-cells, a reduction of mitochondrial ATP levels compared to basal conditions could be observed **(Figure 26B)**, whereas in non-β-cells no decrease of $[ATP]_{mito}$ levels was detected after knock-down of presenilin-1 or pre-treatment with CHIR99021 (**Figure 26C**). These data indicate that the enhanced ER Ca^{2+} yields an enhanced mitochondrial respiratory activity that is coupled by an increased organelle ATP production/levels in β-cells under basal conditions (1).

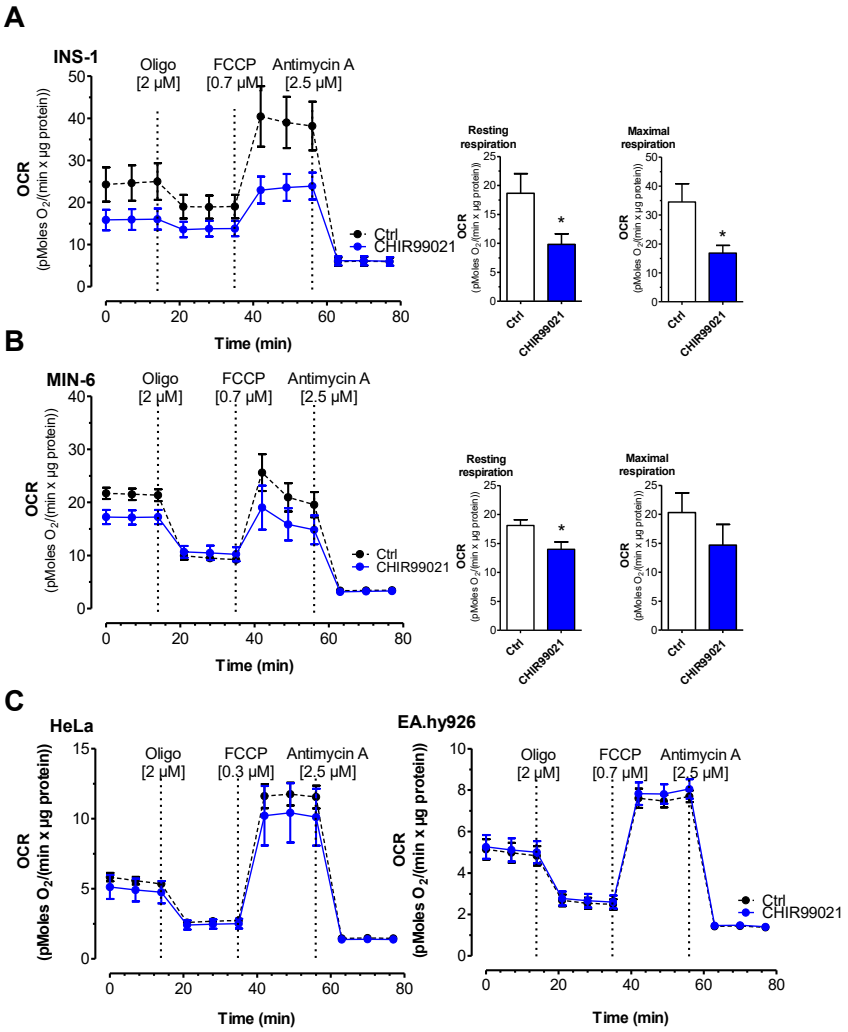

Figure 25 | ER Ca^{2+} fuels increased basal mitochondrial activity (III). OCR of **(A)** INS-1 (*left panel*) and **(B)** MIN-6 *(left panel)* under control conditions (black dotted curve) and after treatment with 2.5 µM of the GSK3β inhibitor CHIR99021 (blue curve). Corresponding bars (*right panels*) represent basal and maximal respiration values. **(C)** OCR of HeLa (*left panel*) and EA.hy926 (*right panel*) under control conditions (black dotted curve) or after treatment with 2.5 µM of the GSK3β inhibitor CHIR99021 (blue curve). **(A-C)** OCR was normalized to protein content. As indicated, cells were treated with 2 µM oligomycin, 0.7 µM FCCP for INS-1, EA.hy926 and MIN-6 and 0.3 µM for HeLa, and 2.5 µM antimycin A. Data represent mean values ± SEM of triplicate repeats (n=6). *p<0.05 versus control using the unpaired Student's t-test. (1)

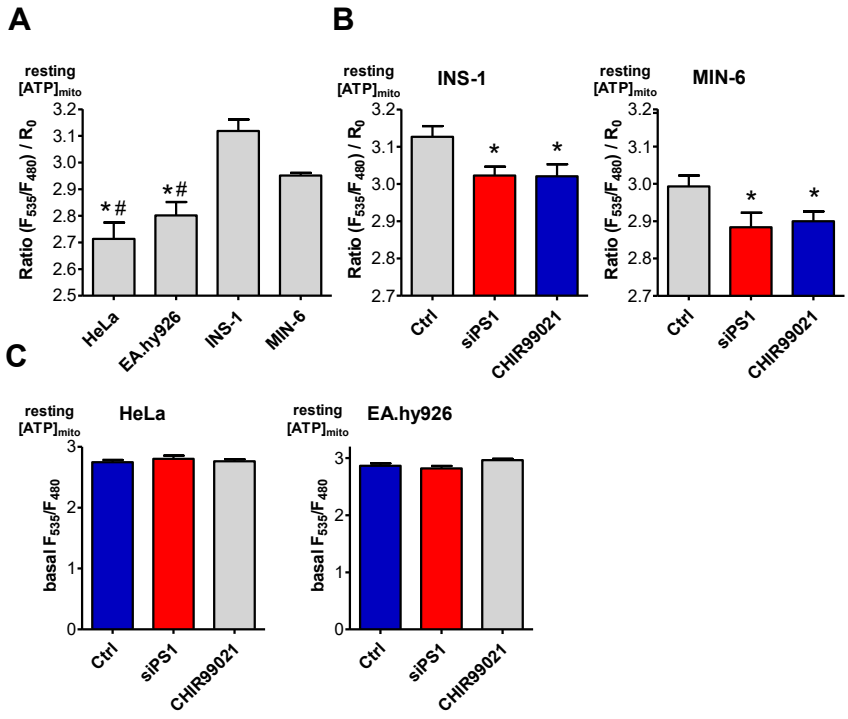

Figure 26 | ER Ca^{2+} leak fuels increased basal mitochondrial activity (IV). **(A)** Bars represent basal $[ATP]_{mito}$ ratio measured with mtAT1.03 in HeLa, EA.hy926, INS-1 and MIN-6 cells under control conditions. **(B,C)** Bars represent basal $[ATP]_{mito}$ ratio measured with mtAT1.03 in **(B)** β-cells and **(C)** non-β-cells under control conditions (grey bars), after knock-down of presenilin-1 with specific siRNAs (red bars) or after treatment with 2.5 µM of the GSK3β inhibitor CHIR99021 (blue bars). *p<0.05 HeLa vs INS-1 and MIN-6, #p<0.05 EA.hy926 vs INS-1 and MIN-6 tested with one way ANOVA. (n≥6). (1)

4.6. ER Ca^{2+} leak is essential for the responsiveness of β-cells

We hypothesize that the observed enhanced basal ER Ca^{2+} release is an important phenomenon that ensures proper responsiveness of β-cells to elevated D-glucose. In particular, the enhanced basal ER Ca^{2+} release might facilitate D-glucose metabolism by Ca^{2+} activated dehydrogenases in the mitochondria and, in turn, accelerate subsequent ATP production for the initiation of K_{ATP} channel inhibition and cytosolic Ca^{2+} spiking as initial steps of insulin secretion. To challenge this hypothesis, β-cells were exposed to elevated D-glucose that yielded initiation of cytosolic Ca^{2+} spiking, thus indicating, that both β-cell lines used in this study were able to exhibit a physiological response to elevated D-glucose (**Figure 27A**). To test the physiological meaning of elevated ER Ca^{2+} leak in β-cells, the elevated ER Ca^{2+} leak was prevented by siRNA-mediated depletion of presenilin-1 or pre-treatment with the GSK3β inhibitor CHIR99021. Importantly, the responsiveness of β-cells with

artificially tightened ER to elevated D-glucose was largely reduced in both β-cell lines used (**Figure 27B,C**). Knock-down of presenilin-1 as well as reduction of its activity by treating the cells with the GSK3β inhibitor CHIR99021 resulted in a delayed onset of oscillations (**Figure 28A**), less amplitutes of the oscillations (**Figure 28B**) as well as to less oscillations over the time period measured (**Figure 28C**). These data indicate, that the enhanced ER Ca^{2+} leak in β-cells is a prerequisite for the cells to ensure fast response to elevated D-glucose.

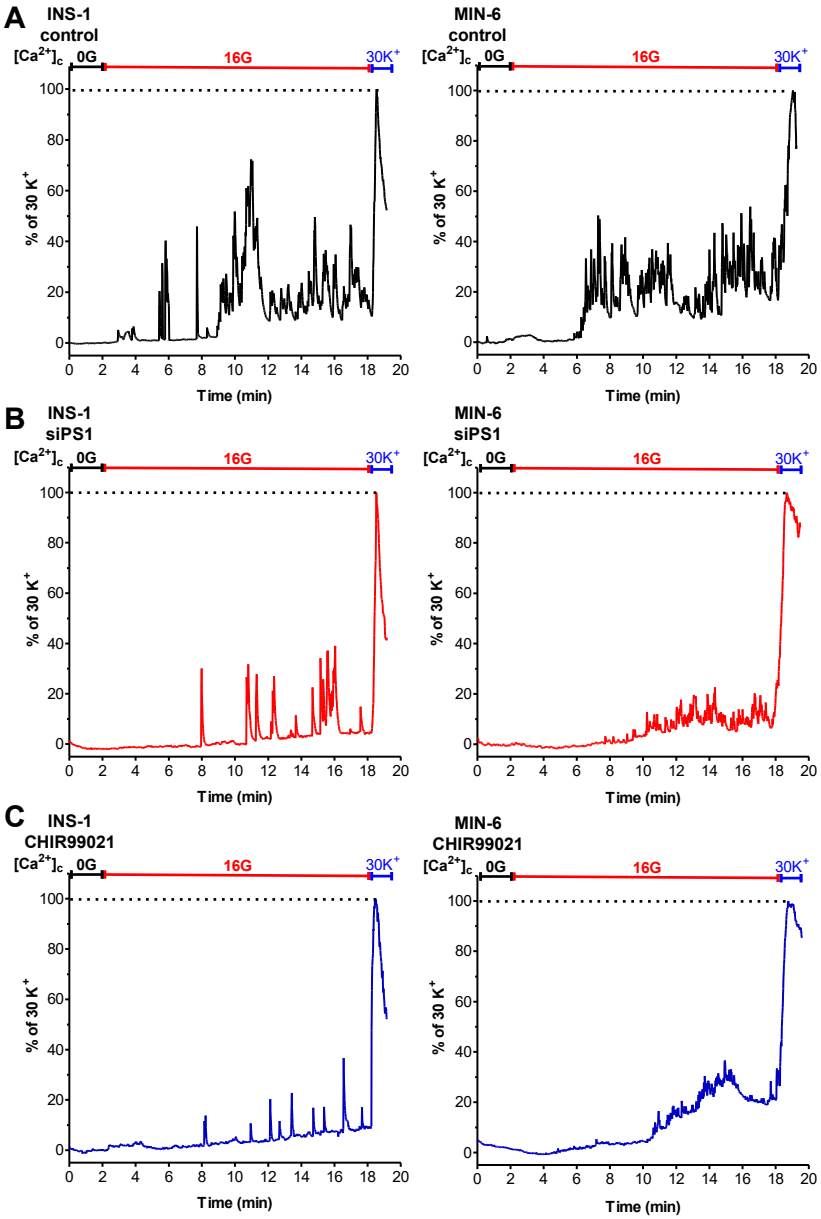

Figure 27 | ER Ca^{2+} leak is essential for the responsiveness of β-cells (I). **(A-C)** Representative curves showing D-glucose induced cytosolic Ca^{2+} oscillations in INS-1 (left panels) and MIN-6 (right panels) either under control conditions **(A)**, after knock-down of presenilin-1 with specific siRNAs **(B)** or after treatment with GSK3β inhibitor CHIR99021 (2.5 μM) **(C).** Cells were loaded with Fura-2/AM in EHL buffer for 40 min, followed by a 20 min

incubation in D-glucose-free buffer (0G) before imaging. On the microscope, cells were perfused with 0G buffer for 2 minutes before switching to 16 mM D-glucose during acquisition, followed by depolarization with 30 mM K^+ to evaluate the maximum Ca^{2+} signal.

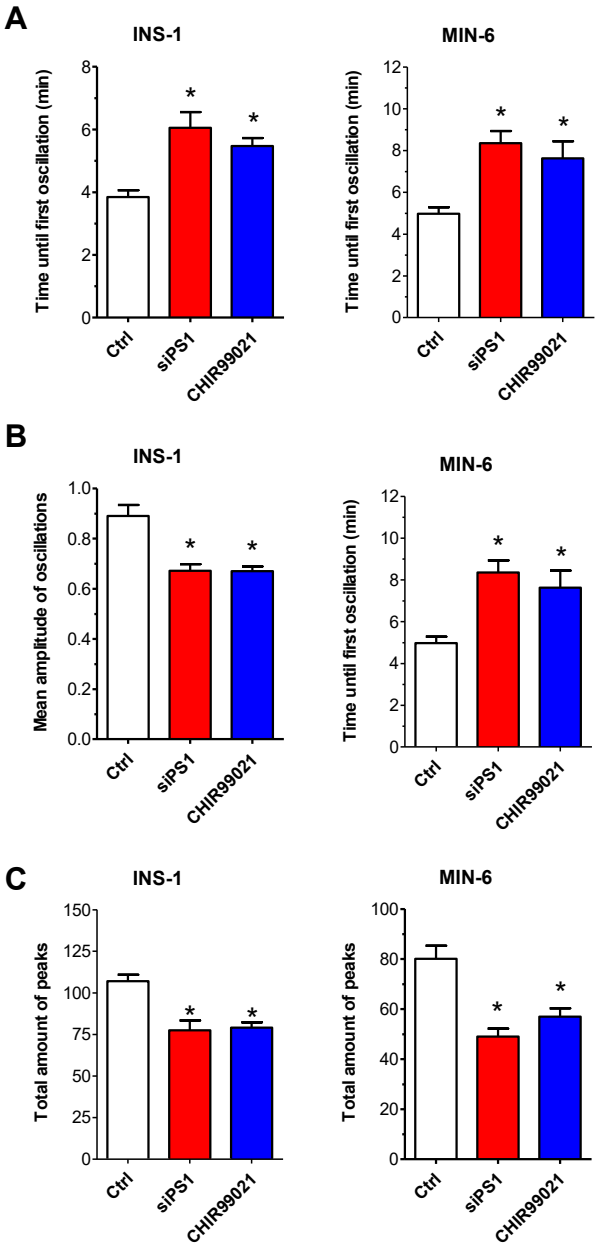

Figure 28 | ER Ca^{2+} leak is essential for the responsiveness of β-cells (II). Corresponding statistical analysis to Figure 27 showing **(A)** the time of oscillation onset, **(B)** the mean amplitude of oscillations and (C) the total amount of oscillations under control conditions (white bars), after knock-down of presenilin-1 (red bars) or after treatment with GSK3β inhibitor CHIR99021 (2.5 µM) (blue bars). *p<0.05 versus control using one-way ANOVA. (n≥6).

4.7. ER Ca^{2+} leak is essential for metabolic TCA cycle in β-cells

Based on our findings that the observed functional coupling between enhanced ER Ca^{2+} leak and mitochondrial Ca^{2+} sequestration under resting conditions establishes a metabolic mitochondrial pre-activation under resting conditions, we hypothesize that the enhanced resting levels of mitochondrial Ca^{2+} pre-stimulate matrix dehydrogenases, thus, these Ca^{2+}-dependent enzymes are capable to convert their substrate sufficiently and independently

from any further Ca^{2+} signal. This concept was tested by comparative NMR-based metabolomics of wild-type vs. presenilin-1-depleted β-cells under resting conditions and upon exposure to elevated D-glucose. Under resting conditions siRNA-mediated depletion of preseninlin-1 yielded accumulation of lactate (**Figure 29B**) while resting levels of citrate (**Figure 29A**) and glutamate (**Figure 29C**) remain rather unchanged. These data point to a reduced citrate cycle activity already under resting conditions (i.e. 3 mM D-glucose).

Within the initial phase of the exposure to high D-glucose (i.e. 4 and 6 min), lactate levels got normalized (**Figure 29B**) due to a transient lactate accumulation in the wild-type cell while glutamate and citrate levels start to decrease (**Figure 29A,C**), reflecting a lack of citrate cycle activity. Hence, cellular L-glutamate levels rapidly decrease (**Figure 29C**), thus, indicating that in presenilin-1 depleted cells citric cycle activity is limited, thus yielding accumulation of end products of the glycolysis and the utilization of L-glutamate to compensate the reduced isocitrate-derived α-ketoglutaric acid formation. After the initial phase of 6 min, the relative lactate levels increase again but started to normalize (**Figure 29B**). Hence, levels of glutamate and citrate started to get normalized as well, thus, indicating that in this phase citrate cycle might get activated even in presenilin-1 depleted cells.

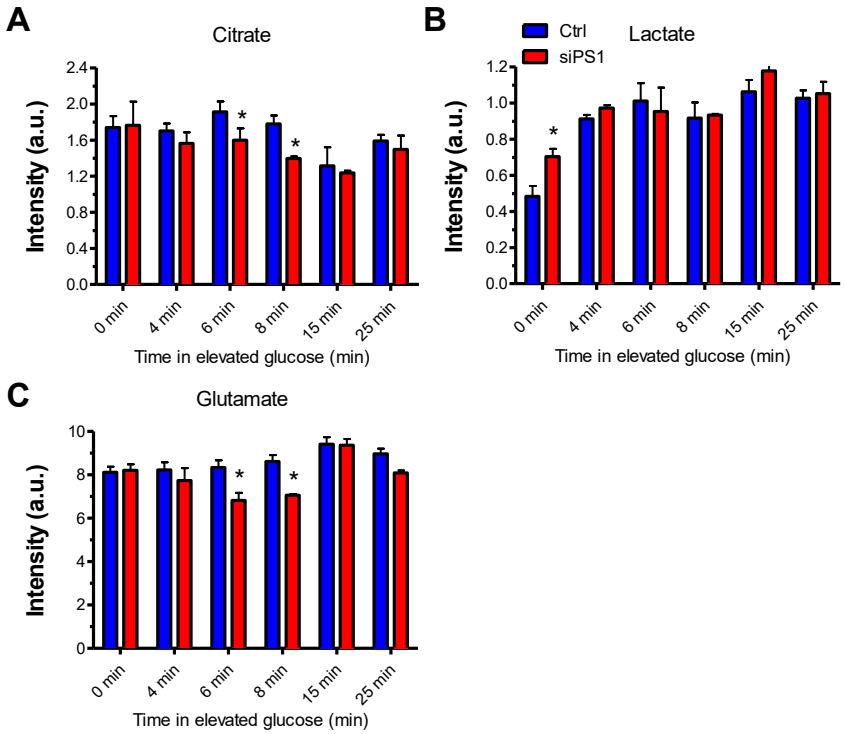

Figure 29 | ER Ca^{2+} leak is essential for metabolic TCA cycle in β-cells. (A-C) Metabolite levels of INS-1 cells represented as binary logarithm of fold changes comparing control condition versus knock-down of presenilin-1 from citrate **(A)**, lactate **(B)** and glutamate **(C)** at distinct time points determined by ^{1}H NMR spectroscopy as

indicated in the graphs. Bars represent mean ± SEM calculated using error propagation. Metabolite differences were determined using a spectral intensity matrix normalized to total metabolite content. (n=6).

4.8. ER Ca^{2+} leak is essentially needed for a physiologic biphasic insulin secretion upon D-glucose stimulus

The above observed increased ER Ca^{2+} leak from β-beta cells seems to be physiologically of crucial importance, since a fast and precise insulin secretion is a major factor to assure balanced blood glucose levels (108). Several studies show a delayed β-cell response/insulin secretion upon glucose stimulus as early irregularity in type 2 diabetes, where the first phase of the normally biphasic insulin response (109) is lost and, thus, leading to a later onset of insulin production (110-113). To elucidate if manipulation of ER Ca^{2+} leak is also in vitro influencing insulin secretion we used an enzyme-linked immunosorbent assay specifically designed to assess insulin secretion rates of rat cells. Therefore, we performed a knock-down of presenilin-1 in INS-1 cells or treated isolated pancreatic islets with GSK3β-inhibitor and monitored the insulin secretion rate compared to control cells after stimulating the cells with experimental buffer containing 16 mM D-glucose. The results prove the importance of the ER Ca^{2+} leak, since manipulating the expression level or the activity of presenilin-1 abolished the first phase of insulin secretion in INS-1 cells as well as pancreatic islets (**Figure 30A,B**), but the total cellular insulin content was comparable between the conditions.

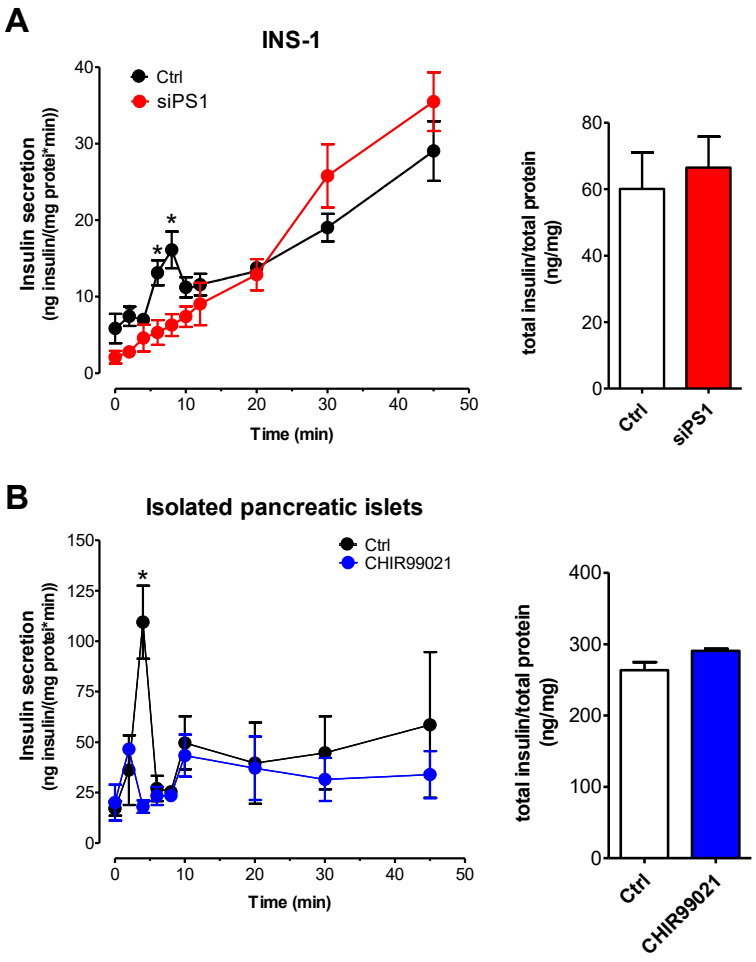

Figure 30 | ER leak is essential for a physiologic insulin secretion. Insulin secretion rate of **(A)** INS-1 cells or **(B)** isolated murine pancreatic islets was measured via insulin-specific enzyme-linked immunosorbent assay under control conditions (black curve) or after knock-down of presenilin-1 with specific siRNAs (red curve) in INS-1 cells or under control conditions (black curve) or after treatment with CHIR99021 (blue curve) in isolated islets. To equilibrate the insulin secretion, cells were kept on HBSS buffer containing 3 mM D-glucose for 30 minutes. Afterwards medium was changed to HBSS buffer containing 16 mM D-glucose and medium was sampled at the indicated time points. Bars in the insert represent the total insulin content of the cells normalized to total protein content under control conditions (white bars), after knock-down of presenilin-1 with specific siRNAs (red bars) or treatment with GSK3β-inhibitor CHIR99021 (blue bars). *p<0.05 versus control using the unpaired Student's t-test, (n≥5).

5. Discussion

5.1. Summary

In this work a novel and fundamental molecular mechanism is presented how glucose-stimulated-insulin-secretion (GSIS) in β-cells is solely dependent on extracellular glucose levels. A physiologic pre-stimulation of Ca^{2+}-dependent dehydrogenases in the mitochondrial matrix is boosting citric acid cycle activity assuring an optimal mitochondrial ATP formation which is essentially needed for properly triggering GSIS. The first and maybe most central finding of this work was the discovery of an enhanced ER Ca^{2+} leak in clonal β-cells under resting conditions. This leak seems to be specific for this cell type since it could not be detected in the used control cell lines. This ER Ca^{2+} leak is conducted by presenilin-1 and controlled by GSK3β-mediated phosphorylation of two specific serine residues of this protein, namely at position S353 and S357. We could also demonstrate that this leak is independent of IP_3-receptors and is fuelled via the plasma membrane located TRPC3 channel, ensuring a balanced Ca^{2+} content despite the enormous leak-mediated ER Ca^{2+} loss. The leaking Ca^{2+} is directly sequestered by the closely located mitochondria, leading to increased basal mitochondrial matrix Ca^{2+} levels which pre-stimulate dehydrogenases of the citric acid cycle in a substrate independent manner. This metabolic pre-stimulation leads to an increased ATP synthesis in β-cells. Moreover, we could show that β-cell responsiveness, measured as D-glucose induced cytosolic Ca^{2+} oscillations, as well as a proper insulin secretion upon glucose stimulus are essentially regulated by this ER Ca^{2+} leak. In summary, the results presented in this work strongly indicate, that the increased ER Ca^{2+} leak in β-cells is of crucial physiological importance. Therefore, the physiologic consequences of the ER Ca^{2+} leak will be discussed in the next section.

5.2. Physiologic importance of an increased ER Ca^{2+} leak in pancreatic β-cells

There are three main determinants for mitochondrial activity i.e. *i.* metabolic substrates (pyruvate, malate and acylcarnitine), *ii.* electron carriers ($NADH+H^+$, $FADH_2$) and *iii.* matrix Ca^{2+}. The basis for GSIS is an accelerated mitochondrial metabolism triggered by glycolysis-derived signals (114). These signals are

boosting citric acid cycle activity leading to increased mitochondrial ATP production. The augmentation of ATP levels results in an inhibition of ATP-sensitive K^+-channels causing depolarization of the plasma membrane and a consequent Ca^{2+} influx via L-type Ca^{2+} channels is initiated. This cascade is finally triggering the exocytosis of insulin containing granules (115, 116). Three of the citric acid cycle dehydrogenases are Ca^{2+} sensitive i.e. pyruvate dehydrogenase, NAD-isocitrate dehydrogenase, oxoglutarate dehydrogenase (117). Thus, increasing mitochondrial Ca^{2+} stimulates DH activity and serves a key factor for insulin release in pancreatic β-cells.

This aspect offers some contradiction in the current concept, as it is not known at which point during GSIS mitochondrial Ca^{2+} is involved. In fact, in the current concept, the mitochondrial Ca^{2+} increase occurs upon Ca^{2+} entry due to opening of the L-type Ca^{2+} channels, thus, already downstream of the mitochondrial activation by glycolysis-derived pyruvate and ATP production. However, increases in mitochondrial Ca^{2+} are thought to be essential to stimulate Ca^{2+} dependent dehydrogenases of the citric cycle in order to establish suitable enzyme activity to handle the substrate overflow upon elevated blood D-glucose (118). In particular, the responsiveness and proper D-glucose sensing of β-cells to elevated blood D-glucose is determined by the cells pace to produce ATP when exposed to elevated glucose (119). Therefore, we hypothesized that a pre-stimulation of β-cell mitochondrial dehydrogenases, which ultimately are responsible for the necessary ATP production via oxidative phosphorylation, would be of metabolic advantage ensuring a fast and precise insulin response solely controlled by D-glucose. Hence, we speculate that the increased ER Ca^{2+} leak from β-beta cells is of crucial physiological importance to assure a fast and precise insulin secretion is a major factor to assure balanced blood glucose levels (108).

Our data that show a strongly enhanced basal respiratory activity and elevated mitochondrial ATP levels in mitochondria of both clonal β-cell lines in comparison to the non-β-cell lines point to such pre-stimulation of mitochondria in β-cells. These data are in line with the new perspective of GSIS that involves a continuous priming of β-cells based on a weak stimulation of β-cell mitochondria to ensure proper responsiveness to elevated blood D-glucose sensing (120). Our data presented herein provide evidence that besides extracellular stimuli, β-cells have an intrinsic mechanism of mitochondrial pre-stimulation even under resting conditions that builds on an enhanced ER Ca^{2+} leak. This assumption is supported by our

findings that inhibition of ER Ca^{2+} leak by diminution of presenilin-1 or an inhibition of GSK3β abolished the enhanced respiratory activity and elevated basal mitochondrial ATP levels in the clonal β-cells while no effect was found in the non-β-cell lines. These findings and our data that GSK3β is crucially involved in the installation of the ER Ca^{2+} leak that yields pre-activation of mitochondria in the β-cells is in line with the current concept that plasma levels of D-glucose, other nutrients, hormones and/or neural stimulation weakly pre-activate mitochondria even at fasting (120) and may identify GSK3β as target of these priming factors.

The ER Ca^{2+} leak-induced elevation of mitochondrial matrix Ca^{2+} yields basal pre-stimulation of mitochondrial metabolism is further shown by the metabolomics analysis that revealed a considerable reduced basal citric acid activity in β-cells depleted from presenilin-1 (**Figure 29A-C**). Upon exposure to elevated D-glucose β-cells with diminuend presenilin-1 expression rapidly show decreased citrate levels in comparison to the wild-type β-cells, thus, indicating that β-cells that do not have the enhanced ER Ca^{2+} leak are less capable to channel upregulated glycolysis into the citric cycle. Hence, after initial phase, β-cells that lack presenilin-1 further accumulate lactate while citrate levels remain low in comparison with wild-type β-cells (**Figure 29A-C**). Interestingly, β-cell that lack presenilin-1 started to consume L-glutamate, pointing to the utilization of an alternate source for fueling the citric acid if resting mitochondrial Ca^{2+} levels are not intrinsically elevated due to the missing presenilin-1. Because presenilin-1 deleted β-cells metabolize L-glutamate we speculate that the rather low resting mitochondrial Ca^{2+} level that is due to the lack of enhanced ER Ca^{2+} leak is insufficient for activation of isocitrate dehydrogenase. Consequently, the suboptimal activity of isocitrate dehydrogenase, α-ketoglutaric acid formation by this enzyme is attenuated and citrate, acetate and pyruvate are accumulated. Hence our data indicate that the lack of α-ketoglutaric acid is compensated by L-glutamate that keeps citric acid cycle and mitochondrial respiration active. In line with this assumption, from all Ca^{2+}-activated matrix dehydrogenases isocitrate dehydrogenase was found to require the highest matrix Ca^{2+} levels (i.e. 5-50 µM) for stimulation (117). Moreover, our data indicate that besides isocitrate dehydrogenase, other Ca^{2+} activated matrix dehydrogenases might be already activated at reduced mitochondrial Ca^{2+} levels. Accordingly, the enhanced resting levels of mitochondrial Ca^{2+} appears prerequisite to pre-stimulate

isocitrate dehydrogenase, thus, these Ca^{2+}-dependent enzyme is capable to sufficiently convert isocitrate to α-ketoglutaric acid even under resting conditions. Remarkably, by elevating resting matrix Ca^{2+} the activity of citrate cycle activity in β-cells is exclusively linked to glycolysis-derived metabolites without a requirement of a stimulus that increases mitochondrial Ca^{2+} for stimulation of isocitrate dehydrogenase. Therefore, we speculate that presenilin-1dependent ER Ca^{2+} leak is of crucial importance to establish D-glucose sensing in β-cells that is solely controlled by D-glucose but independent from an elevation of mitochondrial Ca^{2+} to activate matrix dehydrogenases. According to this hypothesis, the prevention of enhanced ER Ca^{2+} leak will reduce the activity of the Ca^{2}-dependent matrix dehydrogenases of the citric cycle, thus, yielding to accumulation of end products of the glycolysis while β-cell responsiveness to elevated D-glucose is strongly reduced.

The crucial importance of GSK3β/presenilin-1/ER Ca^{2+} leak-induced mitochondrial pre-stimulation for β-cell responsiveness to elevated D-glucose is demonstrated in our experiments that revealed a much slower and weaker response in cytosolic Ca^{2+} spiking as final trigger for insulin release in presenilin-1 depleted β-cells under conditions of elevated D-glucose. Because the inhibition of GSK3β had similar effects than presenilin-1 knock-down on high D-glucose-induced cytosolic Ca^{2+} spiking, one might speculate that besides its overall importance in D-glucose metabolism (121) this enzyme exhibits a β-cell-unique function in establishing presenilin-1-dependent ER Ca^{2+} leak.

The importance of presenilin-1 established ER Ca^{2+} for the responsiveness of β-cells to elevated D-glucose is further illustrated by our experiments measuring GSIS, as the ultimate readout for β-cell function. In particular our data reveal that presenilin-1-induced ER Ca^{2+} leak is a prerequisite for the initial insulin release within 10 min of GSIS, while no difference was found after 12 min, thus, pointing to a delayed β-cell response to elevated D-glucose yielding disappearance of the initial spike in insulin secretion normally found in β-cells (109). Notably, several studies show a delayed β-cell response/insulin secretion upon glucose stimulus as early irregularity in type 2 diabetes, where the first phase of the normally biphasic insulin response (109) is lost and, thus, leading to a later onset of insulin production (110-113). The loss of this first phase of insulin response is also known to worsening post-prandial hyperglycemia yielding a progression of the pathologic condition and

ultimately resulting in a clinical relevant hyperglycemia (122). Therefore, the lack of the initial phase of insulin secretion serves as predictive marker for the risk of developing diabetes (123, 124), again highlighting its importance. Our data showing that a decreased ER Ca^{2+} leak ultimately results in reduced mitochondrial metabolism as well as reduced D-glucose induced cytosolic Ca^{2+} oscillations, demonstrate the molecular basis for the loss of first phase insulin response. In line with our findings, recent studies describe the relevance of a functional ER-mitochondrial Ca^{2+} transfer be crucially for an adequate insulin release (103, 125). Accordingly, we hypothesize that disturbances in the presenilin-1 dependent ER Ca^{2+} leak in β-cells hamper the cell's fast and precise first insulin response possibly contributing to development of type 2 diabetes.

More precisely, an imbalanced Ca^{2+} homeostasis by a deranged presenilin-1 leak function could be the trailblazer towards diabetes development. Recent studies support the relevance of a balanced Ca^{2+} homeostasis by showing that ER-mitochondrial membrane integrity and efficient Ca^{2+} transfer between these two organelles to be crucially contributing to an adequate insulin metabolism (103, 125).

5.3. Presenilin-1, the link between diabetes and Alzheimer disease?

There is another devastating disease in which presenilin-1 as well as Ca^{2+} are known to be involved i.e. Alzheimer's disease (AD). Interestingly, there is a profound correlation between type 2 diabetes and AD and type 2 diabetes may lead to cognitive impairment (126, 127). Until recently the amyloid theory was the most supported theory of AD development explaining that β-amyloid plaque formation causes apoptosis induction of neuronal cells (128-130). Supportingly, increased Aβ42/Aβ40 ratios are reported to be an early event in AD development (131). In this respect, presenilin-1 deficiency is shown to lead to a fivefold drop in Aβ production (88). Hence, presenilin-1 together with PEN-2, APH1 and nicastrin forms the γ-secretase complex (86, 87) and since plaque formation is considered as hallmark of AD, γ-secretase function is implicated to AD pathogenesis (85).

Recently the amyloid theory as sole mechanisms causing AD got challenged (85, 132, 133). Because presenilin-1 is necessary for Aβ production one would expect AD associated mutations in presenilin-1 to gain the protein's function (88). However, most mutations decrease activity *in vitro* and in cells (134-138) and also enzymatic

inhibition fails to reduce symptoms in AD patients (139). Moreover, there is obviously only a moderate correlation between occurrence of plaques and plaque count with emergence and severity of AD and are also found in healthy individuals (140, 141) and presenilin-1 mutations are also found in front temporal dementia (FTD) that comes with similar functional defects while no plaque formation occurs (142-144). Accordingly, all these findings fuel the assumption that protease activity of γ-secretase may not anymore considered as the only causative factor of AD. One alternative/additional hypothesis states that neuronal dysfunction being the basis of chronic brain disorders is triggered by persistent disruption of intracellular Ca^{2+} signaling. Mutations in the presenilin-1 gene are the most common cause of familial Alzheimer's disease (FAD) (145). According to the "*Alzheimer Disease & Frontotemporal Dementia Mutation Database*" there are approximately 219 presenilin-1 mutations related to AD pathology (146). Notably, all so far tested presenilin-1 mutations also influence in some aspect of cellular Ca^{2+} handling (90, 91, 147) (**Table 2**).

Table 2 | Localization and effects of certain presenilin-1 mutations

Mutation	Localization	[1]Known influence on Ca^{2+}	[3]Possible GSK3β target	[2]Known link to AD	Selected literature
S353A	c	√	√	-	[1] current work
S357A	c	√	√	-	[1] current work
S169P	TMIII	-	√	√	[2]Ezquerra 1999, [2]Lleo 2002
S169L	TMIII	-	√	√	[2]Taddei 19998, [2]Takao 2001, [2]Miravalle 2002
S397	TMVII	-	√	-	
A79V	c	X	X	√	[1]Nelson 2007, [2]Cruts 1998, [2]Rogaeva 2001, [2]Wallon 2012
H163R	c	√	X	√	[1]Chui 1999, [2]Campion 1995, [2]Sherrington 1995
L166P	c	√	X	√	[1]Nelson 2007, [2]Moehlmann 2002
E273A	c	√	X	√	[1]Nelson 2007, [2]Kamimura 1998
E280A	c	√	X	√	[1]Sepulveda-Falla 2014, [2]Lendon 1997, [2]Clark 1995
L286V	c	√	X	√	[1]Chui 1999, [1]Guo1996, [1]Furukawa 1998, [2]Sherrington 1995, [2]Ikeuchi 2008, [2]Wallon 2012
M146V	TMII	√	X	√	[1]Nelson 2007, [1]Zhang 2010, [1]Leissring 1999, [1]Begley 1999, [1]Guo1999,[1]Ryazantseva 2013, [2]Clark 1995, [2]Cervenakova 1996, [2]Rogaeva 2001
G206D	TMIV	√	X	√	[1]Chen 2015, [2]Raux 2005, [2]Dobricic 2012
A246E	TMVI	√	X	√	[1]Nelson 2007, [1]Parent 1999, [2]Sherrington 1995, [2]Kowalska 2003, [2]Gliebus 2009
G384A	TMVII	√	X	√	[1]Nelson 2007, [2]Cruts 1995, [2]Tanahashi 1996, [2]Kamumura 1998
P436Q	TMIX	√	X	√	[1]Nelson 2007, [2]Taddei 1998, [2]Houlden 2000, [2]Beck 2004

c, cytoplasmic; TM, transmembrane; -, association not documented so far; √, documented association; x, association excluded. [1]Documented influence of given mutation on Ca^{2+} homeostasis; [2]documented association with AD; [3]predicted target amino acid for GSK3β phosphorylation (GPS webserver used for kinase specific phosphorylation prediction).

Thus, it is tempting to speculate that depending on the mutation(s) present, one or both of presenilin-1 function(s) (i.e. γ-secretase activity and Ca^{2+} handling) are hampered (e.g. ΔE9 affects γ-secretase function, M146V disturbs ER Ca^{2+} handling, L166P affects both (148)). Accordingly, deranged Ca^{2+} homeostasis and β-amyloid toxicity due to mutations of presenilin-1 might act as interdependent causative factors for developing AD. Importantly, the known crucial involvement of presenilin-1 in physiological amyloid degradation (149) and its essential function for β-cells responsiveness presented herein (**Figure 31**), might explain the high incidence of diabetes type 2 in AD patients.

Concluding the above written – changes in cellular Ca^{2+} homeostasis due to alterations in presenilin-1 function could be the missing link for the causative factors of diabetes and Alzheimer's disease development and could shed some light into the correlation of these two diseases. The exact regulation as well as additional mechanisms still need to be further elucidated but this work might be trailblazing for future investigations.

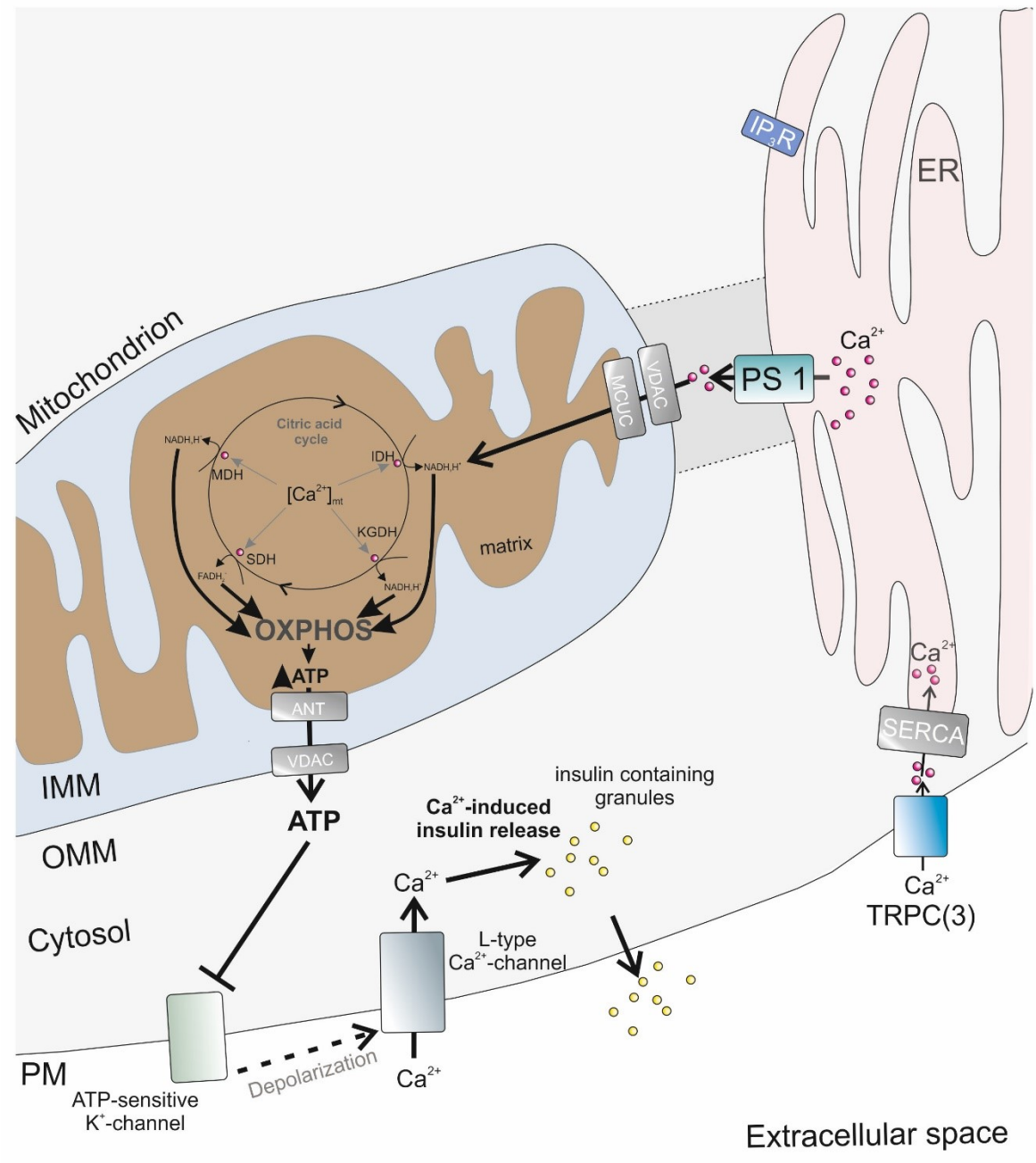

Figure 31 | Graphical summary of presenilin-1-mediated ER Ca^{2+} leak. Schematic representation of our hypothesis of the consequences of presenilin-1 mediated ER Ca^{2+} leak on beta-cell response to glucose stimulus. The presenilin-1 conducted ER Ca^{2+} leak is directly sequestered to mitochondria, leading to increased basal matrix Ca^{2+} levels, where it (substrate-independent) pre-stimulates the Ca^{2+}-dependent dehydrogenases of the citric acid cycle, augmenting resting organelle ATP levels. ATP-sensitive K+-channels are inhibited leading to a depolarization of the cell triggering Ca^{2+} uptake via L-type Ca^{2+} channels. The resulting Ca^{2+}-induced Ca^{2+} release promotes insulin secretion into the extracellular space.

6. REFERENCES

1. Klec C M-SC, Stryeck S, Sachdev V, Duta-Mare M, Gottschalk B, Depaoli MR, Rost R, Hay J, Waldeck-Weiermair M, Kratky D, Madl T, Malli R, Graier WF. Glycogen synthase kinase 3 beta controls presenilin-1-mediated endoplasmic reticulum Ca2+ leak directed to mitochondria in pancreatic islets and beta-cells. Cellular Physiology and Biochemistry. 2018.
2. Ernster L, Schatz G. Mitochondria: a historical review. J Cell Biol. 1981;91(3 Pt 2):227s-55s.
3. Lane N, Martin W. The energetics of genome complexity. Nature. 2010;467(7318):929-34.
4. Friedman JR, Nunnari J. Mitochondrial form and function. Nature. 2014;505(7483):335-43.
5. Neupert W, Herrmann JM. Translocation of proteins into mitochondria. Annu Rev Biochem. 2007;76:723-49.
6. Altman R. Die Elementarorganismen Und Ihre Beziehungen Zu Den Zellen. Leipzig: Veit & comp. 1890:145.
7. Benda C. On spermatogenesis of vertebrates and higher invertebrates, Part II: The histogenesis of sperm. Archiv für Anatomie und Physiologie. 1898(73):393-8.
8. Bensley RRaH, N.L. Studies on cell structure by the freezing-drying method VI. The preparation and properties of mitochondria. The Anatomical Record. 1934;60(4):449-55.
9. Krebs HA, Johnson, W.A. The role of citric acid in intermediate metabolism in animal tissues. Enzymologia. 1937;4:148-56.
10. Mitchell P. Coupling of phosphorylation to electron and hydrogen transfer by a chemi-osmotic type of mechanism. Nature. 1961;191:144-8.
11. Rizzuto R, Simpson AW, Brini M, Pozzan T. Rapid changes of mitochondrial Ca2+ revealed by specifically targeted recombinant aequorin. Nature. 1992;358(6384):325-7.
12. Rizzuto R, Brini M, Pozzan T. Intracellular targeting of the photoprotein aequorin: a new approach for measuring, in living cells, Ca2+ concentrations in defined cellular compartments. Cytotechnology. 1993;11 Suppl 1:S44-6.

13. Kirichok Y, Krapivinsky G, Clapham DE. The mitochondrial calcium uniporter is a highly selective ion channel. Nature. 2004;427(6972):360-4.
14. Trenker M, Malli R, Fertschai I, Levak-Frank S, Graier WF. Uncoupling proteins 2 and 3 are fundamental for mitochondrial Ca2+ uniport. Nat Cell Biol. 2007;9(4):445-52.
15. Perocchi F, Gohil VM, Girgis HS, Bao XR, McCombs JE, Palmer AE, et al. MICU1 encodes a mitochondrial EF hand protein required for Ca(2+) uptake. Nature. 2010;467(7313):291-6.
16. Kuhlbrandt W. Structure and function of mitochondrial membrane protein complexes. BMC Biol. 2015;13:89.
17. Gellerich FN, Trumbeckaite S, Opalka JR, Seppet E, Rasmussen HN, Neuhoff C, et al. Function of the mitochondrial outer membrane as a diffusion barrier in health and diseases. Biochem Soc Trans. 2000;28(2):164-9.
18. Pfanner N, Geissler A. Versatility of the mitochondrial protein import machinery. Nature reviews Molecular cell biology. 2001;2(5):339-49.
19. Zoratti M, Szabo I. Electrophysiology of the inner mitochondrial membrane. J Bioenerg Biomembr. 1994;26(5):543-53.
20. Sjostrand FS. Electron microscopy of mitochondria and cytoplasmic double membranes. Nature. 1953;171(4340):30-2.
21. Carelli V, Chan DC. Mitochondrial DNA: impacting central and peripheral nervous systems. Neuron. 2014;84(6):1126-42.
22. Lightowlers RN, Taylor RW, Turnbull DM. Mutations causing mitochondrial disease: What is new and what challenges remain? Science. 2015;349(6255):1494-9.
23. Mishra P, Chan DC. Metabolic regulation of mitochondrial dynamics. J Cell Biol. 2016;212(4):379-87.
24. Kennedy EP, Lehninger AL. Oxidation of fatty acids and tricarboxylic acid cycle intermediates by isolated rat liver mitochondria. J Biol Chem. 1949;179(2):957-72.
25. Drysdale GR, Lardy HA. Fatty acid oxidation by a soluble enzyme system from mitochondria. J Biol Chem. 1953;202(1):119-36.
26. Sano S, Inoue S, Tanabe Y, Sumiya C, Koike S. Significance of mitochondria for porphyrin and heme biosynthesis. Science. 1959;129(3344):275-6.

27. Williams GS, Boyman L, Chikando AC, Khairallah RJ, Lederer WJ. Mitochondrial calcium uptake. Proc Natl Acad Sci U S A. 2013;110(26):10479-86.
28. Drago I, Pizzo P, Pozzan T. After half a century mitochondrial calcium in- and efflux machineries reveal themselves. EMBO J. 2011;30(20):4119-25.
29. Finkel T, Hwang PM. The Krebs cycle meets the cell cycle: mitochondria and the G1-S transition. Proc Natl Acad Sci U S A. 2009;106(29):11825-6.
30. Antico Arciuch VG, Elguero ME, Poderoso JJ, Carreras MC. Mitochondrial regulation of cell cycle and proliferation. Antioxid Redox Signal. 2012;16(10):1150-80.
31. Tait SW, Green DR. Mitochondria and cell signalling. J Cell Sci. 2012;125(Pt 4):807-15.
32. Wang C, Youle RJ. The role of mitochondria in apoptosis*. Annu Rev Genet. 2009;43:95-118.
33. Rustin P, Kroemer G. Mitochondria and cancer. Ernst Schering Found Symp Proc. 2007(4):1-21.
34. Hockenbery DM. Targeting mitochondria for cancer therapy. Environ Mol Mutagen. 2010;51(5):476-89.
35. Kennedy BE, Madreiter CT, Vishnu N, Malli R, Graier WF, Karten B. Adaptations of energy metabolism associated with increased levels of mitochondrial cholesterol in Niemann-Pick type C1-deficient cells. J Biol Chem. 2014;289(23):16278-89.
36. de Moura MB, dos Santos LS, Van Houten B. Mitochondrial dysfunction in neurodegenerative diseases and cancer. Environ Mol Mutagen. 2010;51(5):391-405.
37. Duchen MR. Mitochondria, calcium-dependent neuronal death and neurodegenerative disease. Pflugers Arch. 2012;464(1):111-21.
38. Griffiths EJ. Mitochondria and heart disease. Adv Exp Med Biol. 2012;942:249-67.
39. Abdallah Y, Kasseckert SA, Iraqi W, Said M, Shahzad T, Erdogan A, et al. Interplay between Ca2+ cycling and mitochondrial permeability transition pores promotes reperfusion-induced injury of cardiac myocytes. J Cell Mol Med. 2011;15(11):2478-85.
40. Parish R, Petersen KF. Mitochondrial dysfunction and type 2 diabetes. Curr Diab Rep. 2005;5(3):177-83.

41. Huttemann M, Lee I, Samavati L, Yu H, Doan JW. Regulation of mitochondrial oxidative phosphorylation through cell signaling. Biochim Biophys Acta. 2007;1773(12):1701-20.
42. Smyth JT, Hwang SY, Tomita T, DeHaven WI, Mercer JC, Putney JW. Activation and regulation of store-operated calcium entry. J Cell Mol Med. 2010;14(10):2337-49.
43. Marchi S, Patergnani S, Missiroli S, Morciano G, Rimessi A, Wieckowski MR, et al. Mitochondrial and endoplasmic reticulum calcium homeostasis and cell death. Cell Calcium. 2018;69:62-72.
44. Bose T, Cieslar-Pobuda A, Wiechec E. Role of ion channels in regulating Ca(2)(+) homeostasis during the interplay between immune and cancer cells. Cell Death Dis. 2015;6:e1648.
45. Chakrabarti R, Chakrabarti R. Calcium signaling in non-excitable cells: Ca2+ release and influx are independent events linked to two plasma membrane Ca2+ entry channels. J Cell Biochem. 2006;99(6):1503-16.
46. Capiod T, Mauger JP, Binet A, Claret M. Regulation of calcium in non-excitable cells. Curr Opin Cell Biol. 1989;1(2):211-4.
47. Brini M, Carafoli E. The plasma membrane Ca(2)+ ATPase and the plasma membrane sodium calcium exchanger cooperate in the regulation of cell calcium. Cold Spring Harb Perspect Biol. 2011;3(2).
48. Newgard CB, McGarry JD. Metabolic coupling factors in pancreatic beta-cell signal transduction. Annu Rev Biochem. 1995;64:689-719.
49. MacDonald PE, Joseph JW, Rorsman P. Glucose-sensing mechanisms in pancreatic beta-cells. Philos Trans R Soc Lond B Biol Sci. 2005;360(1464):2211-25.
50. Wollheim CB, Maechler P. Beta-cell mitochondria and insulin secretion: messenger role of nucleotides and metabolites. Diabetes. 2002;51 Suppl 1:S37-42.
51. Wiederkehr A, Wollheim CB. Impact of mitochondrial calcium on the coupling of metabolism to insulin secretion in the pancreatic beta-cell. Cell Calcium. 2008;44(1):64-76.
52. Wiederkehr A, Szanda G, Akhmedov D, Mataki C, Heizmann CW, Schoonjans K, et al. Mitochondrial matrix calcium is an activating signal for hormone secretion. Cell Metab. 2011;13(5):601-11.

53. Alam MR, Groschner LN, Parichatikanond W, Kuo L, Bondarenko AI, Rost R, et al. Mitochondrial Ca2+ uptake 1 (MICU1) and mitochondrial ca2+ uniporter (MCU) contribute to metabolism-secretion coupling in clonal pancreatic beta-cells. J Biol Chem. 2012;287(41):34445-54.
54. Mazzarello P, Calligaro A, Vannini V, Muscatello U. The sarcoplasmic reticulum: its discovery and rediscovery. Nat Rev Mol Cell Biol. 2003;4(1):69-74.
55. Farquhar MG, Palade GE. The Golgi apparatus: 100 years of progress and controversy. Trends Cell Biol. 1998;8(1):2-10.
56. Schwarz DS, Blower MD. The endoplasmic reticulum: structure, function and response to cellular signaling. Cell Mol Life Sci. 2016;73(1):79-94.
57. English AR, Voeltz GK. Endoplasmic reticulum structure and interconnections with other organelles. Cold Spring Harb Perspect Biol. 2013;5(4):a013227.
58. Clapham DE. Calcium signaling. Cell. 2007;131(6):1047-58.
59. Fill M, Copello JA. Ryanodine receptor calcium release channels. Physiol Rev. 2002;82(4):893-922.
60. Tsujimoto Y, Croce CM. Analysis of the structure, transcripts, and protein products of bcl-2, the gene involved in human follicular lymphoma. Proc Natl Acad Sci U S A. 1986;83(14):5214-8.
61. Yip KW, Reed JC. Bcl-2 family proteins and cancer. Oncogene. 2008;27(50):6398-406.
62. Ikegaki N, Katsumata M, Minna J, Tsujimoto Y. Expression of bcl-2 in small cell lung carcinoma cells. Cancer Res. 1994;54(1):6-8.
63. Monni O, Joensuu H, Franssila K, Klefstrom J, Alitalo K, Knuutila S. BCL2 overexpression associated with chromosomal amplification in diffuse large B-cell lymphoma. Blood. 1997;90(3):1168-74.
64. Tsujimoto Y, Cossman J, Jaffe E, Croce CM. Involvement of the bcl-2 gene in human follicular lymphoma. Science. 1985;228(4706):1440-3.
65. Krajewski S, Tanaka S, Takayama S, Schibler MJ, Fenton W, Reed JC. Investigation of the subcellular distribution of the bcl-2 oncoprotein: residence in the nuclear envelope, endoplasmic reticulum, and outer mitochondrial membranes. Cancer research. 1993;53(19):4701-14.

66. Lithgow T, van Driel R, Bertram JF, Strasser A. The protein product of the oncogene bcl-2 is a component of the nuclear envelope, the endoplasmic reticulum, and the outer mitochondrial membrane. Cell Growth Differ. 1994;5(4):411-7.
67. Akao Y, Otsuki Y, Kataoka S, Ito Y, Tsujimoto Y. Multiple subcellular localization of bcl-2: detection in nuclear outer membrane, endoplasmic reticulum membrane, and mitochondrial membranes. Cancer Res. 1994;54(9):2468-71.
68. Pinton P, Ferrari D, Rapizzi E, Di Virgilio F, Pozzan T, Rizzuto R. The Ca2+ concentration of the endoplasmic reticulum is a key determinant of ceramide-induced apoptosis: significance for the molecular mechanism of Bcl-2 action. EMBO J. 2001;20(11):2690-701.
69. Foyouzi-Youssefi R, Arnaudeau S, Borner C, Kelley WL, Tschopp J, Lew DP, et al. Bcl-2 decreases the free Ca2+ concentration within the endoplasmic reticulum. Proc Natl Acad Sci U S A. 2000;97(11):5723-8.
70. Vervliet T, Parys JB, Bultynck G. Bcl-2 proteins and calcium signaling: complexity beneath the surface. Oncogene. 2016;35(39):5079-92.
71. Schendel SL, Xie Z, Montal MO, Matsuyama S, Montal M, Reed JC. Channel formation by antiapoptotic protein Bcl-2. Proc Natl Acad Sci U S A. 1997;94(10):5113-8.
72. Willecke K, Eiberger J, Degen J, Eckardt D, Romualdi A, Guldenagel M, et al. Structural and functional diversity of connexin genes in the mouse and human genome. Biol Chem. 2002;383(5):725-37.
73. Panchin Y, Kelmanson I, Matz M, Lukyanov K, Usman N, Lukyanov S. A ubiquitous family of putative gap junction molecules. Curr Biol. 2000;10(13):R473-4.
74. Scemes E, Spray DC, Meda P. Connexins, pannexins, innexins: novel roles of "hemi-channels". Pflugers Arch. 2009;457(6):1207-26.
75. Iglesias R, Dahl G, Qiu F, Spray DC, Scemes E. Pannexin 1: the molecular substrate of astrocyte "hemichannels". J Neurosci. 2009;29(21):7092-7.
76. Vanden Abeele F, Bidaux G, Gordienko D, Beck B, Panchin YV, Baranova AV, et al. Functional implications of calcium permeability of the channel formed by pannexin 1. J Cell Biol. 2006;174(4):535-46.
77. Birnbaumer L. The TRPC class of ion channels: a critical review of their roles in slow, sustained increases in intracellular Ca(2+) concentrations. Annu Rev Pharmacol Toxicol. 2009;49:395-426.

78. Vazquez G, Wedel BJ, Aziz O, Trebak M, Putney JW, Jr. The mammalian TRPC cation channels. Biochim Biophys Acta. 2004;1742(1-3):21-36.
79. Bollimuntha S, Cornatzer E, Singh BB. Plasma membrane localization and function of TRPC1 is dependent on its interaction with beta-tubulin in retinal epithelium cells. Vis Neurosci. 2005;22(2):163-70.
80. Berbey C, Weiss N, Legrand C, Allard B. Transient receptor potential canonical type 1 (TRPC1) operates as a sarcoplasmic reticulum calcium leak channel in skeletal muscle. J Biol Chem. 2009;284(52):36387-94.
81. Greenfield JJ, High S. The Sec61 complex is located in both the ER and the ER-Golgi intermediate compartment. J Cell Sci. 1999;112 (Pt 10):1477-86.
82. Laird V, High S. Discrete cross-linking products identified during membrane protein biosynthesis. J Biol Chem. 1997;272(3):1983-9.
83. Wiertz EJ, Tortorella D, Bogyo M, Yu J, Mothes W, Jones TR, et al. Sec61-mediated transfer of a membrane protein from the endoplasmic reticulum to the proteasome for destruction. Nature. 1996;384(6608):432-8.
84. Lang S, Erdmann F, Jung M, Wagner R, Cavalie A, Zimmermann R. Sec61 complexes form ubiquitous ER Ca2+ leak channels. Channels (Austin). 2011;5(3):228-35.
85. Sun L, Zhou R, Yang G, Shi Y. Analysis of 138 pathogenic mutations in presenilin-1 on the in vitro production of Abeta42 and Abeta40 peptides by gamma-secretase. Proc Natl Acad Sci U S A. 2017;114(4):E476-E85.
86. Francis R, McGrath G, Zhang J, Ruddy DA, Sym M, Apfeld J, et al. aph-1 and pen-2 are required for Notch pathway signaling, gamma-secretase cleavage of betaAPP, and presenilin protein accumulation. Dev Cell. 2002;3(1):85-97.
87. Yu G, Nishimura M, Arawaka S, Levitan D, Zhang L, Tandon A, et al. Nicastrin modulates presenilin-mediated notch/glp-1 signal transduction and betaAPP processing. Nature. 2000;407(6800):48-54.
88. De Strooper B, Saftig P, Craessaerts K, Vanderstichele H, Guhde G, Annaert W, et al. Deficiency of presenilin-1 inhibits the normal cleavage of amyloid precursor protein. Nature. 1998;391(6665):387-90.
89. Wolfe MS, Xia W, Ostaszewski BL, Diehl TS, Kimberly WT, Selkoe DJ. Two transmembrane aspartates in presenilin-1 required for presenilin endoproteolysis and gamma-secretase activity. Nature. 1999;398(6727):513-7.

90. Tu H, Nelson O, Bezprozvanny A, Wang Z, Lee SF, Hao YH, et al. Presenilins form ER Ca2+ leak channels, a function disrupted by familial Alzheimer's disease-linked mutations. Cell. 2006;126(5):981-93.
91. Nelson O, Tu H, Lei T, Bentahir M, de Strooper B, Bezprozvanny I. Familial Alzheimer disease-linked mutations specifically disrupt Ca2+ leak function of presenilin 1. J Clin Invest. 2007;117(5):1230-9.
92. Prokesch A, Graef FA, Madl T, Kahlhofer J, Heidenreich S, Schumann A, et al. Liver p53 is stabilized upon starvation and required for amino acid catabolism and gluconeogenesis. FASEB J. 2017;31(2):732-42.
93. Radovic B, Vujic N, Leopold C, Schlager S, Goeritzer M, Patankar JV, et al. Lysosomal acid lipase regulates VLDL synthesis and insulin sensitivity in mice. Diabetologia. 2016;59(8):1743-52.
94. Masumiya H, Shijuku T, Tanaka H, Shigenobu K. Inhibition of myocardial L- and T-type Ca2+ currents by efonidipine: possible mechanism for its chronotropic effect. Eur J Pharmacol. 1998;349(2-3):351-7.
95. Schleifer H, Doleschal B, Lichtenegger M, Oppenrieder R, Derler I, Frischauf I, et al. Novel pyrazole compounds for pharmacological discrimination between receptor-operated and store-operated Ca(2+) entry pathways. Br J Pharmacol. 2012;167(8):1712-22.
96. Maesako M, Uemura K, Kuzuya A, Sasaki K, Asada M, Watanabe K, et al. Gain of function by phosphorylation in Presenilin 1-mediated regulation of insulin signaling. J Neurochem. 2012;121(6):964-73.
97. Cheung KH, Shineman D, Muller M, Cardenas C, Mei L, Yang J, et al. Mechanism of Ca2+ disruption in Alzheimer's disease by presenilin regulation of InsP3 receptor channel gating. Neuron. 2008;58(6):871-83.
98. Gottschalk B, Klec C, Waldeck-Weiermair M, Malli R, Graier WF. Intracellular Ca(2+) release decelerates mitochondrial cristae dynamics within the junctions to the endoplasmic reticulum. Pflugers Arch. 2018;470(8):1193-203.
99. Kirschenbaum F, Hsu SC, Cordell B, McCarthy JV. Substitution of a glycogen synthase kinase-3beta phosphorylation site in presenilin 1 separates presenilin function from beta-catenin signaling. J Biol Chem. 2001;276(10):7366-75.
100. Sutherland C, Leighton IA, Cohen P. Inactivation of glycogen synthase kinase-3 beta by phosphorylation: new kinase connections in insulin and growth-factor signalling. Biochem J. 1993;296 (Pt 1):15-9.

101. Cline GW, Johnson K, Regittnig W, Perret P, Tozzo E, Xiao L, et al. Effects of a novel glycogen synthase kinase-3 inhibitor on insulin-stimulated glucose metabolism in Zucker diabetic fatty (fa/fa) rats. Diabetes. 2002;51(10):2903-10.
102. Ring DB, Johnson KW, Henriksen EJ, Nuss JM, Goff D, Kinnick TR, et al. Selective glycogen synthase kinase 3 inhibitors potentiate insulin activation of glucose transport and utilization in vitro and in vivo. Diabetes. 2003;52(3):588-95.
103. Thivolet C, Vial G, Cassel R, Rieusset J, Madec AM. Reduction of endoplasmic reticulum- mitochondria interactions in beta cells from patients with type 2 diabetes. PLoS One. 2017;12(7):e0182027.
104. Baughman JM, Perocchi F, Girgis HS, Plovanich M, Belcher-Timme CA, Sancak Y, et al. Integrative genomics identifies MCU as an essential component of the mitochondrial calcium uniporter. Nature. 2011;476(7360):341-5.
105. Patron M, Checchetto V, Raffaello A, Teardo E, Vecellio Reane D, Mantoan M, et al. MICU1 and MICU2 finely tune the mitochondrial Ca2+ uniporter by exerting opposite effects on MCU activity. Mol Cell. 2014;53(5):726-37.
106. McCormack JG, Halestrap AP, Denton RM. Role of calcium ions in regulation of mammalian intramitochondrial metabolism. Physiol Rev. 1990;70(2):391-425.
107. Balaban RS. The role of Ca(2+) signaling in the coordination of mitochondrial ATP production with cardiac work. Biochim Biophys Acta. 2009;1787(11):1334-41.
108. Banting FG, Best CH, Collip JB, Campbell WR, Fletcher AA. Pancreatic Extracts in the Treatment of Diabetes Mellitus. Can Med Assoc J. 1922;12(3):141-6.
109. Porte D, Jr., Pupo AA. Insulin responses to glucose: evidence for a two pool system in man. J Clin Invest. 1969;48(12):2309-19.
110. Porte D, Jr. Banting lecture 1990. Beta-cells in type II diabetes mellitus. Diabetes. 1991;40(2):166-80.
111. Davies MJ, Rayman G, Grenfell A, Gray IP, Day JL, Hales CN. Loss of the first phase insulin response to intravenous glucose in subjects with persistent impaired glucose tolerance. Diabet Med. 1994;11(5):432-6.
112. Gerich JE. Pathogenesis and treatment of type 2 (noninsulin-dependent) diabetes mellitus (NIDDM). Horm Metab Res. 1996;28(9):404-12.
113. Bergstrom RW, Wahl PW, Leonetti DL, Fujimoto WY. Association of fasting glucose levels with a delayed secretion of insulin after oral glucose in subjects with glucose intolerance. J Clin Endocrinol Metab. 1990;71(6):1447-53.

114. Kibbey RG, Pongratz RL, Romanelli AJ, Wollheim CB, Cline GW, Shulman GI. Mitochondrial GTP regulates glucose-stimulated insulin secretion. Cell Metab. 2007;5(4):253-64.
115. Maechler P, Wollheim CB. Role of mitochondria in metabolism-secretion coupling of insulin release in the pancreatic beta-cell. Biofactors. 1998;8(3-4):255-62.
116. Kennedy ED, Maechler P, Wollheim CB. Effects of depletion of mitochondrial DNA in metabolism secretion coupling in INS-1 cells. Diabetes. 1998;47(3):374-80.
117. Denton RM. Regulation of mitochondrial dehydrogenases by calcium ions. Biochim Biophys Acta. 2009;1787(11):1309-16.
118. Rutter GA, McCormack JG, Midgley PJ, Denton RM. The role of Ca2+ in the hormonal regulation of the activities of pyruvate dehydrogenase and oxoglutarate dehydrogenase complexes. Ann N Y Acad Sci. 1989;573:206-17.
119. Maechler P, Wang H, Wollheim CB. Continuous monitoring of ATP levels in living insulin secreting cells expressing cytosolic firefly luciferase. FEBS Lett. 1998;422(3):328-32.
120. Komatsu M, Takei M, Ishii H, Sato Y. Glucose-stimulated insulin secretion: A newer perspective. J Diabetes Investig. 2013;4(6):511-6.
121. McManus EJ, Sakamoto K, Armit LJ, Ronaldson L, Shpiro N, Marquez R, et al. Role that phosphorylation of GSK3 plays in insulin and Wnt signalling defined by knockin analysis. EMBO J. 2005;24(8):1571-83.
122. Pratley RE, Weyer C. The role of impaired early insulin secretion in the pathogenesis of Type II diabetes mellitus. Diabetologia. 2001;44(8):929-45.
123. Del Prato S. Loss of early insulin secretion leads to postprandial hyperglycaemia. Diabetologia. 2003;46 Suppl 1:M2-8.
124. Del Prato S, Marchetti P, Bonadonna RC. Phasic insulin release and metabolic regulation in type 2 diabetes. Diabetes. 2002;51 Suppl 1:S109-16.
125. Rieusset J, Fauconnier J, Paillard M, Belaidi E, Tubbs E, Chauvin MA, et al. Disruption of calcium transfer from ER to mitochondria links alterations of mitochondria-associated ER membrane integrity to hepatic insulin resistance. Diabetologia. 2016;59(3):614-23.
126. Reaven GM, Thompson LW, Nahum D, Haskins E. Relationship between hyperglycemia and cognitive function in older NIDDM patients. Diabetes Care. 1990;13(1):16-21.

127. Perlmuter LC, Hakami MK, Hodgson-Harrington C, Ginsberg J, Katz J, Singer DE, et al. Decreased cognitive function in aging non-insulin-dependent diabetic patients. Am J Med. 1984;77(6):1043-8.
128. Pike CJ, Burdick D, Walencewicz AJ, Glabe CG, Cotman CW. Neurodegeneration induced by beta-amyloid peptides in vitro: the role of peptide assembly state. J Neurosci. 1993;13(4):1676-87.
129. Gschwind M, Huber G. Apoptotic cell death induced by beta-amyloid 1-42 peptide is cell type dependent. J Neurochem. 1995;65(1):292-300.
130. Hardy JA, Higgins GA. Alzheimer's disease: the amyloid cascade hypothesis. Science. 1992;256(5054):184-5.
131. Selkoe DJ, Hardy J. The amyloid hypothesis of Alzheimer's disease at 25 years. EMBO Mol Med. 2016;8(6):595-608.
132. Herrup K. The case for rejecting the amyloid cascade hypothesis. Nat Neurosci. 2015;18(6):794-9.
133. Pimplikar SW, Nixon RA, Robakis NK, Shen J, Tsai LH. Amyloid-independent mechanisms in Alzheimer's disease pathogenesis. J Neurosci. 2010;30(45):14946-54.
134. Chavez-Gutierrez L, Bammens L, Benilova I, Vandersteen A, Benurwar M, Borgers M, et al. The mechanism of gamma-Secretase dysfunction in familial Alzheimer disease. EMBO J. 2012;31(10):2261-74.
135. Bentahir M, Nyabi O, Verhamme J, Tolia A, Horre K, Wiltfang J, et al. Presenilin clinical mutations can affect gamma-secretase activity by different mechanisms. J Neurochem. 2006;96(3):732-42.
136. Shimojo M, Sahara N, Murayama M, Ichinose H, Takashima A. Decreased Abeta secretion by cells expressing familial Alzheimer's disease-linked mutant presenilin 1. Neurosci Res. 2007;57(3):446-53.
137. Cacquevel M, Aeschbach L, Houacine J, Fraering PC. Alzheimer's disease-linked mutations in presenilin-1 result in a drastic loss of activity in purified gamma-secretase complexes. PLoS One. 2012;7(4):e35133.
138. Heilig EA, Xia W, Shen J, Kelleher RJ, 3rd. A presenilin-1 mutation identified in familial Alzheimer disease with cotton wool plaques causes a nearly complete loss of gamma-secretase activity. J Biol Chem. 2010;285(29):22350-9.

139. Doody RS, Raman R, Farlow M, Iwatsubo T, Vellas B, Joffe S, et al. A phase 3 trial of semagacestat for treatment of Alzheimer's disease. N Engl J Med. 2013;369(4):341-50.
140. Nordberg A. Amyloid plaque imaging in vivo: current achievement and future prospects. Eur J Nucl Med Mol Imaging. 2008;35 Suppl 1:S46-50.
141. Villemagne VL, Fodero-Tavoletti MT, Pike KE, Cappai R, Masters CL, Rowe CC. The ART of loss: Abeta imaging in the evaluation of Alzheimer's disease and other dementias. Mol Neurobiol. 2008;38(1):1-15.
142. Raux G, Gantier R, Thomas-Anterion C, Boulliat J, Verpillat P, Hannequin D, et al. Dementia with prominent frontotemporal features associated with L113P presenilin 1 mutation. Neurology. 2000;55(10):1577-8.
143. Tang-Wai D, Lewis P, Boeve B, Hutton M, Golde T, Baker M, et al. Familial frontotemporal dementia associated with a novel presenilin-1 mutation. Dement Geriatr Cogn Disord. 2002;14(1):13-21.
144. Dermaut B, Kumar-Singh S, Engelborghs S, Theuns J, Rademakers R, Saerens J, et al. A novel presenilin 1 mutation associated with Pick's disease but not beta-amyloid plaques. Ann Neurol. 2004;55(5):617-26.
145. Sherrington R, Rogaev EI, Liang Y, Rogaeva EA, Levesque G, Ikeda M, et al. Cloning of a gene bearing missense mutations in early-onset familial Alzheimer's disease. Nature. 1995;375(6534):754-60.
146. Cruts M, Theuns J, Van Broeckhoven C. Locus-specific mutation databases for neurodegenerative brain diseases. Hum Mutat. 2012;33(9):1340-4.
147. Supnet C, Bezprozvanny I. Presenilins function in ER calcium leak and Alzheimer's disease pathogenesis. Cell Calcium. 2011;50(3):303-9.
148. Bezprozvanny I. Presenilins and calcium signaling-systems biology to the rescue. Sci Signal. 2013;6(283):pe24.
149. Xia W, Ostaszewski BL, Kimberly WT, Rahmati T, Moore CL, Wolfe MS, et al. FAD mutations in presenilin-1 or amyloid precursor protein decrease the efficacy of a gamma-secretase inhibitor: evidence for direct involvement of PS1 in the gamma-secretase cleavage complex. Neurobiol Dis. 2000;7(6 Pt B):673-81.

7. APPENDIX

In this section the reader can find the corresponding references to **Table 2.**

- Begley JG, Duan W, Chan S, Duff K, Mattson MP. Altered calcium homeostasis and mitochondrial dysfunction in cortical synaptic compartments of presenilin-1 mutant mice. *Journal of neurochemistry* 72, 1030-1039 (1999).
- Campion D*, et al.* Mutations of the presenilin I gene in families with early-onset Alzheimer's disease. *Human molecular genetics* 4, 2373-2377 (1995).
- Chen WT*, et al.* G206D Mutation of Presenilin-1 Reduces Pen2 Interaction, Increases Abeta42/Abeta40 Ratio and Elevates ER Ca(2+) Accumulation. *Mol Neurobiol* 52, 1835-1849 (2015).
- Chui DH*, et al.* Transgenic mice with Alzheimer presenilin 1 mutations show accelerated neurodegeneration without amyloid plaque formation. *Nature medicine* 5, 560-564 (1999).
- Cruts M*, et al.* Molecular genetic analysis of familial early-onset Alzheimer's disease linked to chromosome 14q24.3. *Human molecular genetics* 4, 2363-2371 (1995).
- Cruts M*, et al.* Estimation of the genetic contribution of presenilin-1 and -2 mutations in a population-based study of presenile Alzheimer disease. *Human molecular genetics* 7, 43-51 (1998).
- Dobricic V*, et al.* Genetic testing in familial and young-onset Alzheimer's disease: mutation spectrum in a Serbian cohort. *Neurobiol Aging* 33, 1481 e1487-1412 (2012).
- Ezquerra M, Carnero C, Blesa R, Gelpi JL, Ballesta F, Oliva R. A presenilin 1 mutation (Ser169Pro) associated with early-onset AD and myoclonic seizures. Neurology 52, 566-570 (1999).
- Furukawa K, Guo Q, Schellenberg GD, Mattson MP. Presenilin-1 mutation alters NGF-induced neurite outgrowth, calcium homeostasis, and transcription factor (AP-1) activation in PC12 cells. *Journal of neuroscience research* 52, 618-624 (1998).
- Gliebus G, Rosso A, Lippa CF. Progranulin and beta-amyloid distribution: a case report of the brain from preclinical PS-1 mutation carrier. *American journal of Alzheimer's disease and other dementias* 24, 456-460 (2009).
- Guo Q*, et al.* Alzheimer's PS-1 mutation perturbs calcium homeostasis and sensitizes PC12 cells to death induced by amyloid beta-peptide. *Neuroreport* 8, 379-383 (1996).
- Guo Q*, et al.* Increased vulnerability of hippocampal neurons to excitotoxic necrosis in presenilin-1 mutant knock-in mice. *Nature medicine* 5, 101-106 (1999).

- Ikeuchi T*, et al.* Mutational analysis in early-onset familial dementia in the Japanese population. The role of PSEN1 and MAPT R406W mutations. *Dementia and geriatric cognitive disorders* 26, 43-49 (2008).
- Kamimura K, Tanahashi H, Yamanaka H, Takahashi K, Asada T, Tabira T. Familial Alzheimer's disease genes in Japanese. *Journal of the neurological sciences* 160, 76-81 (1998).
- Kowalska A*, et al.* Molecular genetics of Alzheimer's disease: presenilin 1 gene analysis in a cohort of patients from the Poznan region. *Journal of applied genetics* 44, 231-234 (2003).
- Leissring MA, Paul BA, Parker I, Cotman CW, LaFerla FM. Alzheimer's presenilin-1 mutation potentiates inositol 1,4,5-trisphosphate-mediated calcium signaling in Xenopus oocytes. *Journal of neurochemistry* 72, 1061-1068 (1999).
- Lleo A*, et al.* Frequency of mutations in the presenilin and amyloid precursor protein genes in early-onset Alzheimer disease in Spain. *Archives of neurology* 59, 1759-1763 (2002).
- Nelson O, Tu H, Lei T, Bentahir M, de Strooper B, Bezprozvanny I. Familial Alzheimer disease-linked mutations specifically disrupt Ca2+ leak function of presenilin 1. *The Journal of clinical investigation* 117, 1230-1239 (2007).
- Parent A, Linden DJ, Sisodia SS, Borchelt DR. Synaptic transmission and hippocampal long-term potentiation in transgenic mice expressing FAD-linked presenilin 1. *Neurobiology of disease* 6, 56-62 (1999).
- Raux G*, et al.* Molecular diagnosis of autosomal dominant early onset Alzheimer's disease: an update. *J Med Genet* 42, 793-795 (2005).
- Rogaeva EA*, et al.* Screening for PS1 mutations in a referral-based series of AD cases: 21 novel mutations. *Neurology* 57, 621-625 (2001).
- Ryazantseva M, Skobeleva K, Kaznacheyeva E. Familial Alzheimer's disease-linked presenilin-1 mutation M146V affects store-operated calcium entry: does gain look like loss? *Biochimie* 95, 1506-1509 (2013).
- Sherrington R*, et al.* Cloning of a gene bearing missense mutations in early-onset familial Alzheimer's disease. *Nature* 375, 754-760 (1995).
- Steiner H*, et al.* A pathogenic presenilin-1 deletion causes abberrant Abeta 42 production in the absence of congophilic amyloid plaques. *The Journal of biological chemistry* 276, 7233-7239 (2001).
- Taddei K*, et al.* Two novel presenilin-1 mutations (Ser169Leu and Pro436Gln) associated with very early onset Alzheimer's disease. *Neuroreport* 9, 3335-3339 (1998).

- Takao M*, et al.* Ectopic white matter neurons, a developmental abnormality that may be caused by the PSEN1 S169L mutation in a case of familial AD with myoclonus and seizures. *Journal of neuropathology and experimental neurology* 60, 1137-1152 (2001).
- Tanahashi H, Kawakatsu S, Kaneko M, Yamanaka H, Takahashi K, Tabira T. Sequence analysis of presenilin-1 gene mutation in Japanese Alzheimer's disease patients. *Neuroscience letters* 218, 139-141 (1996).
- Wallon D*, et al.* The French series of autosomal dominant early onset Alzheimer's disease cases: mutation spectrum and cerebrospinal fluid biomarkers. *Journal of Alzheimer's disease : JAD* 30, 847-856 (2012).
- Zhang H, Sun S, Herreman A, De Strooper B, Bezprozvanny I. Role of presenilins in neuronal calcium homeostasis. *The Journal of neuroscience : the official journal of the Society for Neuroscience* 30, 8566-8580 (2010).